Entanglement and confinement in QFT and gauge/gravity.

Warschawski, Michael

Swansea University
Prifysgol Abertawe

Entanglement and Confinement in QFT and Gauge/Gravity

Michael Warschawski
Department of Physics
Swansea University

Abstract

In this thesis our investigation will follow two branches. We will study Entanglement Entropy in Quantum Field Theories and we will study confinement in Holographic Field Theories. In the study of confinement we will mainly focus on field theories dual to a class of backgrounds in Type IIB supergravity, that is obtained by wrapping D5 branes on a two-cycle on the tip of the conifold.

We start by calculating the Entanglement Entropy for a Hilbert Space with a split in field theory degrees of freedom. We apply this novel approach first on a Quantum Field Theory with a light and a heavy scalar and a cubic interaction vertex. We observe divergences in the Entanglement Entropy where the field theory is unstable to decay. We then calculate the Entanglement Entropy for the photon in Quantum Electrodynamics. While the entropy does require a UV-cutoff to remain finite, it is free of singularities.

Then, we move on to the study of Entanglement Entropy in the context of the Gauge/Gravity Correspondence. We establish a connection between the existence of a first-order phase transition in Holographic Entanglement Entropy and confinement of the dual field theory. We notice that non-localities in the UV of the confining field theory can mask the phase transition. We show two methods to resolve this discrepancy. First, we show how novel configurations that show Volume Law divergences rather than the typical Area law divergences, recover the phase transition. Second, we show how a suitable UV completion removing the nonlocalities also leads to discovery. We then provide a Taxonomy of behaviours of the Entanglement Entropy in different confining backgrounds and hint at Invariances of Holographic Entanglement Entropy

Third, we study the Wilson Loop for the confining field theories dual to D5 on S^2. We notice, that the Wilson Loop also admits phase transitions. We interpret the reason why these phase transitions occur and test our assumptions by creating background with multiple phase transitions.

Last, we notice the mathematical similarity between Holographic Entanglement Entropy and the Wilson Loop. We establish and compare the conditions on both quantities to probe confinement. We test these conditions on a selection of backgrounds. While also note the source for the difference in their behaviour and establish the precise term responsible. We conclude by analysing whether it might be possible at all to find backgrounds that have the exact same qualitative behaviour of the Wilson Loop and the Entanglement Entropy.

Contents

Acknowledgements

Undoubtedly, the most difficult task in writing up a thesis is to figure out how to thank all those people that made me who I am and who supported me all these years. Even more so, if I have less than a page to do so.

This work would not have been possible without my advisor Timothy J. Hollowood, who had an incredible amount of patience and always was prepared to reach out a hand when I really needed it. I would also like to thank him and my other collaborators with whom I had the pleasure of making my contributions to the field. A special mention also goes to STFC, who were generous enough to fund my PhD.

It was a delight to work alongside so many talented individuals in Swansea. The older years provided a welcoming atmosphere from the start and had a willingness to sacrifice their time to get me started when I felt hopelessly lost. The people in my year guaranteed that I never felt alone while facing one challenge after the next. And the people of the years below never failed to provide a fresh perspective on physics and the live outside of work. To list all of your names would unfortunately break the confines of this page. That statement in itself conveys how lucky I can count myself to be. You all have my deepest gratitude.

These acknowledgements would mean nothing without mentioning my parents, Alexandra and Georg, as well as my grandmother, Wanda. You surrendered everything you had and more for my success. Let this work be a testament to your unselfish dedication.

Last but not least, my thanks go to Eike Brennenstuhl for her incredible talent to keep me sane when others could not during the tough times when this thesis was written up.

List of Figures

Chapter 1

Introduction

Informally speaking, Entanglement Entropy (EE) is a measure of how much information one subsystem has of another. We will quickly introduce this quantity in Quantum Mechanics and then discuss how it generalises to Quantum Field Theory as well as Gauge/Gravity. In order to formally define it, we first need a bipartite system. This is a Hilbert space that can be written as the direct product of two subsystems,

$$\mathcal{H}_{AB} = \mathcal{H}_A \times \mathcal{H}_B. \tag{1.0.1}$$

Given a quantum state $\rho = \sum_i a_i |\phi_i\rangle \langle\phi_i|$, we can define the reduced density matrix of a subspace A by

$$\rho_A = \mathrm{Tr}_B \, \rho. \tag{1.0.2}$$

The Entanglement Entropy is then given by the von Neumann entropy,

$$S_A = -\mathrm{Tr}\, \rho_A \log \rho_A. \tag{1.0.3}$$

Often, A will represent a subregion of the manifold M on which the theory is embedded. For a general excited state of any quantum system, we will have [1]

$$S_A \sim \mathrm{Vol}(A). \tag{1.0.4}$$

However, when the Hamiltonian is gapped, the ground state of the theory will obey an area law instead[2].

The Entanglement Entropy enjoys several interesting properties. For example, it satisfies the triangle inequality $|S_A - S_B| \leq S_{A\cup B} = S_{AB}$. The mutual information is $I(A,B) \geq 0$,

where

$$I(A,B) = S_A + S_B - S_{AB}. \tag{1.0.5}$$

Also, whenever ρ describes a pure state, we have $S_A = S_B$.

The definition of EE can mathematically be straightforwardly generalised to quantum field theories. However, there are several complications that now have to be considered. First and foremost (1.0.3) is now generally UV divergent. Thus the entropy can usually only be defined up to an infinite additive constant S_{div} that is independent of the dimensionality of $\mathcal{H}_A$. The leading order of the UV cutoff λ the divergence scales as [3, 4]

$$S_{\text{div}} \sim \frac{V_{d-1}}{\lambda^{d-1}}. \tag{1.0.6}$$

Thus it will often be more physically relevant to study derivatives or differences of entropies instead.

While the EE is very difficult to calculate in most QFTs, it provides a tool set that differs greatly from how they are normally studied. Hence it is no surprise that EE is used to prove several facts about QFT that are extremely difficult or impossible to study using other methods. See, for example, the c-Theorem[5], The F-Theorem[6], and the a-Theorem[7]. Of course EE has found many other applications in different branches of Physics. We refer the reader to the papers [8–12] for a further review of these applications and formalism.

The split of the Hilbert space does not necessarily have to be spatial. For example we can also study the EE between different regions of momentum space[13]. With this it can be shown that the Wilsonian effective action is compatible with a description in terms of a density matrix. Though it should be noted that this compatibility is not a 1-to-1 map. The Wilsonian action will always contain more information as it is a functional of time-dependent field configurations. The density matrix is composed only of time-independent configurations.

However, the split can also be done in terms of degrees of freedom corresponding to the different fields of an interacting QFT. With this we can ask what the fundamental entanglement is between these fields, which is present even in the vacuum or a 1 particle state. The study of this concept in relation to the photon and the electron field will be the subject of Chapter 3.

Entanglement Entropy has also been shown to be very useful in the context of the Gauge/Gravity Correspondence [14]. This duality, that is also commonly referred to as 'Holography', enables us to study nonperturbative effects of Quantum Field Theories and Gravity in new and revolutionary ways. The original correspondence between Type IIB String Theory on $AdS_5 \times S^5$

and $\mathcal{N} = 4$ Super Yang Mills was conjectured by Maldacena 18 years ago in 1997. It describes a dictionary that relates quantities in both theories to one another. For example the thermodynamical partition function on both sides of the correspondence are equal to one another $Z_{\text{CFT}}(\beta) = Z_{\text{grav}}(\beta)$, fields in the gravity theory correspond to operators in the CFT, and so on. The duality is often very complex. Weakly coupled quantities in the gravity tend to be connected to strongly coupled quantities in the field theory and vice versa. But it is exactly because of this that the Gauge/Gravity Correspondence has proven to provide new avenues of exploration in theoretical physics. The CFT is thought to live on the conformal boundary of the spacetime. Thus it is common parlance to refer to the gravity side of the duality as 'the bulk' and to the CFT as 'the boundary'. But it should not be forgotten that this is technically inaccurate. Every calculation will be performed either in the framework of one theory or of another. Also the field theory is dual to the whole gravity theory, so in some sense it does live everywhere, too.

The original duality has since been generalised to more realistic models with fewer symmetry. A particular such solution, produced by a twisted compactification of D5 branes on a two-cycle of the resolved conifold is commonly referred to as the Chamseddine-Volkov/Maldacena-Núñez (CVMN) solution [15, 16]. It and its generalisation exhibit many interesting features and will play a central role in this thesis. Thus we will provide a more thorough introduction to them in Chapter 2.

The holographic prescription to calculate the EE was proposed by Ryu and Takayanagi [17, 18]. They noticed that the origin of EE looks analogous to black hole entropy. For once, EE can be understood to be the entropy for an observer who has only access to region A and cannot receive a signal from region B. Furthermore, the leading divergence of EE is proportional to the area of the subsystem A, see (1.0.6). This lead them to generalise the Bekenstein-Hawking Formula [19, 20]

$$S_{\text{BH}} = \frac{\text{A}(\Sigma)}{4G_N}, \tag{1.0.7}$$

where Σ is the event horizon of the black hole, and G_N denotes Newton's Constant. The result was the Ryu-Takayanagi Formula for Holographic Entanglement Entropy for a d dimensional conformal field theory dual to an AdS_{d+2} background

$$S_A = \frac{\text{A}(\gamma_A)}{4G_N^{d+2}}, \tag{1.0.8}$$

where G_N^{d+2} is the generalised Newton's Constant in $d+2$ spacetime dimensions and γ_A is the

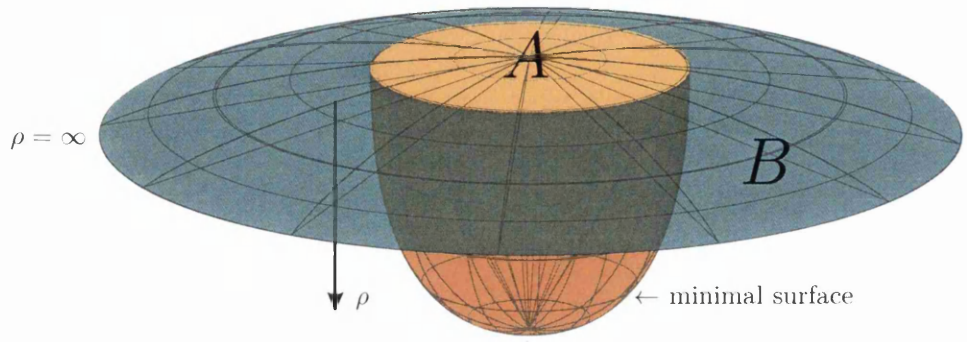

Figure 1.1: A representation of the Ryu-Takayanagi Equation. In order to calculate the entanglement entropy of A, we have to find the minimal surface whose boundary is the same as that of region A.

extremal bulk surface homologous to the boundary region A. Please refer to Figure 1.1 for a visual representation. This conjecture is valid for static backgrounds at zero temperature, where ∂A is a smooth manifold. However, suitable extensions have been proposed for all these cases. Most importantly though, in general areas of the parameter space, the gravity dual is given by string theory, and quantum corrections affect this formula. The authors of [21] have shown that to first order, these corrections are proportional to the entanglement entropy between the two bulk regions separated by γ_A. However, in most cases discussed, such as the strong coupling limits of the QFTs, these correction become negligible and we can treat the formula essentially as exact. In some cases, such as the $(1+1)$ CFT dual to $AdS_3 \times S^7$, where entanglement entropy can be calculated from the field theory side, the formula can be shown to be exact. Another example would be massive quantum field theories by perturbing two-dimensional conformal field theories by relevant perturbations. In some special cases, the formula has been derived directly from the Holography dictionary $Z_{\text{CFT}}(M) = Z_{\text{q.grav.}}(\partial N = M)$ [22].

Klebanov, Kutasov and Murugan (KKM) [23] generalized the prescription of [17] to non-conformal field theories. We know have

$$S = \frac{1}{G_N^{(10)}} \int_\gamma \mathrm{d}\sigma e^{-2\phi} \sqrt{g_{\text{ind}}^{(8)}}, \tag{1.0.9}$$

where $g_{\text{ind}}^{(8)}$ is the induced string frame metric on γ. In particular they found that certain backgrounds, which are holographically dual to confining systems, admit a first order phase

transition upon varying the width of a strip that sets the entangled regions. In this thesis we further explore various aspects of the holographic EE of confining systems.

A special feature of the holographic EE as a diagnostic tool for confinement is the fact that it relates not only the IR behaviour of the geometry, but also has implications on the UV behaviour of the background *.

We study the calculation of the EE in non-local QFTs. We deal with this complicated problem by using holographic duals based on D5 or higher Dp branes ($p > 5$). Then, performing the usual calculation we find that in spite of the background in question having the IR-geometry suitable to be dual to a confining QFT [24], the phase transition in the EE is absent. We will observe that this is an effect of the UV non-locality of the QFT. We will propose a way to fix this situation, by introducing a hard UV cutoff and observing that new configurations appear that would not only recover the phase transition argued in [23], but also solve an stability problem of the configurations that miss the phase transition. Finally, since the UV-cutoff may look like a 'bad fix' for the problem, we will show (with two examples) how a suitable UV-completion to give a local theory, plays a similar role to the UV-cutoff, at least for the purposes of the transition.

This suggest that the EE is not only a quantity useful to diagnose confinement, but also to determine if the QFT in question is local in the far UV.

Another aspect of the Gauge/Gravity Correspondence is its use in the study of non-local operators such as the Wilson loop[25]. It is accessible from the string theory side, which is computationally significant and physically, it provides a basis for gauge invariant gluonic operators.

More importantly, however, the potential of a quark-antiquark($q\bar{q}$) pair can be related to the VEV of a rectangular Wilson loop, whose sides are equal to the $q\bar{q}$ separation and $T \to \infty$. In the gauge theory the Wilson loop $W(\mathcal{C})$ along a curve $\mathcal{C}$ is defined as

$$W(\mathcal{C}) \equiv \frac{1}{N_c} Tr\{P[e^{i \oint_{\mathcal{C}} A_\mu dx^\mu}]\}, \tag{1.0.10}$$

where N_c is the number of colors, P represents the path ordering of the exponential and A_μ are the gauge fields. In this thesis we will assume the gauge fields to be in the fundamental representation, however higher order representations are feasible [26]. On the string side of the

*Here and below, we follow the common parlance according to which the large and small radial position in the string background are associated with the UV and IR of the dual QFT

correspondence we have [27, 28]

$$\left\langle W(\mathcal{C})\right\rangle = \int_{\partial F(\mathcal{C})} \mathcal{D}F e^{-S[F]}, \tag{1.0.11}$$

where F is used to denote all fields of the string theory and ∂F their boundary values along $\mathcal{C}$.

We can approximate (1.0.11) using the steepest descent method. Here, the surface spanned by the strings ending on $\mathcal{C}$ and obeying the Nambu-Goto action $S_{NG}(F)$, is minimised. Now, that we have approximated the VEV of the Wilson loop and we know that we can relate the $q\bar{q}$ potential to this VEV by $\left\langle W(\mathcal{C})\right\rangle \approx e^{-ET}$ we see that

$$E_{q\bar{q}} \approx \frac{S_{NG}}{T}. \tag{1.0.12}$$

Convinced of the importance of Wilson loops, in Chapter 5 we will compute its properties for backgrounds proposed in [29], deepening our understanding of those solutions.

We notice that the functional forms of the length of strip associated with EE and of a Wilson line are similar and further so are the EE and the energy of the WL as a function of the length. We discuss the similarities and the differences of these forms for systems that admit confinement. In an analogous manner to the determination of sufficient conditions for an area law WL [24], we find the sufficient condition for a first order phase transition of the holographic EE. We apply these conditions to several examples including the $AdS_5 \times S^5$, Dp branes compactified on S^1, the hard and soft wall models and the Klebanov-Strassler (KS) model [30].

The material will be organised as follows. Chapter 2 is further review. We will introduce the Chamseddine-Volkov/Maldacena-Núñez solutions and its various extensions in detail. In Chapter 3 we will study the Entanglement of the Photon with the electron, first in a toy scalar theory, and then in QED. This is based on [31]. In Chapter 4 we will discuss the holographic EE of confining theories. This is based on [32]. In Chapter 5 we will study the CVMN solutions and its generalisations using Wilson Loops. This is based on [33]. In Chapter 6, based on [32], we will look at the similarities of these two items of the holographic toolkit and finally, in Chapter 7 we will summarise our results and provide an outlook to possible future work.

Chapter 2

Wrapped brane models

In this thesis, confinement will play a central role. We study this property through the use of entanglement entropy and Wilson Loop calculations. Thus it is no surprise that our main focus will lie on backgrounds dual to confining field theories. A particular class of backgrounds generated by $D5$ branes wrapped on S^2 has emerged that seems particular suitable to this task. It has a relatively simple analytical solution. At the same time it can be generalised and transformed in a myriad of ways. Some of these ways lead to 'problems', such as singularities or non-locality. However, we also have found treatments for most of these ailments. This richness will allow us to separate the issues, features and scales of the theory that will be responsible for the many phenomena that we will observe. This will enable us to zoom in and really understand what role is played by each single component. In order to understand how the variations of this background are related to each other, and thus ease the understanding of the analysis in the chapters to follow, we will introduce these backgrounds in the following.

We will now discuss the main background of interest and its generalisations, see [29]. It is generated from a type IIB string theory that is truncated so that it only includes gravity, a dilaton Φ and Ramond-Ramond (RR) 3-form F_3. In particular, it is produced by a stack of N_c $D5$ branes wrapping an S^2 on the tip of the conifold which is described by a $T^{1,1}$ and extending in the Minkowski direction x^μ, $\mu \in \{0,1,2,3\}$. The field theory described contains a massless vector multiplet as well as a Kaluza-Klein (KK) tower of massive chiral and vector multiplets. The gauge symmetry of the theory is $SU(N_c)$ while the global symmetries are

$$SU(2)_L \times SU(2)_R \times U(1)_R. \tag{2.0.1}$$

More details about the field theory side can be found in [34, 35].

Now to describe the background produced by the above, lets us use the following $SU(2)$ left-invariant one-forms

$$\tilde{\omega}_1 = \cos\psi\, d\tilde{\theta} + \sin\psi \sin\tilde{\theta}\, d\tilde{\varphi}\,, \quad \tilde{\omega}_2 = -\sin\psi\, d\tilde{\theta} + \cos\psi \sin\tilde{\theta}\, d\tilde{\varphi}\,, \quad \tilde{\omega}_3 = d\psi + \cos\tilde{\theta}\, d\tilde{\varphi}\,, \tag{2.0.2}$$

and the vielbeins

$$\begin{aligned} &E^{x^i} = e^{\frac{\Phi}{4}} dx^i\,, \qquad E^{\rho} = e^{\frac{\Phi}{4}+k} d\rho\,, \qquad E^{\theta} = e^{\frac{\Phi}{4}+h} d\theta\,, \qquad E^{\varphi} = e^{\frac{\Phi}{4}+h} \sin\theta\, d\varphi\,, \\ &E^1 = \frac{1}{2} e^{\frac{\Phi}{4}+g}(\tilde{\omega}_1 + a\, d\theta)\,, \quad E^2 = \frac{1}{2} e^{\frac{\Phi}{4}+g}(\tilde{\omega}_2 - a\, \sin\theta\, d\varphi)\,, \quad E^3 = \frac{1}{2} e^{\frac{\Phi}{4}+k}(\tilde{\omega}_3 + \cos\theta\, d\varphi)\,. \end{aligned} \tag{2.0.3}$$

Then, in the Einstein frame, we have

$$\begin{aligned} ds_E^2 &= \alpha' g_s \sum_{i=1}^{10} (E^i)^2\,, \\ F_3 &= e^{-\frac{3}{4}\Phi}\Big(f_1 E^{123} + f_2 E^{\theta\varphi 3} + f_3(E^{\theta 23} + E^{\varphi 13}) + f_4(E^{\rho 1\theta} + E^{\rho\varphi 2})\Big)\,, \end{aligned} \tag{2.0.4}$$

where we defined

$$\begin{aligned} &E^{ijk..l} = E^i \wedge E^j \wedge E^k \wedge ... \wedge E^l\,, \\ &f_1 = -2N_c e^{-k-2g}\,, \qquad f_2 = \frac{N_c}{2} c^{-k-2h}(a^2 - 2ab + 1)\,, \\ &f_3 = N_c e^{-k-h-g}(a-b)\,, \qquad f_4 = \frac{N_c}{2} e^{-k-h-g} b'\,. \end{aligned} \tag{2.0.5}$$

With the foresight that we would like to study rectangular Wilson loops and entanglement entropy, we will move from the Einstein frame to the string frame in the following. The metric can be obtained by multiplying ds_E^2 by $e^{\frac{\Phi}{2}}$. The metric relevant for both computations becomes

$$ds_{str}^2 = \alpha' g_s \sum_{i=1}^{10} (e^i)^2\,, \tag{2.0.6}$$

where the vielbeins are given by

$$\begin{aligned} &e^{x^i} = \frac{e^{\frac{\Phi}{2}}}{\alpha' g_s} dx^i\,, \qquad e^{\rho} = e^{\frac{\Phi}{2}+k} d\rho\,, \qquad e^{\theta} = e^{\frac{\Phi}{2}+h} d\theta\,, \qquad e^{\varphi} = e^{\frac{\Phi}{2}+h} \sin\theta\, d\varphi\,, \\ &e^1 = \frac{1}{2} e^{\frac{\Phi}{2}+g}(\tilde{\omega}_1 + a\, d\theta)\,, \quad e^2 = \frac{1}{2} e^{\frac{\Phi}{2}+g}(\tilde{\omega}_2 - a\, \sin\theta\, d\varphi)\,, \quad e^3 = \frac{1}{2} e^{\frac{\Phi}{2}+k}(\tilde{\omega}_3 + \cos\theta\, d\varphi)\,. \end{aligned}$$

To ease the understanding we will now set $\alpha' g_s = 1$ for the rest of the chapter. There are 6 functions in the background (a, b, Φ, g, h, k) which depend on the radial coordinate ρ. The background is determined by solving the equations of motion for these functions. A system

of BPS equations can be derived[36–38].It is sometimes more efficient, to 'change the basis' to describe the background and RR fields from the functions $[a, h, g, k, \Phi]$ to another set of functions $[P, Q, \tau, Y, \Phi]$. This is useful because in terms of the second set, the BPS equations decouple. It is then possible to solve the non-linear ordinary BPS equations, so that everything is left in terms of a function $P(\rho)$, that satisfies a non-linear ordinary second order differential equation. The change of basis is

$$4e^{2h} = \frac{P^2 - Q^2}{P\cosh\tau - Q}, \quad e^{2g} = P\cosh\tau - Q, \quad e^{2k} = 4Y, \quad a = \frac{P\sinh\tau}{P\cosh\tau - Q}, \quad N_c b = \sigma. \tag{2.0.7}$$

After having solved for $[Y, Q, \tau, \Phi]$ and choosing integration constants to avoid singularities, we have

$$\begin{aligned} e^{2k} &= \frac{P'}{2}, \qquad e^{2h} = \frac{1}{4}\frac{P^2 - Q^2}{P\coth(2\rho) - Q}, \quad e^{2g} = P\coth(2\rho) - Q, \\ a &= \frac{P}{P\cosh(2\rho) - Q\sinh(2\rho)}, \quad e^{4\Phi - 4\Phi_0} = \frac{2\sinh(2\rho)^2}{(P^2 - Q^2)P'}. \end{aligned} \tag{2.0.8}$$

These equations show that all background functions can be expressed in terms of $Q(\rho)$ and $P(\rho)$, where

$$Q(\rho) = (Q_o + N_c)\coth(2\rho - 2\rho_\Lambda) + N_c\,(2\rho\coth(2\rho - 2\rho_\Lambda) - 1), \tag{2.0.9}$$

and P is a solution to the following differential equation

$$P'' + P'\Big(\frac{P' + Q'}{P - Q} + \frac{P' - Q'}{P + Q} - 4\coth(2\rho - 2\rho_\Lambda)\Big) = 0. \tag{2.0.10}$$

This is sometimes called 'master equation' in the bibliography [37], as this is the only equation that needs to be solved to generate the background. ρ_Λ and Q_o are constants of integration. In order to avoid a background that is singular in the IR, we are required to set $Q_o = -N_c$. Furthermore, we are free to set $\rho_\Lambda = 0$. This sets the dynamical scale against which all other parameters are measured against, to one. Different solutions to the master equation have been discussed and classified in [29, 37, 39].

One simple solution of this 'master' equation for the function $P(\rho)$ (2.0.10), leading to a smooth background, is known analytically and given by

$$P = 2N_c\rho. \tag{2.0.11}$$

It leads to the background discussed in [16]. One can check by replacing in eq.(2.0.8) that the

dilaton behaves as $e^{4\Phi} \sim \frac{e^{4\rho}}{\rho}$. The background functions of this solution are

$$\frac{e^{2g}}{N_c} = \frac{e^{2k}}{N_c} = 1, \qquad \frac{e^{2h}}{N_c} = \rho \coth 2\rho - \frac{\rho^2}{\sinh^2 2\rho} - \frac{1}{4},$$
$$a = b = \frac{2\rho}{\sinh 2\rho}, \qquad e^{4\Phi - 4\phi_0} = \frac{N_c}{4} e^{-2h} \sinh^2 2\rho. \tag{2.0.12}$$

Other solutions can be found semi-analytically. We can derive UV and IR expansions, but are required to find a smooth interpolation between them numerically. Nevertheless this suffices to be able to show that a generic solution to the master equation can be approximated by the following:

$$P(\rho) \simeq P_a \equiv \sup\left\{c_0, 2N_c\rho, c_+ e^{4\rho/3}\right\}. \tag{2.0.13}$$

$c_+, c_0 \geq 0$ are two constants of integration. Please note that the real solutions to the master equation are smooth $\forall \rho \geq 0$. However several useful facts can already be seen, such as the fact that P and P' will always be monotonically increasing and $P > Q$.

In this thesis we will only concentrate on solutions for which $c_0 = 0$. We then have

$$\begin{aligned} P \;&= e^{4\rho/3}\Big[c_+ + \frac{e^{-8\rho/3}N_c^2}{c_+}\left(4\rho^2 - 4\rho + \frac{13}{4}\right) + e^{-4\rho}\left(c_- - \frac{8c_+}{3}\rho\right) + \\ &+ \frac{N_c^4 e^{-16\rho/3}}{c_+^3}\left(\frac{18567}{512} + \frac{2781}{32}\rho + \frac{27}{4}\rho^2 + 36\rho^3\right) + \mathcal{O}(e^{-20\rho/3})\Big] \end{aligned} \tag{2.0.14}$$

as our UV expansion. c_- is a constant related to c_0. It turns out that if we treat c_+ and c_- as completely independent, the background will in general be mildly singular, with a divergent Kretschmann Scalar $K = R_{abcd}R^{abcd}$, where R_{abcd} is the Riemann curvature tensor, in the IR. Please also note, that our solutions are mostly derived from supergravity. These solutions are only valid outside of singularities. Otherwise we would expect α' near the singularities. We will avoid all this by setting $c_- = 0$*.

The IR expansion can be written as[36]

$$P = h_1\rho + \frac{4h_1}{15}\left(1 - \frac{4N_c^2}{h_1^2}\right)\rho^3 + \frac{16h_1}{525}\left(1 - \frac{4N_c^2}{3h_1^2} - \frac{32N_c^4}{3h_1^4}\right)\rho^5 + \mathcal{O}(\rho^7). \tag{2.0.15}$$

$h_1 > 2N_c$ is again a constant of integration. Naively it appears as if we now have two independent constants to consider, h_1 and c_+. However, the requirement for both expansions to match leads to the fact that there is a dependency between the two constants. Given the value of one

*$c_- = 0$ follows automatically from $c_0 = 0$. For completeness, it should be mentioned that less severe restrictions can be found that still circumvent the singularity

constants allows us in principle to determine the value of the other, though it should be noted that a closed form relationship is generally not known.

We see that the small radius expansion is quite similar to the one of the exact solution $P = 2N_c\rho$. Indeed, for the constant $h_1 = 2N_c$ we recover the exact solution. On the other hand, the large radius expansion of the solution for the function $P(\rho)$ is quite different from the linear behaviour of the exact solution. These differences and similarities suggest that the dynamics of the QFT dual to the second solution is actually afflicted by an irrelevant operator. In the paper [40], this point was made precise (see also the discussion in [29]). The operator can be seen to be of dimension eight. The situation is not so different from the case of 'keeping the constant factor' in the warp factor of the D3 branes solution $\hat{h} = 1 + \frac{L^4}{r^4}$. Indeed, it can be shown that the factor '1' makes the background of N_c D3 branes dual to $N = 4$-SYM with a dimension eight operator inserted. In order to UV-complete this QFT one needs to insert back the whole tower of string modes.

Such a completion is given by a U-duality as it is described in [41].This procedure has also been referred to as a rotation. It is a solution generating technique that schematically unites the backgrounds, by taking a solution to our master equation and mapping it to another background where new fluxes are turned on. While neither the background functions, nor Q and P change, the metric does and new fluxes are turned on. It can be described by the following steps.

- Perform a compactification of the spatial Minkowski directions and perform T-dualisation along them

- Uplift to M-Theory and perform the following boost in the $t - x^\sharp$ plane, where $x^\sharp$ is the newly introduced direction :

$$t \to \cosh\hat{\beta}t - \sinh\hat{\beta}x^\sharp, \qquad x^\sharp \to -\sinh\hat{\beta}t + \cosh\hat{\beta}x^\sharp. \tag{2.0.16}$$

- Downlift back to String theory and T-dualise back along the Minkowski directions.

This rotation changes the metric and turns on extra fluxes, but F_3 remains invariant. Also the relation between the background functions is unchanged, thus we can solve them the exact same way using the same master equation. To describe the new metric we can use the $SU(2)$

left-invariant one-forms defined in (2) and the following vielbeins:

$$
\begin{aligned}
&e^{x^j} = e^{\frac{\Phi}{4}}\hat{h}^{-\frac{1}{4}}\,dx^j, \qquad e^{\rho} = e^{\frac{\Phi}{4}+k}\hat{h}^{\frac{1}{4}}\,d\rho, \qquad e^{\theta} = e^{\frac{\Phi}{4}+h}\hat{h}^{\frac{1}{4}}\,d\theta, \qquad e^{\varphi} = e^{\frac{\Phi}{4}+h}\hat{h}^{\frac{1}{4}}\sin\theta\,d\varphi,\\
&e^1 = \frac{1}{2}e^{\frac{\Phi}{4}+g}\hat{h}^{\frac{1}{4}}(\tilde{\omega}_1 + a\,d\theta), \qquad e^2 = \frac{1}{2}e^{\frac{\Phi}{4}+g}\hat{h}^{\frac{1}{4}}(\tilde{\omega}_2 - a\sin\theta\,d\varphi),\\
&e^3 = \frac{1}{2}e^{\frac{\Phi}{4}+k}\hat{h}^{\frac{1}{4}}(\tilde{\omega}_3 + \cos\theta\,d\varphi).
\end{aligned}
\tag{2.0.17}
$$

The full background is the given by

$$
\begin{aligned}
ds_E^2 &= \sum_i (e^i)^2,\\
F_3 &= \frac{e^{-\frac{3}{4}\Phi}}{\hat{h}^{\frac{3}{4}}}\Big[f_1 e^{123} + f_2 e^{\theta\varphi 3} + f_3(e^{\theta 23} + e^{\varphi 13}) + f_4(e^{\rho 1\theta} + e^{\rho\varphi 2})\Big],\\
H_3 &= -\kappa\frac{e^{\frac{5}{4}\Phi}}{\hat{h}^{\frac{3}{4}}}\Big[-f_1 e^{\theta\varphi\rho} - f_2 e^{\rho 12} - f_3(e^{\theta 2\rho} + e^{\varphi 1\rho}) + f_4(e^{1\theta 3} + e^{\varphi 23})\Big],\\
C_4 &= -\kappa\frac{e^{2\Phi}}{\hat{h}}\,dt\wedge dx_1\wedge dx_2\wedge dx_3,\\
F_5 &= \kappa e^{-\frac{5}{4}\Phi - k}\hat{h}^{\frac{3}{4}}\partial_\rho\left(\frac{e^{2\Phi}}{\hat{h}}\right)\left[e^{\theta\varphi 123} - e^{tx_1x_2x_3\rho}\right].
\end{aligned}
\tag{2.0.18}
$$

We should note that there is an additional B_2 defined by $H_3 = dB_2$. $\hat{h}$ is the new warp factor and is defined by

$$
\hat{h} = 1 - \kappa^2 e^{2\Phi}. \tag{2.0.19}
$$

κ has to be carefully chosen so that we remove the dimension 8 irrelevant operator and decouple the QFT from gravity. Then we UV complete with the precise matter content such that the UV of the resulting QFT is as healthy as the Klebanov-Strassler (KS) QFT.

To explain better what we mean by healthy, remember that the modern, Wilsonian definition of a field theory is a conformal UV fixed point and an RG flow. The study of these RG flows through the Gauge/Gravity Correspondence comes in different varieties of 'cleanliness'. $\mathcal{N} = 4$ SYM flowing into $\mathcal{N} = 1*$ Yang-Mills is an example of a completely clean realization. Klebanov-Strassler, while still highly successful and non-trivial, has some downsides in the realisation of the field theory group flow. It introduces a deformation in the string bulk that corresponds to an imbalance of the ranks of the gauge groups in the field theory side. However, this deformation does not switch itself off and the theory never reaches a conformal fixed point in the UV. Instead it follows a cascade of Seiberg dualities, each pushing the theory towards a new fixed point described by field theories whose rank grows without bound. Nevertheless, the resulting system shows behaviour that is closely resembling $4d$ field theories. The D_5 on S^2 is another

step below on this ladder. A weak coupling analysis of the dual theory shows an infinite tower of equidistant modes. This leads to many headaches, like the operator coupling to gravity. In the UV, the theory never reaches a fixed point. Naively, we should regard these theories as effective field theories. They have interesting and healthy low energy dynamics but are broken in the UV. The U-duality fixes that. On the field theory side, this operation connects the IR behaviour to the UV of KS via a Higgsing cascade. See the discussion in [40] for further explanation of this point.

If $\kappa = e^{-\Phi_\infty}$, where Φ_∞ is the UV limit of the dilaton, we achieve our goal of asymptoting the KS UV dynamics. The warp factor of the background asymptotes to zero and this switches off the dimension-eight irrelevant operator discussed above. These backgrounds form a continuous set of solutions parametrised by h_1. They span the whole baryonic branch of the dual field theory. Notice also that this expression for $\hat{h}$ implies that this U-duality or rotation of the $SU(3)$-structure can only be performed in the case in which the dilaton is stabilised at large radius, namely $\Phi(\infty)$ is a finite value. In other words, we cannot use this for the analytical solution $P = 2N_c\rho$, that has linearly growing dilaton. Only the solutions described around eq.(2.0.14) and (2.0.15) can be used. But we can regard $P = 2N_c\rho$ to be a direct analytic continuation of the set of baryonic branch solutions given by $h_1 \in (2N_c, \infty)$. The $h_1 \to \infty$ limit yields the KS model [30].

2.1 Sources

The KS dual has a bulk geometry given by $AdS_5 \times T^{1,1}$, where $T^{1,1}$ is the base of the conifold. It has kN_c $D3$ branes and N_c fractional $D5$ branes. On the field theory side we have a minimally supersymmetric QFT with two bifundamental matter fields. It has a two-node quiver of gauge groups of equal rank, given by $SU(kN_c) \times SU(kN_c + N_c)$. It lives on the baryonic branch of the moduli space of the theory.

However, the above solutions can also be moved to the mesonic branch. In order to do this, we need to de-tune the ranks of the two gauge groups. The unbalance is achieved by adding matter that in the dual string theory is represented by D5 branes with induced D3 brane charge. This will change the gauge group to $SU(kN_c+n_f) \times SU(kN_c+N_c+n_f+\frac{N_f}{2})$. The N_f-D5 and n_f-D3 branes are added as sources; namely the background is a solution to the equations of motion of Type IIB Supergravity plus the Born-Infeld Wess-Zumino action for the sources. The associated solutions were discussed in detail in [39], [29]. The formalism used in deriving these

backgrounds runs parallel to the one described above, in the sense that a 'change of basis' and a second order differential 'master' equation can be written for a single function $P(\rho)$ that in this case will contain the effect of the (n_f, N_f) D3-D5 sources. A rotation of the $SU(3)$-structure forms is used to generate the solutions dual to the mesonic branch of the KS field theory. It now takes the following form

$$P'' + (P' + N_f)\Big[\frac{P' + Q' + 2N_f}{P - Q} + \frac{P' - Q' + 2N_f}{P + Q} - 4\coth(2\rho)\Big] = 0\,,$$
$$Q(\rho) = \frac{2N_c - N_f}{2}(2\rho\coth(2\rho) - 1)\,. \tag{2.1.1}$$

Our background functions now are dependent on P and Q in the following way:

$$e^{2k} = \frac{P' + N_f}{2}\,, \qquad e^{2h} = \frac{1}{4}\frac{P^2 - Q^2}{P\coth(2\rho) - Q}\,, \quad e^{2g} = P\coth(2\rho) - Q\,,$$
$$a = \frac{P}{P\cosh(2\rho) - Q\sinh(2\rho)}\,, \quad e^{4\Phi - 4\Phi_0} = \frac{2\sinh(2\rho)^2}{(P^2 - Q^2)(P' + N_f)}\,. \tag{2.1.2}$$

We require new IR asymptotes reflecting the addition of N_f sources. The ones befitting our case are [39]

$$P(\rho) = h_1\rho + \frac{4N_f}{3}\left(-\rho\log\rho - \frac{1}{12}\rho\log(-\log\rho) + \mathcal{O}\left(\frac{\rho\log(-\log\rho)}{\log\rho}\right)\right) + \mathcal{O}(\rho^3\log\rho)\,. \tag{2.1.3}$$

As before, h_1 can be tuned to a value h_{1c} so that P has linear behaviour in the UV. Then the dilaton Φ will grow without bound. For all values $h_1 > h_{1c}$, P will have exponential asymptotes and Φ will have a finite value in the UV. It is for these solutions that we again can apply the rotation procedure to UV complete these new solutions.

Unfortunately, we have adopted an IR singularity caused by the high density stacking of the source branes near $\rho = 0$ [42].

As described in [43], we can avoid this singularity by distributing the sources such that not all sources reach $\rho = 0$. Of importance is the fact that the density profile for the sources has a Maclaurin series with leading term at least of order $\mathcal{O}(\rho^3)$. A profile that preserves the same SUSY as the background and avoids all singularities, can be derived to be [43],

$$\mathcal{S}(\rho) = N_f\tanh(2\rho)^4. \tag{2.1.4}$$

Note that its IR expansion is

$$\mathcal{S}(\rho) = 16\rho^4 - \frac{256}{3}\rho^6 + \frac{1536}{5}\rho^8 + \mathcal{O}[\rho^{10}] \tag{2.1.5}$$

as required. Also, this profile can be 'translated' according to

$$\mathcal{S}(\rho) = N_f\,\Theta(\rho - \rho_*)\tanh(2\rho - 2\rho_*)^4 \tag{2.1.6}$$

and still preserve SUSY and avoid singularities everywhere.

Following [43], we now have the master equation

$$\begin{aligned}
&(P'' + N_f\mathcal{S}') + (P' + N_f\mathcal{S})\Big[\frac{P' + Q' + 2N_f\mathcal{S}}{P - Q} + \frac{P' - Q' + 2N_f\mathcal{S}}{P + Q} - 4\coth(2\rho)\Big] = 0\,, \qquad (2.1.7)\\
&Q = \coth(2\rho)\Big[\int_0^\rho dx \frac{2N_c - N_f\mathcal{S}(x)}{\coth^2(2x)}\Big]\,,\\
&e^{2k} = \frac{P' + N_f\mathcal{S}}{2}\,,\\
&e^{4\Phi - 4\Phi_0} = \frac{2\sinh(2\rho)^2}{(P^2 - Q^2)(P' + N_f\mathcal{S})}\,.
\end{aligned}$$

Please note, comparing with the case without source profile, it seems that the analysis was simply generalised by replacing $N_f \to N_f\mathcal{S}(\rho)$ everywhere. This is not quite true, seen for example at the new form the equation governing Q takes. We get Figure 2.1.

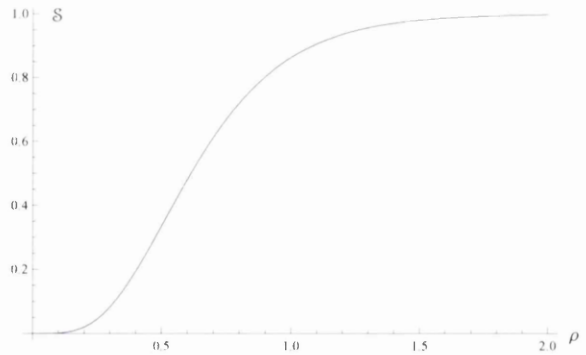

Figure 2.1: $\mathcal{S}(\rho)$

In the papers [39], [29] a solution encoding the effect of the sources was found. The large radius asymptotics for the warp factor $\hat{h}$ in eq.(2.0.19) is given in eq.(2.25) of the paper [29],

using the radial coordinate $r = e^{2\rho/3}$ we have,

$$\lim_{r\to\infty} \hat{h} \sim \frac{N_f r^2 + 3N_c^2 \log r}{r^4} \,. \tag{2.1.8}$$

This deviates (by what seems to be the addition of an irrelevant operator of dimension-six) from the cascading behaviour of the Klebanov-Strassler QFT.

The field theoretic logic is again, that the number of D3 sources, n_f, grows very fast — as was discussed in [29]

$$n_f \sim \mathcal{S}(\rho)(\sinh(4\rho) - 4\rho)^{1/3} \sim e^{4\rho/3}, \tag{2.1.9}$$

and this rapid growth of the gauge group ranks going to higher energies (due to Higgsing every time a source D3 is crossed) implies that the QFT looses the 4-d character of the KS system.

The asymptotic form of the warp factor in eq.(2.1.8), strongly indicates that the QFT is not behaving as a 4-d QFT, in the sense of 'locality' being lost. It was understood in [29] that this is due to a very rapid growth of degrees of freedom.

In backgrounds where the profile for the sources is $\mathcal{S} \sim \tanh(2\rho)^4$, this is reflected by the fact that the flow to the UV of the QFT is described by a superposition of Seiberg dualities — the logarithmic term in eq.(2.1.8) — and a Higgsing, represented by the term quadratic in the radial variable. Another interplay between Higgsing and Seiberg cascade was previously observed in [44].

We would like this mesonic branch solution of the KS field theory to behave like a 4-d QFT. In order to do this, we will slow-down the growth of degrees of freedom, by proposing a *phenomenological* profile for the sources. This is phenomenological in the sense that is not derived from first principles (as a kappa symmetric embedding of sources with this profile). Nevertheless, the profile we will propose has the following properties [29]:

- The background still satisfies BPS equations, suggesting SUSY preservation.
- The energy density of the sources T_{00} is positive definite for profiles that decay at most as fast as the one we will propose.
- The central charge of the dual QFT when calculated with this profile is a monotonic and growing function.

As argued in [29], the UV behaviour is improved by using a profile that decays like $e^{\frac{-4\rho}{3}}$. This is due to the fact that to preserve the KS like UV asymptotic behaviour, we need a profile that decays at least that fast. The presence of an exponentially increasing number of source

branes, as is the case for a profile where $S \to 1$, behaves like the insertion of an irrelevant operator that deforms the UV dynamics. We also would not want a profile that decays faster to keep $T^{\text{sources}}_{x_0 x_0}$, representing the mass density of the sources, positive everywhere. To have $T^{\text{sources}}_{x_0 x_0} \to 0$ exactly, a profile that decays like $(\sinh(4\rho) - 4\rho)^{-1/3}$ is needed. Thus the following two profiles will be of importance. See [43, 45] for more details.

$$\mathcal{S}(\rho) = \tanh^4(2\rho) e^{\frac{-4\rho}{3}}\,, \tag{2.1.10}$$

$$\hat{\mathcal{S}}(\rho) = \frac{\tanh^4(2\rho)}{(\sinh(4\rho) - 4\rho)^{1/3}}\,, \tag{2.1.11}$$

which look like

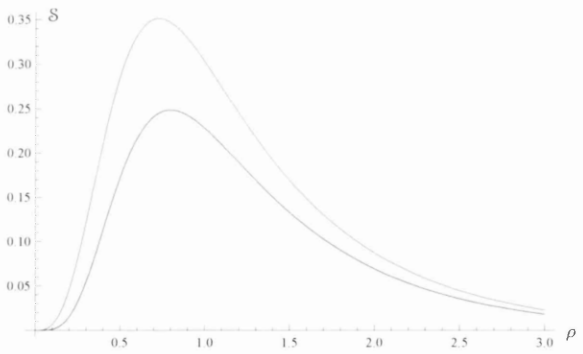

Figure 2.2: $\mathcal{S}(\rho)$ is blue while $\hat{\mathcal{S}}(\rho)$ is red

Note that $\hat{\mathcal{S}}(0) = \frac{0}{0}$. While this can be quite easily analytically continued to be $\hat{\mathcal{S}}(0) = 0$, numerical calculations using this profile have to be dealt with carefully. The approach in this thesis is based on the following idea. As the IR expansion of this profile is

$$\hat{\mathcal{S}}(\rho) = 6^{\frac{1}{3}}(4\rho^3 - \frac{112}{5}\rho^5 + \mathcal{O}[\rho^7])\,, \tag{2.1.12}$$

we define $\hat{\mathcal{S}}(\rho) = a\rho^3 + b\rho^5$ for $0 < \rho < \epsilon$. We then solve for a and b by demanding that $\hat{\mathcal{S}}(\rho)$ and $\hat{\mathcal{S}}'(\rho)$ are continuous at ϵ.

Chapter 3

Entanglement of the Photon

Before we move to the study of confinement using entanglement entropy and the Gauge/Gravity Correspondence, we would like to present some findings using EE in QFT directly. Most often, the study of entanglement entropy in the literature is done through a regional split of degrees of freedom. As aforementioned, we are free to choose different splits, and this has led to some interesting results. See, for example [13] for a study of a split in momentum space. In the following, we will try an even different approach. We will split in field degrees of freedom. This will allow us to study the EE associated between different types of interacting fields. We will see this exists even in the vacuum as well when we only have a state with a single particle. We will start with a derivation of the setup. We then apply it to a toy model scalar field theory with two fields of differing masses. Finally we move on to calculate the entanglement entropy of a single photon state in Quantum Electrodynamics (QED).

3.1 Derivation of main formula

Consider a system $\mathcal{H}_A \times \mathcal{H}_B$ with a Hamiltonian $H = H_A + H_B + \lambda H_I$. The unperturbed eigenstates are $|\psi_{ia}\rangle = |\phi_i\rangle \otimes |\chi_a\rangle$. We assume the eigenstates to have a non-degenerate spectrum. The usual first order shift in the state vector is

$$|\psi'_{ia}\rangle = |\psi_{ia}\rangle + \lambda \sum_{jb} |\psi_{jb}\rangle \frac{\langle \psi_{jb}| H_I |\psi_{ia}\rangle}{E_{ia} - E_{jb}} , \tag{3.1.1}$$

where we have assumed that

$$\langle \psi_{ia}| H_I |\psi_{jb}\rangle = 0 \quad \text{if} \quad i = j \quad \text{or} \quad a = b. \tag{3.1.2}$$

This means that the first order shift term does not include states $|\phi_i\rangle$ of A or $|\chi_a\rangle$ of B.

The reduced density matrix of A to order λ^2 is then

$$\rho = \mathrm{Tr}_B\, |\psi'_{ia}\rangle\, \langle\psi'_{ia}| = \big(1 - \lambda^2 \sum_j A_{jj}\big)\, |\phi_i\rangle\, \langle\phi_i| + \lambda^2 \sum_{jk} |\phi_j\rangle\, A_{jk}\, \langle\phi_k| \ , \tag{3.1.3}$$

where

$$A_{jk} = \sum_b \frac{\langle\psi_{jb}|\, H_I\, |\psi_{ia}\rangle}{E_{ia} - E_{jb}} \frac{\langle\psi_{ia}|\, H_I\, |\psi_{kb}\rangle}{E_{ia} - E_{kb}} \, . \tag{3.1.4}$$

Note that the sum in (3.1.3) excludes terms with $j = i$ or $k = i$ because of (3.1.2).

If ξ_j are the eigenvalues of A_{jk}, then the entanglement entropy to order λ^2 is

$$\begin{aligned} S = -\,\mathrm{Tr}\,(\rho \log \rho) &= -\big(1 - \lambda^2 \sum_j \xi_j\big) \log\big(1 - \lambda^2 \sum_j \xi_j\big) - \sum_j \lambda^2 \xi_j \log\big(\lambda^2 \xi_j\big) \\ &= -\lambda^2 \log\big(\lambda^2\big) \sum_j \xi_j + \lambda^2 \sum_j \xi_j \big(1 - \log(\xi_j)\big) + \mathcal{O}(\lambda^4) \\ &= -\lambda^2 \sum_j \log\big(\lambda^2 e^{-1} \xi_j\big) \xi_j + \mathcal{O}(\lambda^4) \, . \end{aligned}$$

The leading order contribution is at order $\lambda^2 \log(\lambda^2)$,

$$S = -\lambda^2 \log\big(\lambda^2\big)\, \mathrm{Tr}\, A + \mathcal{O}(\lambda^2) \, . \tag{3.1.5}$$

3.2 The Entanglement of the Scalar Photon A

In this section we will discuss a QFT with two scalars, A of mass m, and Φ of mass M. We will set $m < M$. The scalar fields interact with each other via the interaction Hamiltonian $H_{int} = \int \Phi^2 A$. We will refer to the light scalar A as the photon and to the heavy scalar Φ as the electron in this section when needed. We will first be discussing the 1-particle state with only one photon, then discuss the vacuum, and finally have a look at the 1-electron state.

Let us denote the states as $|\boldsymbol{k}_1, \ldots, \boldsymbol{k}_n; \boldsymbol{p}_1, \ldots, \boldsymbol{p}_m\rangle = |\boldsymbol{k}_1, \ldots, \boldsymbol{k}_n\rangle \otimes |\boldsymbol{p}_1, \ldots, \boldsymbol{p}_m\rangle$, where n and m are the particle numbers of the photon/electron respectively. The initial state is the 1-particle A state $|\boldsymbol{k}; \mathrm{vac}\rangle$ and the non-trivial matrix elements of the interaction are

$$\langle \mathrm{vac}; \boldsymbol{p}_1, \boldsymbol{p}_2|\, H_I\, |\boldsymbol{k}; \mathrm{vac}\rangle \qquad \text{and} \qquad \langle \boldsymbol{k}, \boldsymbol{k}'; \boldsymbol{p}_1, \boldsymbol{p}_2|\, H_I\, |\boldsymbol{k}; \mathrm{vac}\rangle \ . \tag{3.2.1}$$

In the latter case,

$$\langle \boldsymbol{k}, \boldsymbol{k}'; \boldsymbol{p}_1, \boldsymbol{p}_2|\, H_I\, |\boldsymbol{k}; \mathrm{vac}\rangle = \langle \boldsymbol{k}'; \boldsymbol{p}_1, \boldsymbol{p}_2|\, H_I\, |\mathrm{vac}; \mathrm{vac}\rangle \ , \tag{3.2.2}$$

so is independent of the original 1-particle state. We will see this is the vacuum contribution to the EE.

So in this case,

$$\mathrm{Tr}\, A = \sum_{\boldsymbol{p}_1,\boldsymbol{p}_2} \left| \frac{\langle \mathrm{vac}; \boldsymbol{p}_1, \boldsymbol{p}_2 | \, H_I \, | \boldsymbol{k}; \mathrm{vac} \rangle}{\omega_m(\boldsymbol{k}) - \omega_M(\boldsymbol{p}_1) - \omega_M(\boldsymbol{p}_2)} \right|^2 + \sum_{\boldsymbol{k}';\boldsymbol{p}_1,\boldsymbol{p}_2} \left| \frac{\langle \boldsymbol{k}'; \boldsymbol{p}_1, \boldsymbol{p}_2 | \, H_I \, | \mathrm{vac}; \mathrm{vac} \rangle}{\omega_m(\boldsymbol{k}') + \omega_M(\boldsymbol{p}_1) + \omega_M(\boldsymbol{p}_2)} \right|^2 . \quad (3.2.3)$$

$\omega_m(\boldsymbol{p}) = \sqrt{\boldsymbol{p}^2 + m^2}$. It is clear that the second contribution is just the contribution of the vacuum to the entanglement entropy and so we can define

$$S_{\text{1-particle}} = S - S_{\text{vac}} = -\lambda^2 \log(\lambda^2) \sum_{\boldsymbol{p}_1,\boldsymbol{p}_2} \left| \frac{\langle \mathrm{vac}; \boldsymbol{p}_1, \boldsymbol{p}_2 | \, H_I \, | k; \mathrm{vac} \rangle}{\omega_m(\boldsymbol{k}) - \omega_M(\boldsymbol{p}_1) - \omega_M(\boldsymbol{p}_2)} \right|^2 , \quad (3.2.4)$$

as well as

$$S_{\text{vac}} = \sum_{\boldsymbol{k}';\boldsymbol{p}_1,\boldsymbol{p}_2} \left| \frac{\langle \boldsymbol{k}'; \boldsymbol{p}_1, \boldsymbol{p}_2 | \, H_I \, | \mathrm{vac}; \mathrm{vac} \rangle}{\omega_m(\boldsymbol{k}') + \omega_M(\boldsymbol{p}_1) + \omega_M(\boldsymbol{p}_2)} \right|^2 . \quad (3.2.5)$$

We will now study the contributions separately as they both have information of different physics.

3.2.1 $S_{\text{1-particle}}$

The contribution we want comes from A coupling to the 2-ϕ state. The A spatial momentum is fixed, and we may as well work in the rest frame $\boldsymbol{k} = 0$. To continue, we will now work towards calculating matrix element $\langle \mathrm{vac}; \boldsymbol{p}_1, \boldsymbol{p}_2 | \, H_I \, | \boldsymbol{k}; \mathrm{vac} \rangle$. We will first define the theory to be defined inside a cube of size L with periodic boundary conditions. After calculating the matrix element, we take $L \to \infty$ to derive our final formula for the entanglement entropy. However, we must be careful with factors of L to make sure that the entanglement entropy will be intensive as we would expect. The canonical quantization approach to QFT lets us expand the fields as

$$\begin{aligned} \Phi(x) &= \frac{1}{L^{\frac{d}{2}}} \sum_p \frac{1}{\sqrt{2\omega_p}} (a_p e^{-ip\cdot x} + a_p^\dagger e^{ip\cdot x}) , \\ A(x) &= \frac{1}{L^{\frac{d}{2}}} \sum_k \frac{1}{\sqrt{2\omega_k}} (b_k e^{-ik\cdot x} + b_k^\dagger e^{ik\cdot x}) . \end{aligned} \quad (3.2.6)$$

From that we can calculate the matrix element to be

$$\langle \mathrm{vac}; \boldsymbol{p}_1, \boldsymbol{p}_2 | \, H_I \, | \boldsymbol{k}; \mathrm{vac} \rangle = \frac{1}{2^{3/2} L^{d/2}} \frac{\delta_{\boldsymbol{p}_1 + \boldsymbol{p}_2 - \boldsymbol{k}}}{\sqrt{\omega_M(\boldsymbol{p}_1)\omega_M(\boldsymbol{p}_2)\omega_m(\boldsymbol{k})}} . \quad (3.2.7)$$

When we put A on-shell in the rest frame $\boldsymbol{k} = 0$ then we have $\omega_m(0) = m$.

The delta function enforces spatial momentum conservation, and we will write $\boldsymbol{p}_1 \equiv \boldsymbol{p} + \frac{1}{2}\boldsymbol{k}$ and $\boldsymbol{p}_2 = -\boldsymbol{p} + \frac{1}{2}\boldsymbol{k}$. So we only have to sum (integrate) over $\boldsymbol{p}$.

We then take $L \to \infty$ and make the replacements.

$$\sum_{\vec{p}} \to \left(\frac{L}{2\pi}\right)^d \int d^d p\,. \qquad\qquad \delta_{\vec{p}} \to \left(\frac{2\pi}{L}\right)^d \delta^d(p). \tag{3.2.8}$$

There are factors L^d for each integral p_1 and p_2 and L^{-d} from the delta function. Finally $(L^{-d/2})^2$ from the square of the matrix element. So the factors of L cancel.

The entanglement entropy of the particle in its rest frame is therefore intensive rather than extensive as we require of a single particle:

$$\begin{aligned} S_{\text{1-particle}} &= -\frac{\lambda^2 \log(\lambda^2)}{(2\pi)^d 2^3 m} \int d^d\boldsymbol{p}_1\, d^d\boldsymbol{p}_2 \frac{\delta(\boldsymbol{p}_1 + \boldsymbol{p}_2)}{\omega_M(\boldsymbol{p}_1)\omega_M(\boldsymbol{p}_2)\left(\omega_M(\boldsymbol{p}_1) + \omega_M(\boldsymbol{p}_2) - m\right)^2} \\ &= -\frac{\lambda^2 \log(\lambda^2)}{(2\pi)^d 2^3 m} \int d^d\boldsymbol{p}\, \frac{1}{\left(\boldsymbol{p}^2 + M^2\right)\left(2\sqrt{\boldsymbol{p}^2 + M^2} - m\right)^2}\,, \end{aligned}$$

where the m comes from $(1/\sqrt{\omega_m(0)})^2$ in the matrix element. The dimensions work out because the coupling λ has dimensions $L^{d/2-5/2}$ so S is dimensionless.

The above equals

$$S_{\text{1-particle}} = -\frac{\lambda^2 \log(\lambda^2)}{(2\pi)^d 2^5 m} \text{Vol}(S^{d-1}) M^{d-4} Q(m/2M)\,, \tag{3.2.9}$$

where

$$Q(x) = \int_0^\infty \frac{p^{d-1} dp}{(p^2+1)(\sqrt{p^2+1} - x)^2}\,. \tag{3.2.10}$$

It is clear that the entropy is UV safe for $d < 4$, i.e. $D = d + 1 < 5$.

One way to proceed is to use the substitution $p = \sinh\theta$,

$$Q(x) = \int_0^\infty \mathrm{d}\theta\, \frac{\sinh^{d-1}(\theta)}{\cosh(\theta)(\cosh(\theta) - x)^2}. \tag{3.2.11}$$

We then get the solutions

$D = 2$ (i.e. $d = 1$)

$$Q(x) = -\frac{\left(\pi\left(x^2-1\right) - 2x\right)\sqrt{1-x^2} + \left(4 - 8x^2\right)\tan^{-1}\left(\frac{x}{\sqrt{1-x^2}}\right) + \left(4 - 8x^2\right)\tan^{-1}\left(\sqrt{\frac{2}{x+1} - 1}\right)}{2x^2\left(1 - x^2\right)^{3/2}}, \tag{3.2.12}$$

$D = 3$ (i.e. $d = 2$)

$$Q(x) = \frac{\log(1-x) - \frac{x}{x-1}}{x^2}, \tag{3.2.13}$$

$D = 4$ (i.e. $d = 3$)

$$Q(x) = \frac{(2x+\pi)\left(-\sqrt{1-x^2}\right) + 4\tan^{-1}\left(\frac{x}{\sqrt{1-x^2}}\right) + 4\tan^{-1}\left(\sqrt{\frac{2}{x+1}-1}\right)}{2x^2\sqrt{1-x^2}}. \tag{3.2.14}$$

It is interesting that as $x \to 1$ the entanglement entropy diverges, see Figure 3.1. This corresponds to $m \to 2M$ which is the point at which A becomes unstable to decay to $\phi\phi$,

$$D = 4: \quad Q(x) \longrightarrow \frac{\pi}{\sqrt{2}\sqrt{1-x}}, \tag{3.2.15}$$

$$D = 3: \quad Q(x) \longrightarrow \frac{1}{1-x}, \tag{3.2.16}$$

$$D = 2: \quad Q(x) \longrightarrow \frac{\pi}{2\sqrt{2}(x-1)^{3/2}}. \tag{3.2.17}$$

Another curious fact is that for $D = 2$ and $D = 4$ we have $\lim_{x\to 0} Q(x) = \frac{\pi}{4}$, while for $D = 3$ we have $\lim_{x\to 0} Q(x) = \frac{1}{2}$.

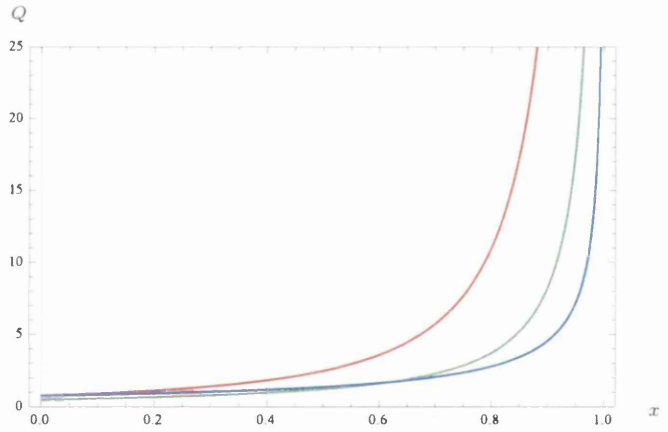

Figure 3.1: $Q(x)$ for the scalar QFT in various space dimensions. Red represents $d = 1$, green $d = 2$ and blue $d = 3$.

3.2.2 S_{vac}

Now let us focus on the vacuum contribution to the EE. In a very similar fashion we can calculate that we have

$$\frac{S_{vac}(a)}{L^d} = -\lambda\log(\lambda)M^{2(d-1)}\frac{(2\pi)^{d(\frac{3}{2}-n)}}{2^{n-1}\Gamma(\frac{d}{2})}\int \mathrm{d}r\mathrm{d}\rho\frac{r^{d-1}\rho^{d-1}}{\omega_r\omega_\rho\omega_{r+\rho}(\omega_r+\omega_\rho+\omega_{r+\rho})^2}. \tag{3.2.18}$$

We will use the rapidity substitution $r = M\sinh(\theta_1)$ and $\rho = M\sinh(\theta_2)$. We will refer to the integrand as $s(\tau_1, \tau_2, a)$.

In $d = 1$ we will have to solve

$$Q(a) = \frac{1}{M^4}\int_{-\infty}^{\infty} \mathrm{d}\theta_1 \mathrm{d}\theta_2 s(\theta_1, \theta_2, a) \ , \tag{3.2.19}$$

where

$$s(\theta_1, \theta_2, a) = \frac{1}{\sqrt{(\sinh\theta_1 + \sinh\theta_2)^2 + a^2}(\cosh\theta_1 + \cosh\theta_2 + \sqrt{(\sinh\theta_1 + \sinh\theta_2)^2 + a^2})^2} \ , \tag{3.2.20}$$

and $a = \frac{m}{M}$. Mathematica cannot integrate (3.2.19) symbolically, unfortunately. So we have to do it numerically. We found that an integration limit at 10^3 was most suitable. The results can be seen in Figure 3.2.

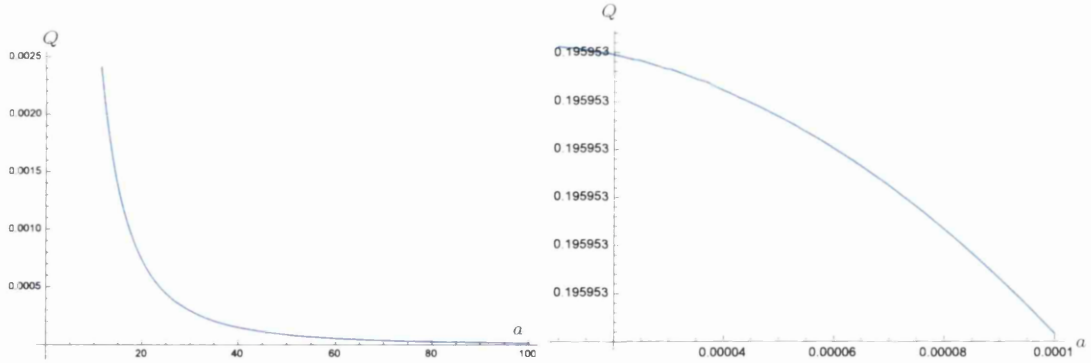

Figure 3.2: The integral as a function of the mass ratio a (left panel) and the same function plotted very close to the origin (right panel).

Indeed, on first sight it seems as if $\lim_{a\to 0} S_A = \infty$ and $\lim_{a\to\infty} S_A = 0$, but a closer look at our results begs more scrutiny. As we see on the right panel, when we look at S_A very close to the origin, we see that S_A changes it's apparent behaviour and that S_A instead converges to a finite value as $a \to 0$. Let us show this analytically.

We find a Taylor expansion around the point $(\theta_1, \theta_2, a) = (x_1, x_2, 0 \vee \infty)$ of the form

$$s(\theta_1, \theta_2, a) = \sum_{i=0}^{\infty} f_i(\theta_1, \theta_2) a^i \ , \tag{3.2.21}$$

where

$$f_i(\theta_1, \theta_2) = \sum_{i=0}^{\infty} \tilde{f}_i(\theta_1)\theta_2^i \,, \tag{3.2.22}$$

and similarly

$$\tilde{f}_i(\theta_1) = \sum_{i=0}^{\infty} c_i \theta_1^i \,, \tag{3.2.23}$$

where c_i are constants.

We can then assume that

$$S_A(a) = \sum_{i=0}^{\infty} F_i a^i \,, \tag{3.2.24}$$

where

$$F_i = \int_{-\infty}^{\infty} f_i(\theta_1, \theta_2) \mathrm{d}\theta_1 \mathrm{d}\theta_2 \,. \tag{3.2.25}$$

As the radius of convergence should be ∞ this approach is justified. Computationally we of course have the limitation that that we cannot compute infinite terms, thus we should not integrate to ∞ but only up to some N where the truncated series approximation starts to deviate from the actual integral. To still make sure that we get fairly accurate results, the integral must be carried by a finite region. However, this is also required if we want the improper integral to be finite, so we should not expect to have any problems here. We then have to find the centre of this region in order to determine the optimal value for x_i.

So, let us plot $s(\theta_1, \theta_2, a)$:

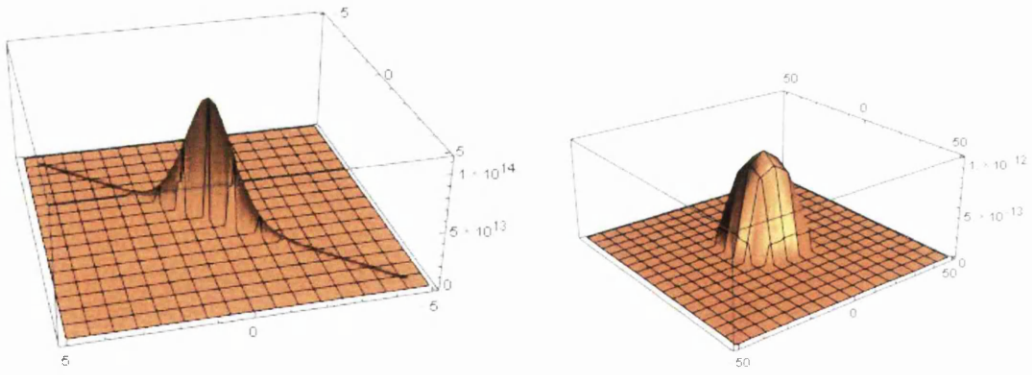

Figure 3.3: $s(\theta_1, \theta_2, a)$ plotted over the (θ_1, θ_2) plane. We have chosen $a = 0$ (left panel) and $a = 10^4$ (right panel).

As we can see, for both small and large a, the integrand fits our criteria. We can also see that the best choice to expand around is given by $(x_1, x_2) = (0, 0)$ for both expansions. Following the procedure outlined above and setting $M = 1$, we can come to the conclusion that for small

a we have:

$$S_A = F_0 + F_2 a^2 + \mathcal{O}(a^4)\,, \tag{3.2.26}$$

where F_2 is negative. Hence for small a, S_A should approach a constant quadratically from below, in accordance with our numerical integration.

In the limit $a \to \infty$ we get the expansion

$$S_A = a^{-3} + \mathcal{O}(a^{-4})\,. \tag{3.2.27}$$

Note that $F_3 = 1$ exactly. This confirms our suspicion that $S_A \to 0$ and additionally shows us how rapidly this happens.

Now for $d > 1$ we have

$$Q(a) = M^{2d-6} \int_0^\infty \mathrm{d}\theta_1 \mathrm{d}\theta_2 s(\theta_1, \theta_2, a)\ , \tag{3.2.28}$$

where

$$s(\theta_1, \theta_2, a) = \frac{\sinh^{d-1}\theta_1 \sinh^{d-1}\theta_2}{\sqrt{(\sinh\theta_1 + \sinh\theta_2)^2 + a^2}(\cosh\theta_1 + \cosh\theta_2 + \sqrt{(\sinh\theta_1 + \sinh\theta_2)^2 + a^2})^2}\,. \tag{3.2.29}$$

We can analyse the behaviour of s as we take $\theta_1, \theta_2 \to \infty$. The symmetries of the function guarantee us that we can take $\theta_2 = n\theta_1$, where $0 \leq n \leq 1$*. Thus, ignoring factors we can deduce

$$s \propto e^{\theta_1((d-1)(n+1)-3)} \tag{3.2.30}$$

for large θ_1.

So we now that the integral will converge whenever

$$d < \frac{5}{2}\,. \tag{3.2.31}$$

Thus it does not make much sense to go beyond $d = 2$. Numerically, not much changes in $d = 2$ compared to $d = 1$.

*Note that if $n > 1$ we can instead take $\theta_1 = \frac{1}{n}\theta_2$ as the function is invariant under $\theta 1 \leftrightarrow \theta_2$

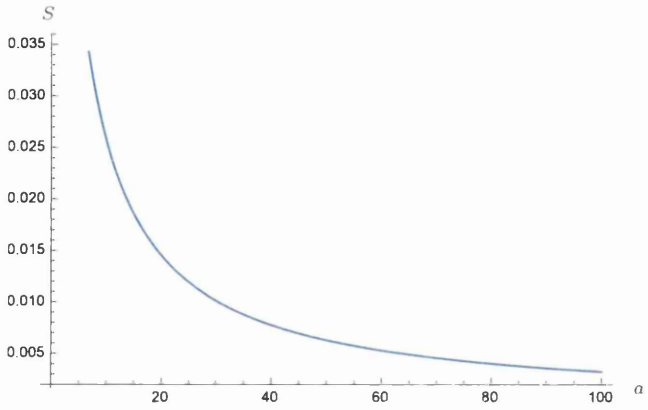

Figure 3.4: $S(a)$ for the vacuum

The asymptotes for the vacuum also have the same form for $d = 2$ as for $d = 1$. The only slight difference is that $F_3 \neq 1$ any more for the $a \to \infty$ expansion of the entanglement entropy.

3.2.3 The Heavy Particle

We can also calculate the entanglement entropy for the heavy particle. Since the vacuum term is equivalent to last section, we just have to look at the 1-particle to two particle term. In this case, the two particle state has one heavy and one light particle: $\omega_M(0) = M$, $\omega_M(\boldsymbol{p}) = \sqrt{\boldsymbol{p}^2 + M^2}$ and $\omega_m(\boldsymbol{p}) = \sqrt{\boldsymbol{p}^2 + m^2}$. We find that

$$S = \frac{M^{d-4}\pi^{\frac{d}{2}}}{\Gamma(\frac{d}{2}+1)} Q(x), \tag{3.2.32}$$

where

$$Q(x) = \int \mathrm{d}p \frac{p^{d-1}}{\sqrt{\boldsymbol{p}^2+1}\sqrt{\boldsymbol{p}^2+x^2}(\sqrt{\boldsymbol{p}^2+1}+\sqrt{\boldsymbol{p}^2+x^2}-1)^2}, \tag{3.2.33}$$

and $x = \frac{m}{M}$.

In $d = 2$, this equation can be solved very simply analytically. We get

$$Q = \frac{1}{x} + \log\left(\frac{x}{x+1}\right). \tag{3.2.34}$$

We can see that $\lim_{x\to 0} Q(x) = \frac{1}{x}$ and $\lim_{x\to\infty} Q(x) = \frac{1}{2x^2}$. In other dimensions, the integral can in principle be solved analytically in terms of elliptical integrals. However, firstly, we have to do it separately in 4 pieces. One for each of the regions $(0,1), (1,1.5), (1.5,2), (2,\infty)$. These pieces can smoothly pieced together to give our function. Though the formula for each piece is

horrendous. For example, in $d = 1$ we get for $Q(x)$ in the region $(0, 1)$

$$Q(x) = \frac{x^2-2}{x^2\left(x^2-4\right)} + \frac{2\tanh^{-1}\left(\frac{x^2-2}{x\sqrt{x^2-4}}\right)}{x\left(x^2-4\right)^{3/2}} + \frac{2i\sqrt{x-1}x\sqrt{x^2-4}\left(x^2-2\right)E\left(\frac{1}{x^2}\right)}{\sqrt{x-1}x^2\left(x^2-4\right)^{3/2}\left(x^2-2\right)} + \frac{\pi\sqrt{\frac{1}{4-x^2}}}{x\left(x^2-4\right)}$$
$$+ \frac{-2\left(-2\sqrt{\frac{1}{x^2}-1}\sqrt{x-1}\sqrt{\frac{1}{1-x^2}}\sqrt{x^2-4}K\left(1-x^2\right)\left(x^2\right)^{3/2}\right) + 4x^2K\left(1-x^2\right)\sqrt{x-1}\sqrt{x^2-4}}{\sqrt{x-1}x^2\left(x^2-4\right)^{3/2}\left(x^2-2\right)}$$
$$+ \frac{-2\left(-\sqrt{x-1}\sqrt{x^2-4}\left(x^2-2\right)\left(\sqrt{\frac{1}{x^2}-1}\sqrt{-\frac{x^2}{x^2-1}}-1\right)E\left(1-x^2\right)\right)}{\sqrt{x-1}x^2\left(x^2-4\right)^{3/2}\left(x^2-2\right)} + \frac{1}{4-x^2} - \frac{2\tanh^{-1}\left(\frac{x}{\sqrt{x^2-4}}\right)}{x\left(x^2-4\right)^{3/2}}$$
$$+ \frac{-2\left(-i\sqrt{\frac{1}{1-x}}x^4\sqrt{x^2-4}F\left(\frac{1}{2}\left(\pi-2\cos^{-1}\left(\sqrt{\frac{x-1}{x+1}}\right)\right)|\frac{(x+1)^2}{(x-1)^2}\right) - x^4K\left(1-x^2\right)\sqrt{-\frac{x^3-x^2}{(x^2-1)^2}}\sqrt{x^2-4}\right)}{\sqrt{x-1}x^2\left(x^2-4\right)^{3/2}\left(x^2-2\right)}$$
$$+ \frac{-2\left(-3i\sqrt{x-1}x^2\sqrt{x^2-4}K\left(x^2\right) - \sqrt{x-1}x^4\sqrt{x^2-4}K\left(1-x^2\right) - 2\sqrt{x-1}x\sqrt{x^2-4}K\left(1-\frac{1}{x^2}\right)\right)}{\sqrt{x-1}x^2\left(x^2-4\right)^{3/2}\left(x^2-2\right)}$$
$$+ 4\frac{\sqrt{\frac{1}{1-x}}x^3\Pi\left(\frac{(x+1)\left(-2i+x\sqrt{x^2-4}\right)}{(x-1)\left(2i+x\sqrt{x^2-4}\right)};\frac{1}{2}\left(\pi-2\cos^{-1}\left(\sqrt{\frac{x-1}{x+1}}\right)\right)|\frac{(x+1)^2}{(x-1)^2}\right)}{\sqrt{x-1}x^2\left(x^2-4\right)^{3/2}\left(x^2-2\right)}$$
$$- 4\frac{x^3\Pi\left(\frac{(x+1)\left(2i+x\sqrt{x^2-4}\right)}{(x-1)\left(-2i+x\sqrt{x^2-4}\right)};\frac{1}{2}\left(\pi-2\cos^{-1}\left(\sqrt{\frac{x-1}{x+1}}\right)\right)|\frac{(x+1)^2}{(x-1)^2}\right)\sqrt{\frac{1}{1-x}}}{\sqrt{x-1}x^2\left(x^2-4\right)^{3/2}\left(x^2-2\right)}$$
$$+ \frac{+i\left(x^2-2\right)E\left(x^2\right)\sqrt{x-1}\sqrt{x^2-4} + ix^4K\left(x^2\right)\sqrt{x-1}\sqrt{x^2-4} + 2iK\left(x^2\right)\sqrt{x-1}\sqrt{x^2-4}}{\sqrt{x-1}x^2\left(x^2-4\right)^{3/2}\left(x^2-2\right)}$$
$$+ \frac{x^4K\left(1-x^2\right)\sqrt{x-1}\sqrt{x^2-4}\sqrt{-\frac{x^2}{x^2-1}}\sqrt{\frac{1}{x^2}-1} + 2i\left(x^2-2\right)E\left(x^2\right)\sqrt{x-1}\sqrt{x^2-4}}{\sqrt{x-1}x^2\left(x^2-4\right)^{3/2}\left(x^2-2\right)}$$
$$+ 2\frac{x^2K\left(1-x^2\right)\sqrt{x-1}\sqrt{x^2-4} + x^3K\left(1-\frac{1}{x^2}\right)\sqrt{x-1}\sqrt{x^2-4} + ix^4K\left(x^2\right)\sqrt{x-1}\sqrt{x^2-4}}{\sqrt{x-1}x^2\left(x^2-4\right)^{3/2}\left(x^2-2\right)}$$
$$- 2\frac{-3i\sqrt{x-1}x^2\sqrt{x^2-4}K\left(x^2\right) - \sqrt{x-1}x^4\sqrt{x^2-4}K\left(1-x^2\right) - 2\sqrt{x-1}x\sqrt{x^2-4}K\left(1-\frac{1}{x^2}\right)}{\sqrt{x-1}x^2\left(x^2-4\right)^{3/2}\left(x^2-2\right)}$$
$$- 2\frac{\sqrt{\frac{1}{1-x}}x^3\Pi\left(\frac{(x+1)\left(-2i+x\sqrt{x^2-4}\right)}{(x-1)\left(2i+x\sqrt{x^2-4}\right)};\frac{1}{2}\left(\pi-2\cos^{-1}\left(\sqrt{\frac{x-1}{x+1}}\right)\right)|\frac{(x+1)^2}{(x-1)^2}\right) + 2iK\left(x^2\right)\sqrt{x-1}\sqrt{x^2-4}}{\sqrt{x-1}x^2\left(x^2-4\right)^{3/2}\left(x^2-2\right)}$$
$$+ 2\frac{x^3\Pi\left(\frac{(x+1)\left(2i+x\sqrt{x^2-4}\right)}{(x-1)\left(-2i+x\sqrt{x^2-4}\right)};\frac{1}{2}\left(\pi-2\cos^{-1}\left(\sqrt{\frac{x-1}{x+1}}\right)\right)|\frac{(x+1)^2}{(x-1)^2}\right)\sqrt{\frac{1}{1-x}} + x^3K\left(1-\frac{1}{x^2}\right)\sqrt{x-1}\sqrt{x^2-4}}{\sqrt{x-1}x^2\left(x^2-4\right)^{3/2}\left(x^2-2\right)}$$
$$+ \frac{2\sqrt{\frac{1}{x+1}-1}\left(-2\Pi\left(\frac{(x+1)\left(2i+x\sqrt{x^2-4}\right)}{(x-1)\left(-2i+x\sqrt{x^2-4}\right)};\sin^{-1}\left(\sqrt{\frac{2}{x+1}-1}\right)|\frac{(x+1)^2}{(x-1)^2}\right)\right)}{\sqrt{1-\frac{4}{x^2}}(x-2)(x-1)\sqrt{\frac{x}{x+1}}(x+2)\left(x^2-2\right)}$$

$$+\frac{+2\Pi\left(\frac{(x+1)\left(-2i+x\sqrt{x^2-4}\right)}{(x-1)\left(2i+x\sqrt{x^2-4}\right)};\sin^{-1}\left(\sqrt{\frac{2}{x+1}-1}\right)|\frac{(x+1)^2}{(x-1)^2}\right)+ixF\left(\sin^{-1}\left(\sqrt{\frac{2}{x+1}-1}\right)|\frac{(x+1)^2}{(x-1)^2}\right)\sqrt{x^2-4}}{\sqrt{1-\frac{4}{x^2}}(x-2)(x-1)\sqrt{\frac{x}{x+1}}(x+2)\left(x^2-2\right)}.$$

Where $K(z)$ is the complete elliptic integral of the first kind, with $K(z) = F(\frac{\pi}{2}|z)$ and

$$F(z|m) = \int_0^z \frac{\mathrm{d}t}{\sqrt{1-m\sin^2(t)}}. \tag{3.2.35}$$

$E(z)$ is the complete elliptic integral of the second kind, defined by $E(z) = E(\frac{\pi}{2}|z)$, and

$$E(z|m) = \int_0^z \mathrm{d}t\sqrt{1-m\sin^2(t)}. \tag{3.2.36}$$

$\Pi(n;z|m)$ is the incomplete elliptic integral of the third kind, defined by

$$\Pi(n;z|m) = \int_0^z \frac{\mathrm{d}t}{(1-n\sin^2(t))\sqrt{1-m\sin^2(t)}}. \tag{3.2.37}$$

Please note that while it might seem that this function is complex, all the imaginary parts cancel exactly to give us a real answer in the end.

Despite the increase in complexity, the general behaviour remains the same. We have a divergence as $x \to 0$ and then the function monotonically decreases to 0. Again the divergence occurs when $m = 0$ and thus the emission of A becomes unstable.

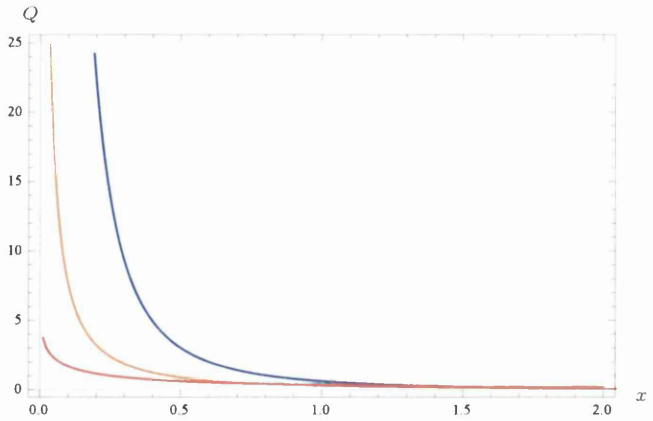

Figure 3.5: $Q(x)$ for the Heavy Particle. Blue represents $d = 1$, orange $d = 2$ and red $d = 3$.

3.3 The Entanglement of the QED Photon

In the last section we have developed tools that we can extend to phenomenologically more relevant theories. Thus let us calculate the Entanglement of the Photon with the Electron field in Quantum Electrodynamics.

3.3.1 $S_{\text{1-particle}}$

Here, we need to calculate the matrix element

$$\langle \text{vac}; \boldsymbol{p}_1, \boldsymbol{p}_2 | \, H_I \, | \boldsymbol{k}; \text{vac} \rangle = \langle e^-(\boldsymbol{p}_1) e^+(\boldsymbol{p}_2) | \, H_{\text{int}} \, | \gamma(\vec{k}) \rangle \, . \tag{3.3.1}$$

In this case there's no rest frame so this is a complication because we have to deal with the photon's momentum.

Most of the calculation nevertheless generalises trivially to this case. We get, however, an extra ingredient from the spinor factors

$$\sum_{\text{spins}} \left| \bar{v}(p') \gamma^i u(p) \right|^2 , \tag{3.3.2}$$

where $p = (\omega_1, \boldsymbol{p} + \frac{1}{2}\boldsymbol{k})$ and $p' = (\omega_2, \boldsymbol{p} - \frac{1}{2}\boldsymbol{k})$ and the photon's polarization is along the direction i. The e^- and e^+ are on-shell,

$$\omega_{1,2}^2 = (\boldsymbol{p} \pm \tfrac{1}{2}\boldsymbol{k})^2 + m^2 \, . \tag{3.3.3}$$

According to the usual rules, the above equals

$$\text{Tr}\left((\not{p}' - m) \gamma^i (\not{p} + m) \gamma^i \right) = 4\left(2 p'^i p^i + p \cdot p' - m^2 \right) . \tag{3.3.4}$$

If the photon is travelling along the z-axis, $\boldsymbol{k} = (0, 0, \omega)$ and the polarization is along the x direction, the factor is equal to

$$4\omega_1\omega_2 + 4p_1^2 - 4p_2^2 - 4p_3^2 + \omega^2 - 4m^2 = -2(\omega_1 - \omega_2)^2 + 8p_1^2 + 2\omega^2 \, . \tag{3.3.5}$$

The relevant integral is

$$Q(\omega) = \int \mathrm{d}^3\boldsymbol{p} \, \frac{4p_1^2 + \omega^2 - (\omega_1 - \omega_2)^2}{\omega_1\omega_2(\omega_1 + \omega_2 - \omega)^2} \, . \tag{3.3.6}$$

In order to deal with this integral we do the following. Firstly, let us define $\boldsymbol{\rho} = \boldsymbol{p} + \frac{1}{2}\boldsymbol{k}$. We then change to spherical coordinates $\mathrm{d}\boldsymbol{\rho}_1\mathrm{d}\boldsymbol{\rho}_2\mathrm{d}\boldsymbol{\rho}_3 \to \mathrm{d}\rho\mathrm{d}\theta\mathrm{d}\phi$ so that we have

$$\begin{aligned}\boldsymbol{\rho}_1 &= \rho\cos(\theta)\sin(\phi)\,,\\ \boldsymbol{\rho}_2 &= \rho\sin(\theta)\sin(\phi)\,,\\ \boldsymbol{\rho}_3 &= \cos(\phi)\,.\end{aligned} \tag{3.3.7}$$

In these coordinates the Jacobian is $\rho\sin(\theta)$ and we have

$$\begin{aligned}\omega_1^2 &= \rho^2 + m^2\,,\\ \omega_2^2 &= \rho^2 + m^2 + \omega^2 - 2\rho\cos(\phi)\omega.\end{aligned} \tag{3.3.8}$$

We can in principle perform the integrals over the angles analytically, however the integral over ϕ gives such an overly complicated expression, that it would take several dozen pages to even write it down and hence, we choose to do this integral either numerically or at points later in the analysis. Lastly note the for the rest of the chapter we set $m = 1$.

We can now write

$$Q(\omega) = \int_0^\infty \int_0^\pi \mathrm{d}r\mathrm{d}\phi \frac{4\pi r^2\sin(\phi)\left(\sqrt{(r^2+1)\left(r^2-2r\omega\cos(\phi)+\omega^2+1\right)} + r\cos(\phi)(\omega - r\cos(\phi)) - 1\right)}{\sqrt{(r^2+1)\left(r^2-2r\omega\cos(\phi)+\omega^2+1\right)}\left(\sqrt{r^2-2r\omega\cos(\phi)+\omega^2+1}+\sqrt{r^2+1}-\omega\right)^2}. \tag{3.3.9}$$

Please Note that this integral is divergent. In order to illustrate this, let us refer to the integrand as $q(r,\omega) = \int_0^\pi \mathrm{d}\phi\, q(r,\omega,\phi)$. We will find an expansion at $r = \infty$ for $q(r,\omega,\phi)$ and then integrate each term separately over ϕ to get an expansion for $q(r,\omega)$. We get

$$q(r,\omega) = \frac{4\pi\omega}{3} + \frac{4\pi\left(\omega^2-2\right)}{3r} + \frac{2\pi\omega\left(8\omega^2-25\right)}{15r^2} + \mathcal{O}\left(\left(\frac{1}{r}\right)^3\right). \tag{3.3.10}$$

As we can see, a quick and dirty way to get rid of the main divergence is to shift the integrand downwards by $\frac{4\pi\omega}{3}$. However there is a physically more elegant way. In the context of Entanglement Entropy in position space, it is well known[23] that EE is in general divergent. The entropy can only be defined up to a scale independent infinite additive constant. Thus, the physical interesting quantities to look at are either derivatives of the entropy or differences.

With that in mind let us study $\lim_{\omega\to 0} Q(\omega)$. We can check that in this case,

$$\begin{aligned} Q(0) &= \int \mathrm{d}^3\boldsymbol{\rho}\frac{\boldsymbol{\rho}_1^2}{\omega_1^4} \\ &= \int_0^\lambda \mathrm{d}r\frac{4\pi r^4}{3\left(r^2+1\right)^2} \\ &= \frac{2}{3}\pi\left(\lambda\left(\frac{1}{\lambda^2+1}+2\right)-3\tan^{-1}(\lambda)\right). \end{aligned} \tag{3.3.11}$$

In the limit $\lambda\to\infty$ this becomes

$$Q = \frac{4\pi\lambda}{3} - \pi^2. \tag{3.3.12}$$

Here we explicitly see the infinite additive constant. So to proceed we will now redefine our EE to be $Q(\omega)\to\hat{Q}(\omega) = Q(\omega) - Q(0)$. We get

$$\begin{aligned} \hat{Q}(\omega) = \int_0^\infty\int_0^\pi \mathrm{d}r\mathrm{d}\phi\ \pi r^2\sin(\phi) \\ \left(\frac{4\left(r^2+1\right)^{3/2}\left(\sqrt{r^2+1}\sqrt{r^2-2r\omega\cos(\phi)+\omega^2+1}+r\cos(\phi)(\omega-r\cos(\phi))-1\right)}{\left(r^2+1\right)^2\sqrt{r^2-2r\omega\cos(\phi)+\omega^2+1}\left(\sqrt{r^2-2r\omega\cos(\phi)+\omega^2+1}+\sqrt{r^2+1}-\omega\right)^2}-\right. \\ \left.\frac{r^2\sin^2(\phi)\sqrt{r^2-2r\omega\cos(\phi)+\omega^2+1}\left(\sqrt{r^2-2r\omega\cos(\phi)+\omega^2+1}+\sqrt{r^2+1}-\omega\right)^2}{\left(r^2+1\right)^2\sqrt{r^2-2r\omega\cos(\phi)+\omega^2+1}\left(\sqrt{r^2-2r\omega\cos(\phi)+\omega^2+1}+\sqrt{r^2+1}-\omega\right)^2}\right). \end{aligned} \tag{3.3.13}$$

By performing a similar analysis as above, we can show that

$$\hat{q}(r,\omega) = \frac{4\pi\omega}{3r}+\frac{4\pi\omega^2}{3r^2}+\frac{2\pi\left(8\omega^2-25\right)\omega}{15r^3}+\mathcal{O}\left(r^{-4}\right). \tag{3.3.14}$$

As we can see, we managed to get rid of the main singularity. And even though $\lim_{r\to\infty}\hat{q}=0$, we see that this does not happen fast enough and that a logarithmic divergence remains. Thus we still have use a UV-cutoff λ in order to completely regularize our integral.

It should be noted that in other areas in the study of entanglement entropy, similar structures have been observed. It has been shown [1] that, for example, the EE of any CFT between a region A and B in even spacetime dimension will have the form

$$S_A^{\mathrm{CFT}} = b_{d-2}(\frac{L_A}{\epsilon_{UV}})^{d-2}+b_{d-4}(\frac{L_A}{\epsilon_{UV}})^{d-4}+\cdots+(-1)^{\frac{d-2}{2}}\tilde{S}\log\frac{L_A}{\epsilon_{UV}}+\mathcal{O}\left(\epsilon_{UV}\right). \tag{3.3.15}$$

L_A is the diameter of the region, ϵ_{UV} is a UV-cutoff defined through a lattice spacing, and $\tilde{S}$ is the renormalised entanglement entropy. While the analysis that lead to the equation above

is not trivially transferable to the cases discussed in this chapter, the similarities nonetheless suggest that there is something more to be understood here.

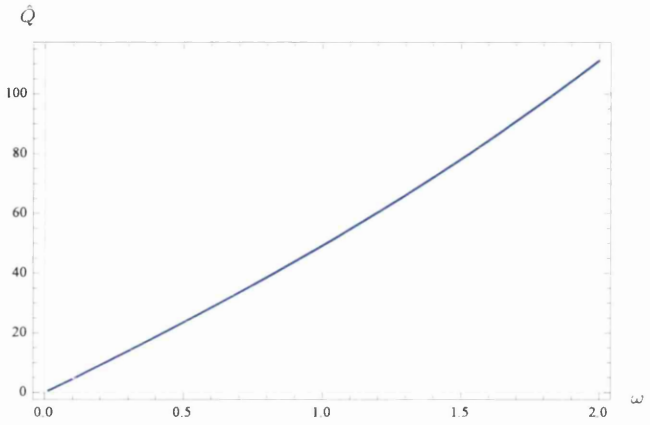

Figure 3.6: $\hat{Q}(\omega)$ for the QED Photon. We have chosen a UV cutoff at $\lambda = 10^6$.

If we compare Figure 3.6 with Figure 3.1, we can see that while both functions are monotonically increasing, there are interesting differences. For once the QED photon seems to behave linearly for small ω, while the scalar photon is constant in the small mass limit. This is not so surprising as in QED the constant factor turned out to be infinite and we removed it in order to regularise our integral. Furthermore the EE of the QED photon remains non-singular for all values of ω. This is more surprising and begs further analysis what part of QED is responsible from this departure in behaviour when compared to the scalar toy model.

Chapter 4

Holographic Entanglement Entropy

In this chapter we will study Entanglement Entropy (EE) in holographic theories and see how it relates to the confinement and the locality of the field theory. Let us start by discussing some ideas that motivated the research presented in this chapter.

Consider a theory like QCD: it was argued that this theory has a Hagedorn density of states. For a mass M, the number of states $N(M)$ is

$$N(M) \sim \left(\frac{M}{T_H}\right)^{2b} e^{+\frac{M}{T_H}}.$$

Here T_H is some energy scale and b a number. The Partition Function will roughly be,

$$Z \sim \int DM\, M^{2b} e^{+\frac{M}{T_H} - \beta M}.$$

We see that for a high enough temperature, this Partition Function is divergent and not well-defined.

In the case of QCD, this is not an effect one would actually measure, because hadrons have a natural width and at energies high enough, they would start decaying into each other, there would also be pair creation, etc. But in a 'truly confining' QFT, like for example Yang-Mills or minimally SUSY Yang-Mills, we would have — if we take the large N_c limit — infinite hadrons (glueballs) that will be very narrow and they will present the Hagedorn behaviour above (although generically, the deconfinement occurs before the Hagedorn transition). Just like it happens in a typical theory of strings.

The authors of [23], have argued that something similar happens to the EE of a confining theory. An intuitive reasoning lead them to write the EE as

$$S \sim \int DM\, M^{2b} e^{+\beta_H M - 2ML_{EE}},$$

where they used that for scalar non-interacting degrees of freedom — our 'large N_c' glueballs for example — the EE goes like $e^{-2ML_{EE}}$, where L_{EE} is the separation between the entangled regions. So it was argued in [23], that 'truly confining' QFTs should present a phase transition in the EE, when $2L > \beta_H$. This phase transition is *phenomenologically* similar to the confinement-deconfinement one. So, it is expected that for a given $L_{EE,crit}$ the EE behaves in a 'constant' manner — that is N^0 — for $L > L_{EE,crit}$, or grows very rapidly, like N^2, for for $L < L_{crit}$ respectively. We will see this in various examples below.

One may argue that in some QFTs the reasoning above might fail, if for example the density of states grows differently or if the behaviour of the EE for many scalars changes and hence the argument breaks down. We will see that a way of having some analytic control over the problem is to first introduce a cutoff at high energy, find the phase transition exploring regions close to the cutoff and then take the cutoff to infinity. These limits need not commute. A similar situation but in a different context was encountered in [46] and we will find this to be the case in theories with non-local UV-behaviour. Similarly we will observe that a local and honest UV-completion of non-local theories plays the same role as the regularisation with a cutoff.

This chapter is organised as follows: First, we will summarise the results of [23]. Then we will look at D5 on S^1 to study why some theories can show confinement but not show a phase transition in the EE. We will argue that the naive calculation is missing some key configurations. We further motivate the configurations through UV-cutoffs. We will then make the analysis explicit on a 4d QFT with non-local UV, which also need the cutoff. We will then see how a suitable UV-completion removing the nonlocality also behaves like the cutoff-QFT. This emphasises the point that the cutoff is capturing 'real physics'. We will classify key scales and features of the backgrounds in question and how they relate to the entanglement entropy behaviour. Last but not least we will present other interesting material that was observed during the study of the main body of work.

Let us start with the brief summary of the results of Klebanov, Kutasov and Murugan (KKM) [23], who studied the EE in gravity duals of confining large N_c gauge theories. KKM

have generalized the Ryu-Takayanagi conjecture to non-conformal theories, and suggested that the EE in these cases is given by

$$S = \frac{1}{G_N^{(10)}} \int_\gamma d^8\sigma e^{-2\phi} \sqrt{G^{(8)}_{ind}}\,, \tag{4.0.1}$$

where $G_N^{(10)}$ is the 10-dimensional Newton constant and $G^{(8)}_{ind}$ is the induced string frame metric on γ. The EE is obtained by minimizing the action (4.0.1) over all surfaces that approach the boundary of the entangling surface. KKM have considered, as the entangling surface, a strip of length L. In this case, they found that there are two local minima of the action (4.0.1) for a given L. The first is a disconnected surface, which consists of two cigars which are separated by a distance L. The second is a connected surface, in which the two cigars are connected by a tube whose width depends on L. Please note that the disconnected solution should actually be regarded as a connected solution, with two cusps. It is only that the connecting tube, given by the red dotted line in Figure 4.3 has a length of 0 for this solution. This is due to the fact that its length has a factor of the internal volume which vanishes at ρ_Λ for confining theories with a mass gap. The so called disconnected solution can be deduced as the extremal limit of a continuous sequence of non-extremal solutions parametrised by different ρ_*, which is the minimum value of ρ the surface reaches. The connected solution would be the local maxima of this sequence, then the surface area of the other curves would shrink as they approach the shape of the disconnected solution, a local minima of the sequence.

The gravitational background in the string frame is of the form

$$ds^2 = \alpha(\rho)\left[\beta(\rho)d\rho^2 + dx^\mu dx_\mu\right] + g_{ij}d\theta^i d\theta^j\,, \tag{4.0.2}$$

where x^μ ($\mu = 0, 1, \ldots, d$) parametrise $\mathbb{R}^{d+1}$, ρ is the holographic radial coordinate

$$\rho_\Lambda < \rho < \infty \tag{4.0.3}$$

(ρ_Λ can be zero in some cases) and θ^i ($i = d+2, \ldots, 9$) are the $8-d$ internal directions. There is also a dilaton field that we denote with ϕ. Some RR and NS fluxes complete the background, but they will not be relevant to our analysis. The volume of the internal manifold (described by the $\vec{\theta}$ coordinates) is $V_{int} = \int d\vec{\theta}\sqrt{\det[g_{ij}]}$. We also define the quantity

$$H(\rho) = e^{-4\phi}V_{int}^2\alpha^d\,. \tag{4.0.4}$$

The functions $H(\rho)$ and $\beta(\rho)$ will play an essential role in the following and all along the rest of this chapter. We will mention few important properties of these functions. KKM have argued that in confining backgrounds $H(\rho)$ is typically a monotonically *increasing* function while $\beta(\rho)$ is typically a monotonically *decreasing* function. Since $H(\rho)$ includes a factor of the volume of the internal manifold, it typically shrinks to zero size at $\rho = \rho_\Lambda$, in agreement with the vanishing of the central charge at zero energies. On the other hand, $\beta(\rho)$ is less restricted and it can either diverge or approach a finite value at $\rho = \rho_\Lambda$.

Denoting the minimal value of ρ along the connected surface in the bulk by ρ_0, its EE is given by

$$S_C(\rho_0) = \frac{V_{d-1}}{2G_N^{(10)}} \int_{\rho_0}^{\infty} d\rho \sqrt{\frac{\beta(\rho)H(\rho)}{1 - \frac{H(\rho_0)}{H(\rho)}}} \,. \tag{4.0.5}$$

The length of the line segment for the connected solution as a function of ρ_0 is

$$L(\rho_0) = 2 \int_{\rho_0}^{\infty} d\rho \sqrt{\frac{\beta(\rho)}{\frac{H(\rho)}{H(\rho_0)} - 1}} \,. \tag{4.0.6}$$

On the other hand, the EE of the disconnected solution does not depend on ρ_0 and is given by

$$S_D(\rho_0) = \frac{V_{d-1}}{2G_N^{(10)}} \int_{\rho_\Lambda}^{\infty} d\rho \sqrt{\beta(\rho)H(\rho)} \,. \tag{4.0.7}$$

The EE is in general UV divergent, but the difference between the EE of the connected and disconnected phases is finite

$$\frac{2G_N^{(10)}}{V_{d-1}} S(\rho_0) \equiv \frac{2G_N^{(10)}}{V_{d-1}} (S_C - S_D) = \int_{\rho_0}^{\infty} d\rho \sqrt{\frac{\beta(\rho)H(\rho)}{1 - \frac{H(\rho_0)}{H(\rho)}}} - \int_{\rho_\Lambda}^{\infty} d\rho \sqrt{\beta(\rho)H(\rho)} \,. \tag{4.0.8}$$

Depending on the value of L (or alternatively of ρ_0) S would either be positive or negative. In the first case the true solution will be a disconnected surface, while in the later case the connected solution will be the true one. The phase transition between the two solutions is a characteristic of confining theories, and is described in Figure 4.1.

The connected solution exists only in a finite range of lengths $0 < L < L_{\max}$. In this range there are two possible values for the connected solution, corresponding to the two branches in Figure 4.1. The upper branch is an unstable solution. This double valuedness, which is called the "butterfly shape", corresponds to the double valuedness in the graph of $L(\rho_0)$. As a result of the double valuedness, there is a first order phase transition at the point $L = L_c$ between the

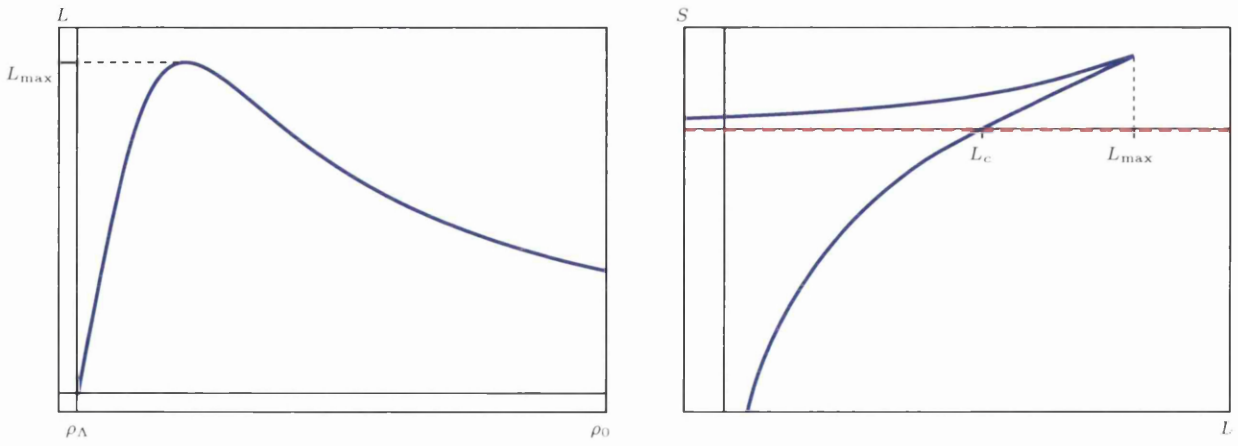

Figure 4.1: The phase diagram for the entanglement entropy in confining theories. On the left, the length of the connected solution as a function of the minimal radial position in the bulk $L(\rho_0)$, which is a non-monotonic function in confining theories. On the right, the entanglement entropy of the strip as a function of its length. The solid blue line represent the connected solution while the dashed red line is the disconnected solution. At the point $L = L_c$ there is a first order phase transition between the two solutions. This type of first-order phase transition behaviour is called the "butterfly shape" in the bibliography.

connected and the disconnected solutions. The scale that sets the phase transition is governed by the same effect that governs the different confinement phases. From the gravity side it is given by $\bar{\rho}$, the point at which $P(\rho)$, the solution to the master equation changes its behaviour outlined in (2.0.13). For this reason KKM have argued that a signal for a phase transition, and therefore also for confinement, is the non-monotonicity of the function $L(\rho_0)$. Indeed, as we will show later in different examples, every peak in $L(\rho_0)$ corresponds to a possible phase transition in the entanglement entropy $S(L)$.

4.1 Volume and Area Laws, UV-cutoffs and Confinement

This section will aim to provide an example as to why some confining theories might not present a phase transition in the EE. We will briefly analyse the case of $AdS_5 \times S^5$, then quickly move into NS5 and D5 branes, where an important role will be played by the non-locality of the associated field theory. The analogue to the confining Witten's model, but with D5 branes that wrap S^1 will close the analysis of this section.

Let us discuss the well understood case of $AdS_5 \times S^5$, as it will be a basis for comparison for more complicated cases. The metric and other relevant functions for the case of $AdS_5 \times S^5$

are given by

$$ds^2_{AdS} = \frac{R^2}{\rho^2}d\rho^2 + \frac{\rho^2}{R^2}dx^2_{1,3} + R^2 d\Omega^2_5, \quad \beta(\rho) = \frac{R^4}{\rho^4}, \; H(\rho) = \left(\frac{8\pi^2}{3}\right)^2 R^4\rho^6. \tag{4.1.1}$$

The length of the strip $L(\rho_0)$ as well as the S can be exactly computed and are plotted in

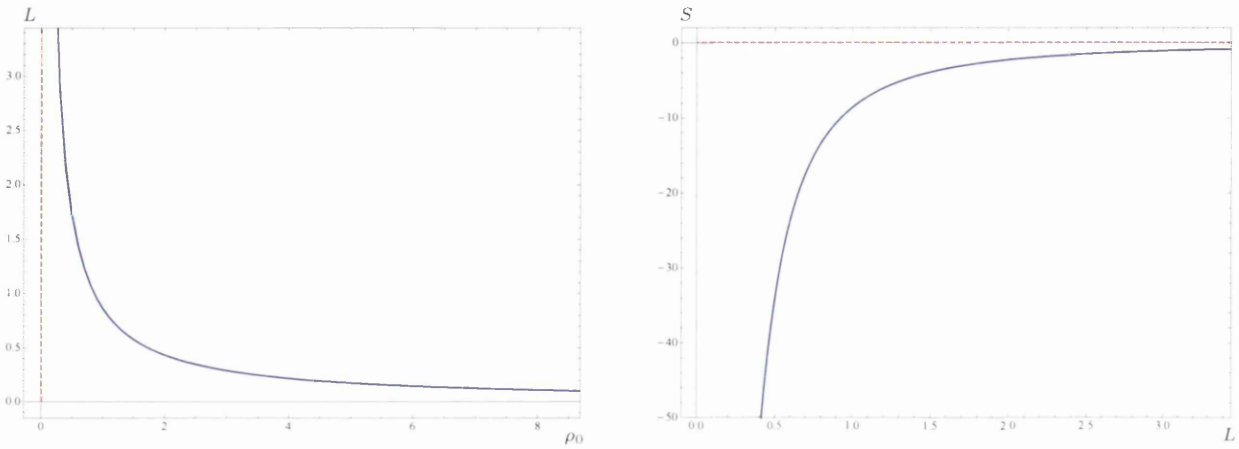

Figure 4.2: The case of $AdS_5 \times S^5$ — Here we plot $L(\rho_0)$ and $S(L)$.

Figure 4.2. We find that the connected solution is always the minimal solution for the EE and is always preferred to the disconnected solution for all values of L which has a higher EE. The connected solutions asymptote the disconnected ones from below for large L. For a local field theory, the EE follows what is called a "Heisenberg-like" relation, such that $L(\rho_0) \sim \rho_0^{-1}$ for some region (typically for large ρ_0) of the minimal solution. This type of behaviour can be seen in Figure 4.3 by considering only the navy blue lines (both solid and dashed). We should further note that they have the correct concavity for stability [47],[48],

$$\frac{d^2S}{dL^2} < 0. \tag{4.1.2}$$

The $AdS_5 \times S^5$ has the usual Area Law for the EE when we analyse the divergent parts.

Introducing confinement in this theory can be thought of as an effect on the IR region of the corresponding $AdS_5 \times S^5$ plot. This effect can be modelled by a soft-wall solution as we will see in chapter 6. We replace the IR region with the usual $L \sim \rho_0^{-1}$ behaviour for the connected solution, with an *unstable* branch (c.f. the green lines in Figure 4.3) [*]. This has the effect of moving the disconnected branch down such that it now meets the *stable* connected branch at

[*]Notice that this solution does not satisfy the criteria for the concavity given in eq.(4.1.2).

a finite value of $L = L_c$ (see the right panel of Figure 4.3). Thus within backgrounds of this type we find that there exists a critical value L_c, such that for $L > L_c$, the minimal solution is now the disconnected branch, and for $L < L_c$ we still have the original AdS-like connected behaviour in the UV (*stable* branch). The presence of the *unstable* branch will occur for all theories we will study that exhibit confinement (for zero temperature at least). Again these solutions follow the usual Area Law for the divergent parts of the EE.

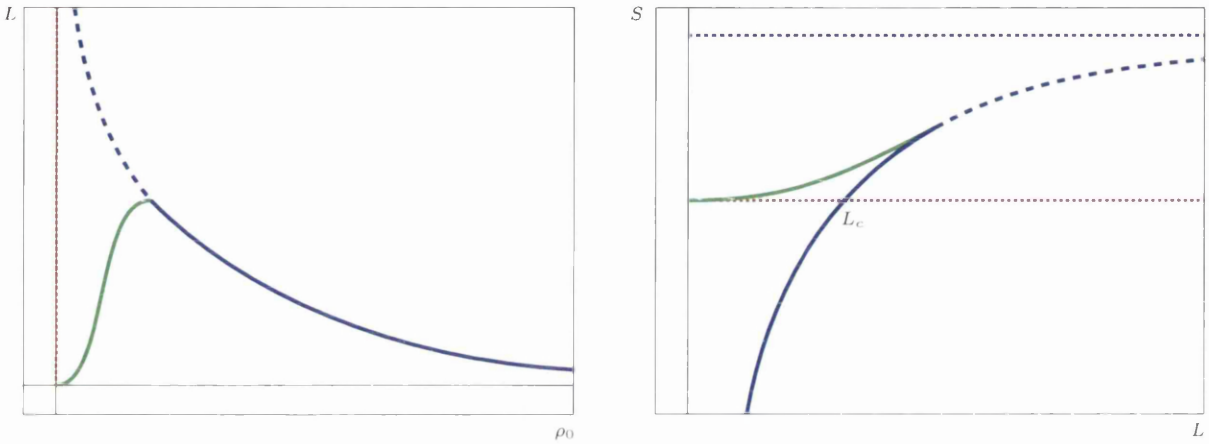

Figure 4.3: Here are cartoons of the change in L and S when we have a theory with confinement. The navy blue lines (solid and dashed) in both plots represent the behaviour of the connected part of conformal solutions like that of $AdS_5 \times S^5$ (i.e. $L(\rho_0) \sim \rho_0^{-1}$), the green line is the *unstable* branch introduced by confinement (like in the soft-wall model). The dotted red and navy lines represent the disconnected solution. We can see that in the confining case there is a phase transition at the point L_c.

Something peculiar occurs if we now consider the case of D5/NS5 branes, as discussed in [49]. In this case, we find that the separation of the connected branch is constant, given by $L(\rho_0) = \pi R/2$ where $R^2 = \alpha' g_s N_c$. Thus there is an infinite number of connected solutions which are parametrised by the depth to which they probe but all have the same fixed value of L (as in the left panel of Figure 4.4).

The authors of [49] argued that the solutions for smaller values of $L < L_c$ (using the approximation of a capped cylinder similar to the one we will discuss shortly), are exactly those that must live near the UV-cutoff, with the contribution to the EE coming from the cap, which present a Volume-Law, once the divergent part of the EE is considered.

Another interesting case occurs in the context of D5 branes wrapped on S^1, which as explained, is a model of a confining 4 + 1-d QFT. Here we find that the connected branch of the

EE is similar to that of the IR *unstable* branch of the soft-wall model, but that there is no *stable* branch as we move into the UV. This would be akin to only keeping the green line in Figure 4.3 (in this specific case the connected branch asymptotically approaches that of the NS5/D5, i.e. $L = \frac{\pi R}{2}$) — see the third row in Figure 6.1. The example of D5 wrapped on S^1 then presents the IR features of a confining model (like a soft-wall model), but the UV behaviour of a non-local QFT (like flat NS or D5 branes). It presents only an unstable branch and a disconnected one and the absence of a phase transition in spite of displaying a confining Wilson loop. We will appeal to cutoff-effects to solve this issue. Below, we will clarify the details of this example. Before that, we present a useful approximation to some of the quantities involved in the calculations.

4.1.1 A Useful Quantity

As an aside, we would like to introduce a combination of background functions that (we have checked) approximates very well the function $L(\rho_0)$ in all the cases studied in this thesis. This is useful, because in the examples dealt with in the following sections, the functions defining the background are only known numerically (or in semi-analytic expansions). Hence the integrals defining L and S are very time-consuming. Instead, the quantity

$$\mathcal{Y}(\rho_0) = 2\pi \left. \frac{H(\rho)\sqrt{\beta(\rho)}}{H'(\rho)} \right|_{\rho=\rho_0} \tag{4.1.3}$$

can be seen to approximate very precisely the complicated integral in (4.0.6) that defines $L(\rho_0)$. The analogue of this function also appeared in studies of Wilson loops and other probes [50], [51].

4.1.2 Study of the D5 branes on S^1 System

Here, we will emphasize that the presence of a phase transition for the entanglement entropy in confining theories is sensitive to the UV behaviour of the field theory. We will make this point by considering the simplest confining field theory in $4+1$ dimensions that one can construct by wrapping N_c D5 branes on a circle and imposing periodic (anti-periodic) boundary conditions for the bosons (fermions) of this field theory. This is in analogy with the example introduced by Witten in [52] by double-Wick rotating a black-brane solution.

Indeed we will have that the string frame metric reads,

$$\frac{ds^2}{\alpha'} = \left(\frac{u}{R}\right)[dx_{1,4}^2 + h(u)d\varphi_c^2] + \frac{R}{uh(u)}du^2 + Rud\Omega_3^2, \quad R^2 = g_s\alpha' N_c.$$

where the functions $h(u)$ and the dilaton are,

$$h(u) = 1 - \left(\frac{\Lambda}{u}\right)^2, \quad e^{\phi} = g_s\alpha'\left(\frac{u}{R}\right).$$

It is more convenient to change from the 'energy' variable u to the radial variable $r = \alpha' u$. The background and relevant functions for our calculations are,

$$\begin{aligned}
ds^2 &= \left(\frac{r}{R}\right)[dx_{1,4}^2 + \alpha' h(r)d\varphi^2] + \frac{R}{rh(r)}dr^2 + Rrd\Omega_3^2, \quad R^2 = g_s\alpha' N_c, \\
h(r) &= 1 - \left(\frac{R_\Lambda}{r}\right)^2, \; e^{\phi} = g_s\frac{r}{R}, \quad R_\Lambda = \alpha'\Lambda, \\
\alpha(r) &= \frac{r}{R}, \; \beta(r) = \frac{R^2}{r^2 h(r)}, \; V_{int}^2 = (4\pi)^4 l_\varphi^2 R^2 h(r) r^4, \\
H(r) &= \frac{(4\pi)^4 R^2 l_\varphi^2}{g_s^4} h(r) r^4, \quad l_\varphi = \sqrt{\alpha'}\oint d\varphi.
\end{aligned} \tag{4.1.4}$$

Using the approximation discussed in eq.(4.1.3), one can compute that the function $L(r_0)$ asymptotes (from below) to a constant value

$$L(r_0 \to \infty) \sim \mathcal{Y}(r \to \infty) = \lim_{r_0 \to \infty} \frac{\pi R\sqrt{r^2(r^2 - R_\Lambda^2)}}{(2r^2 - R_\Lambda^2)} = \frac{\pi}{2}\sqrt{g_s\alpha' N_c}\,, \tag{4.1.5}$$

hence preventing any form of double-valuedness and phase transition. See the third row in Figure 6.1 for a plot of the calculation done with the background in eq.(4.1.4). Notice again, that the connected solution has the wrong concavity, hence it is unstable. This would lead us to believe that the disconnected solution would always be the minimal EE solution for all values of L. With this case in mind one can instead ask the question

- *Question:* Are there other solutions which have smaller EE that we should consider ?

As we anticipated above, the answer goes like this: in [49], the authors discuss how non-locality affects EE calculations. They argue that one should add a UV-cutoff and also consider solutions which live close to it (represented by B in Figure 4.4). These solutions can minimise the EE in cases which exhibit non-locality. There is a difference between these solutions and the ones we have discussed so far, in that these solutions no longer follow the standard Area Law but instead follow a "Volume Law" for the divergent part of the EE. This observation was also made

in other contexts by [53–55]. From this insight we can try to understand in which cases these new Volume Law solutions may be relevant to our question.

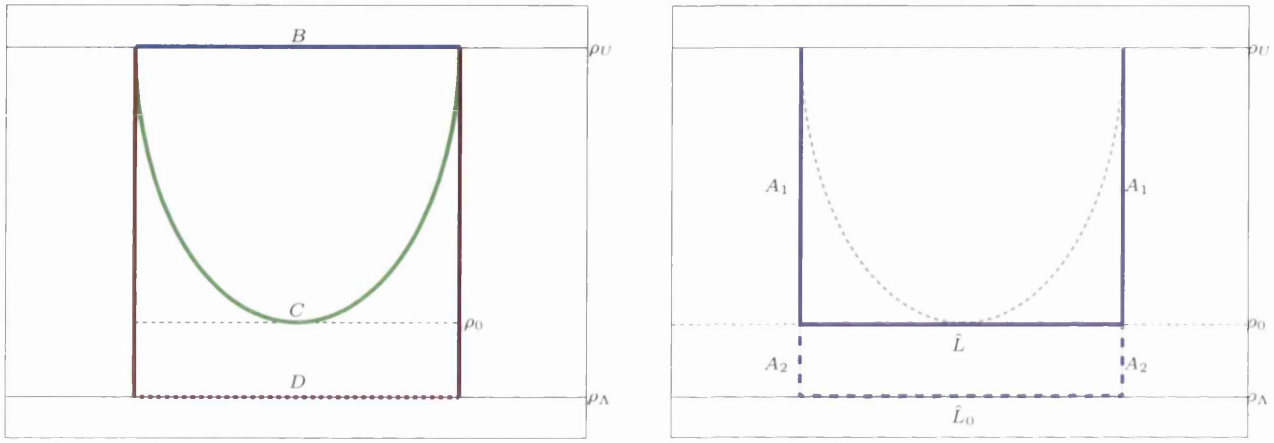

Figure 4.4: Here are cartoons of the types of solutions we shall be considering in the left panel and details of the approximation in the right panel. In both, ρ_U represents the UV boundary and ρ_Λ is the IR end of the space. In the left panel, the red lines (including the dashed line at ρ_Λ) represent the disconnected solution (D), the green line represents a generic connected solution (C) which probes down to a depth ρ_0 and finally in blue are the solutions which live close to the boundary (B) and behave under the Volume Law for the EE. In the right panel, we outline the various sections of the approximation. The purple solid lines map out the approximation to the connected dashed green solution, which we split into three parts: two vertical contributions labelled as A_1 and a horizontal contribution labelled $\hat{L}$. The surface mapped out by the dashed purple lines, which is useful when we regularise our approximation, consists again of three parts: the two vertical contributions labelled A_2 and the horizontal contribution labelled $\hat{L}_0$.

We start by making clear what is meant in each of the cases of Volume/Area-Law along the lines of [49]. We consider a QFT in d-space dimensions. It is known that the structure of divergences of the HEE, when written in terms of some UV cutoff ϵ, is given by

$$S[V] = \frac{g_{d-1}[\partial V]}{\epsilon^{d-1}} + \frac{g_{d-2}[\partial V]}{\epsilon^{d-2}} + ... + \frac{g_1[\partial V]}{\epsilon} + g_0[\partial V]\log\epsilon + S_{finite}\,, \tag{4.1.6}$$

where $g_i[\partial V]$ are extensive functions of $[\partial V]_{d-1}$ which is the boundary surface of V and are homogeneous of degree i. When a QFT is local we find

$$S_{HEE} = N_{eff}\frac{|\partial V|}{\epsilon^{d-1}} \tag{4.1.7}$$

and this is known as an Area-Law as mentioned in the above. Further, that when a QFT is non-local

$$S_{HEE} = N_{eff}\frac{|V|}{\epsilon^{d}}\,, \tag{4.1.8}$$

we find extensive behaviour or a Volume-Law, where in both expressions the N_{eff} is the effective number of degrees of freedom.

Furthermore, it is possible to have a phase transition between these two types of behaviour (Volume Law $\leftrightarrow$ Area Law). We will find that the Volume Law behaviour is always linked with the non-local UV behaviour of our theories. So, we may wonder what this implies for the case of the D5 branes wrapped on S^1 ? In this case, we are introducing a confinement scale and thus we will introduce an *unstable* branch, joining our disconnected solutions, which have a degenerate point at one end of the confinement branch (point X in the right panel of Figure 4.5), to our near UV solutions, which have a degenerate point at the other end of the confinement branch (point Y in the right panel of Figure 4.5). The practicalities of realising this UV branch of solutions will be discussed shortly.

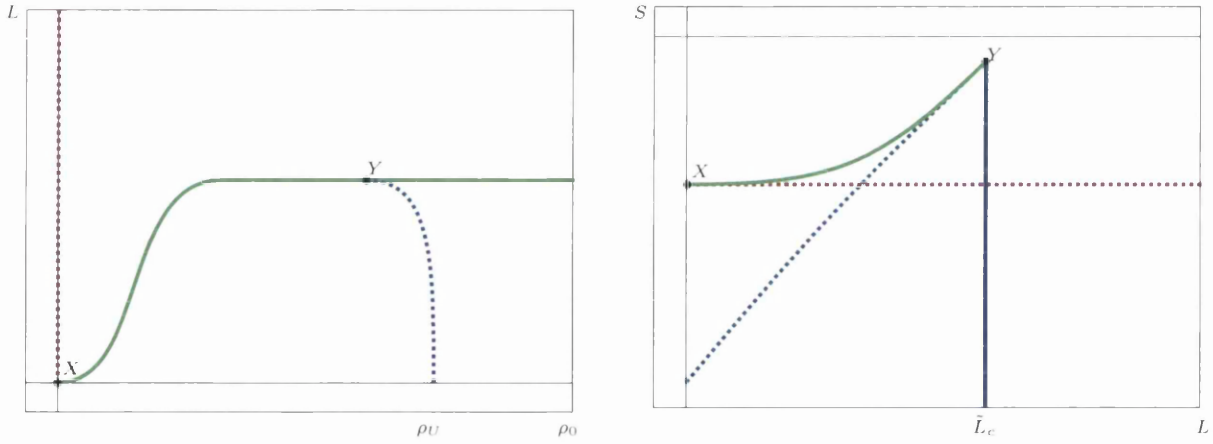

Figure 4.5: Here are cartoons of the behaviour in a background like that of the D5 branes wrapped on an S^1. The dashed red line represents the disconnected solution, and the green that of the confinement branch, which join at the point X. With finite UV cutoff ρ_U, we would find something similar to the dashed navy blue branch in both plots for solutions near the cutoff scale. If we increase the UV cutoff (meaning the point Y moves to larger ρ_0), we find that the gradient of the UV branch becomes steeper, such that in the limit that we remove the cutoff completely, it becomes the vertical solid navy blue line and we reproduce exactly the extensive solutions.

Note that in the cartoon in Figure 4.5, the introduction of solutions like B (c.f. 'short solutions' in Figure 4.4) mean that for the EE, there is now a phase transition between the disconnected solutions and the extensive solutions at the point $\tilde{L}_c$. In the cases we shall consider, we can argue that a transition to a region in the UV where an extensive behaviour of the EE is the minimal solution, is a sign of non-locality [49, 53, 54], but further to that, a sign that one

may want to look to UV complete these theories in a non-trivial way, if they are to be correct duals to "nice" field theories. Let us now be more precise about the 'short solutions'.

4.1.3 Finding the 'Short Configurations'

Now we would like to motivate the existence of these new 'short configurations' explicitly and then use them as a completion for some specific EE diagrams. To this end we will use a particular *approximation*. We let our surface be rectangular in shape, such that the sides follow the same path as the disconnected surface from $\rho = \rho_U$ to $\rho = \rho_0$ (we can take $\rho_U \to \infty$ later). Then we connect the two vertical surfaces A_1 with the horizontal surface $\hat{L}$ at constant ρ_0 (depicted as the solid purple lines in the right panel of Figure 4.4). Initially, we shall rewrite the EE of the disconnected solution S_D, by splitting it into two parts joined at ρ_0,

$$S_D = 2(A_1 + A_2) + \hat{L}_0\,, \tag{4.1.9}$$

where A_1 is the contribution from ρ_U down to ρ_0, while A_2 is the contribution from ρ_0 down to the end of space ρ_Λ. Note that $\hat{L}_0$ would be a contribution from the horizontal piece at the end of space which is vanishing in the cases we consider. From this, we can now write the surface area of our approximating surface as

$$S_{app} = 2A_1 + \hat{L}. \tag{4.1.10}$$

It should be noted here that the approximate surfaces S_{app} are *not* extremal surfaces as they are not proper solutions of the equations of motion. Nevertheless, we note that for a fixed value of ρ_0, A_1 and A_2 are strictly constant, while $\hat{L} \propto L$, thus when $L \to 0$ then $\hat{L} \to 0$. *This means that, no matter how small A_2 is, there exists small enough values of L such that we have $\hat{L} < 2A_2$, and thus $S_{app} < S_D$.* The existence of these configurations would indicate, that for small L there will exist solutions that have lower EE than the disconnected case, and that there exists actual extremal solutions also with lower EE than the disconnected one.

Now let us derive the precise formula for the area of S_{app}. Starting with $\hat{L}$, we notice that since the surface is volume filling in all but the $\{x_1, \rho\}$ directions, we have

$$\hat{L} = \int \prod_{i=1}^{8-d} \prod_{j=1}^{d} d\theta_i dx_j \sqrt{g_{\text{ind}}} \int du \sqrt{g_{\mu\nu}\dot{x}^\mu \dot{x}^\nu}. \tag{4.1.11}$$

Using the parametrisation $x^\mu = \{\hat{\rho}, u\}$, with $u \in \{-\frac{L}{2}, \frac{L}{2}\}$, we can easily deduce that

$$\hat{L} \propto V_{int}\alpha^{\frac{d}{2}}e^{-2\phi}|_{\rho=\rho_0}L = \sqrt{H(\rho_0)}L\,. \tag{4.1.12}$$

The two sides A_1 are given by

$$2A_1 = 2\int_{\rho_0}^{\rho_U} d\rho\sqrt{\beta(\rho)H(\rho)}\,. \tag{4.1.13}$$

Note that A_1 is divergent for $\rho_U \to \infty$. Thus we renormalise using the same approach as for the extremal solutions; we subtract the disconnected surface area $S_D = 2\int_{\rho_\Lambda}^{\rho_U} d\rho\sqrt{\beta(\rho)H(\rho)}$. Thus overall we have*

$$S_{app}(L) = \frac{2}{\pi}V_{int}\alpha^{\frac{d}{2}}e^{-2\phi}|_{\rho_0}L - 2\int_{\rho_\Lambda}^{\rho_0} d\rho\sqrt{\beta(\rho)H(\rho)}. \tag{4.1.14}$$

Notice that this last formula is an approximation of the expression in (6.0.4). We now study what happens in the examples discussed so far.

If we take $\rho_0 \to \rho_\Lambda$ we will have that $V_{int}\alpha^{d/2}e^{-2\Phi} \to 0$ — as we observed, it happens in all our models that $H_{EE}(\rho_\Lambda) \to 0$—see eq.(6.0.8). We then recover the disconnected solutions and due to our renormalisation scheme, it is easy to see that the solution will always sit on top of the L-axis of our $S_{app}(L)$ plots. This is a feature of all backgrounds studied here. In the other limit $\rho_0 \to \rho_U$ our surface becomes the S_{app}-axis of the $S_{app}(L)$ plot, and we have a smooth interpolation in between — see the top left of Figure 4.6. Note that these lines map out the actual connected solution and thus approximate this case very well. A quantity that proves to be very useful is the point at which the surfaces cross the L-axis. We know that $S_{app} = 0$ whenever

$$L = \frac{\pi\int_{\rho_\Lambda}^{\rho_0} d\rho\sqrt{\beta(\rho)H(\rho)}}{V_{int}\alpha^{\frac{d}{2}}e^{-2\phi}|_{\rho_0}} \equiv T(\hat{\rho})\,. \tag{4.1.15}$$

Thus in cases like that of $AdS_5 \times S^5$, $T(\hat{\rho})$ will be monotonically decreasing function with T varying between $(\infty, 0]$ as ρ_0 varies between $[0, \infty)$.

If we now study the soft-wall case (see the top-right panel of Figure 4.6), we can see that the solutions again near the UV look similar to that of the $AdS_5 \times S^5$ case above, as expected. The difference lies in the solutions near the IR, where the surfaces initially begin to move into the positive plane of the S_{app} plot, meaning they have higher EE than the disconnected solution. A phase transition appears as one would expect. This change can also be seen in the behaviour

*Note that we have added the extra multiplicative factor to take care of the sharp edges of our surfaces that otherwise make the surface a worse approximation to the actual minimal solutions.

of $T(\rho_0)$. Indeed, now $T \to \{0,0\}$ as $\rho_0 \to \{0,\infty\}$. Additionally $T(\rho_0)$ is an increasing function for small ρ_0 (below the confinement scale) and a decreasing function above it.

Now let us discuss backgrounds which exhibit non-locality. First we look at the case of D5 branes as studied in [49] and depicted in the bottom-left panel of Figure 4.6. We see that the surfaces all intercept the axis at $L = \pi/2$ (as we have set $R = 1$) with increasing gradient as we move towards the UV. Thus in the limit we would expect to find a vertical line at $L = \pi/2$. This agrees with the expectations of our discussion above.

Finally, we move to the D5 wrapped on S^1 that mostly occupied us in this section. The associated plot can be seen in the bottom-right panel of Figure 4.6. Here we find that the surfaces initially move up into the positive plane of the S_{app} plot and they then asymptote the same value as the flat D5 solution leading again to a vertical line at $L = \pi/2$ (choosing $R = 1$) in the UV. The two D5 cases discussed differ in a subtle point. While the phase transition in the two cases is always between Area $\leftrightarrow$ Volume Law behaviour, in the flat D5 case, all the connected solutions sit at the transition point.

These 'short configurations' living at the cutoff appear and play an important role, every time we have a non-local QFT. They are *needed* in order to avoid having only a connected-unstable and the disconnected solutions. The short configurations imply the existence of a phase transition between connected-stable and disconnected branches of the EE [*].

In the next section, we will study another example of this 'cutoff effect' when studying the behaviour of the EE in one of the 'trademark' models of confining field theory (but with a non-local UV). We will also learn that a similar job as the one done by the cutoff can be done by a UV-completion of the QFT. This gives a well-behaved EE-phase transition, with an area law for the divergent part of the EE, etc.

4.2 The Absence of Phase Transitions in (some) Confining Models

The reader might object that the example of D5 wrapped on S^1 discussed above is not such a good model for a confining field theory. In principle theories in $4+1$ dimensions have strongly coupled UV behaviour, their IR tends to be weakly coupled and what we observed is just an effect of these features, in contradiction with us imposing the model to be confining. One may imagine that for duals to field theories in $3+1$ dimensions the phase transition should reappear.

[*]Notice that we are taking limits in a given order; first $\rho_0 \to \rho_U$ followed by $\rho_U \to \infty$. This is very reminiscent of the treatment in [46]

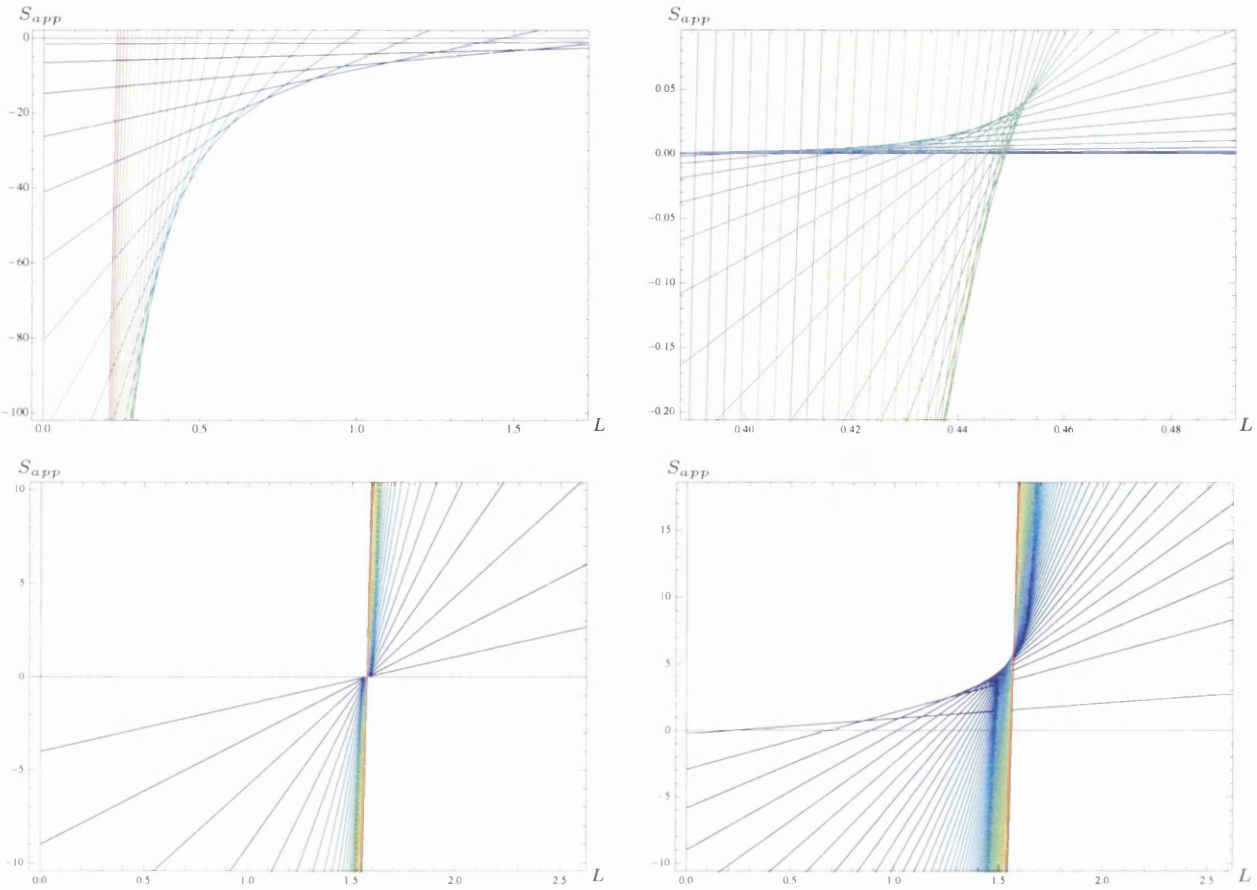

Figure 4.6: In the above we have plotted a number of the surfaces $S_{app}(L)$. The colour scheme is such that purple lines are surfaces with ρ_0 approaching 0, and the red solutions which have ρ_0 approaching ρ_U. The top-left panel is that of $AdS_5 \times S^5$, then in the top-right the Soft-Wall, the bottom-left is flat D5 branes and the bottom-right is D5 branes wrapped on S^1.

Below, we will analyse this claim, by first studying the case of a dual QFT obtained by wrapping N_c D5 branes on a two-cycle of the resolved conifold [16]. We will discover that the behaviour in the UV is not much different from the one of the flat-D5 brane just analysed above. The reader may argue that this is due to the fact that at energies high enough, the dual QFT becomes higher dimensional, an infinite set of KK-modes coming from the compactification of the D5 branes on the two-cycle indicate the higher dimensional character of the QFT. This is of course correct, but the point is subtle. Indeed, as Andrews and Dorey [35] have shown (in the perturbative regime), the field theory is completely equivalent to four-dimensional $\mathcal{N} = 1^*$ Yang-Mills, expanded at a particular point of its Higgs branch, which is a well-defined 4-d QFT. Also, the same sort of KK-modes appear if we compactify a stack of D4 branes on S^1 and in that confining model the phase transition is present, see [23] and Section 6.2.2 . We will then

carefully calculate the entanglement entropy for this QFT based on wrapped D5 branes.

The details of this background have been introduced in Chapter 2. The metric is given by (2.0.6). The functions needed to calculate the entanglement entropy in this string-frame background are,

$$\begin{aligned} &\alpha = e^{\Phi}, && \beta = \alpha' g_s e^{2k}, \\ &V_{int}^2 = (2\pi)^6 (\alpha' g_s)^5 e^{4h+4g+5\Phi+2k}, && H = (2\pi)^6 (\alpha' g_s)^5 e^{4\Phi+4g+4h+2k}. \end{aligned} \tag{4.2.1}$$

We will first focus on the solution (2.0.11). We obtain a behaviour similar to the one around eq.(4.1.4), considering the change in the radial variable between one description and the other (that for large radius is $\rho \sim \log r$), both are examples of 'linear dilaton' backgrounds.

Indeed, calculating the entanglement entropy $S(\rho_0)$, the separation between regions $L(\rho_0)$ and then plotting parametrically $S(L)$, we find that there is no minimal solution present, only the disconnected and the unstable connected ones. The latter exists over a finite range for $0 < L < \frac{\pi}{2}\sqrt{g_s \alpha' N_c}$ with $S_c(0) = 0$ and $S_c(\frac{\pi}{2}\sqrt{g_s \alpha' N_c}) = \infty$. Using the approximation of

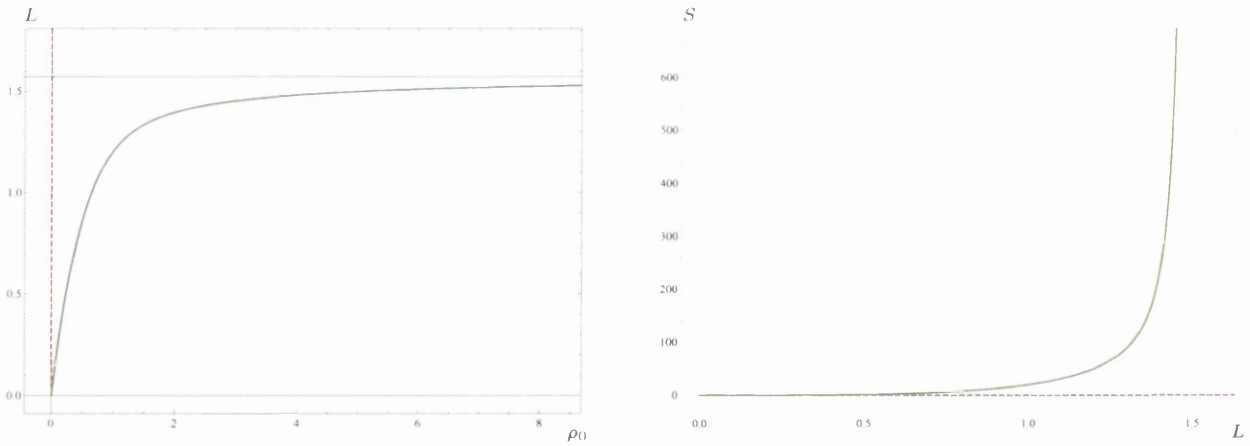

Figure 4.7: The system of D5s on a two-cycle — Here we plot $L(\rho_0)$ and $S(L)$.

eq.(4.1.3), we find,

$$\begin{aligned} L(\rho) \sim \mathcal{Y}(\rho) &= \sqrt{\alpha' g_s}\pi \frac{e^k}{2\Phi' + 2h' + 2g' + k'} = \\ &= \frac{\pi\sqrt{\alpha' g_s P'}}{\sqrt{2}} \frac{(P^2 - Q^2)}{(2P^2 \coth(2\rho) + PP' - QQ' - 2Q^2 \coth(2\rho))}. \end{aligned} \tag{4.2.2}$$

Which for the exact solution

$$P = 2N_c\rho, \quad Q = N_c(2\rho \coth(2\rho) - 1),$$

gives the approximated asymptotics for the function $L(\rho_0)$,

$$L(\rho_0 \to \infty) \sim \frac{\pi\sqrt{\alpha' g_s N_c}}{2}(1 - \frac{1}{4\rho_0}), \quad L(\rho_0 \to 0) \sim \frac{\pi\sqrt{\alpha' g_s N_c}}{2}\rho_0.$$

Notice that the Heisenberg-like relation $L \sim \rho_0^{-1}$ is violated here. Also note that the entropy scales as

$$\frac{G_{10} S_c}{V_2} \sim (\alpha' g_s)^3 N_c^{\frac{3}{2}}.$$

Like in the example of the compactified D5 branes on S^1 above, we see that the connected configuration is unstable — not satisfying the concavity condition of eq.(4.1.2). We do not see the possibility of a phase transition. But here is where the 'short configurations' and the effects of the UV cutoff enter to cure the problem [*].

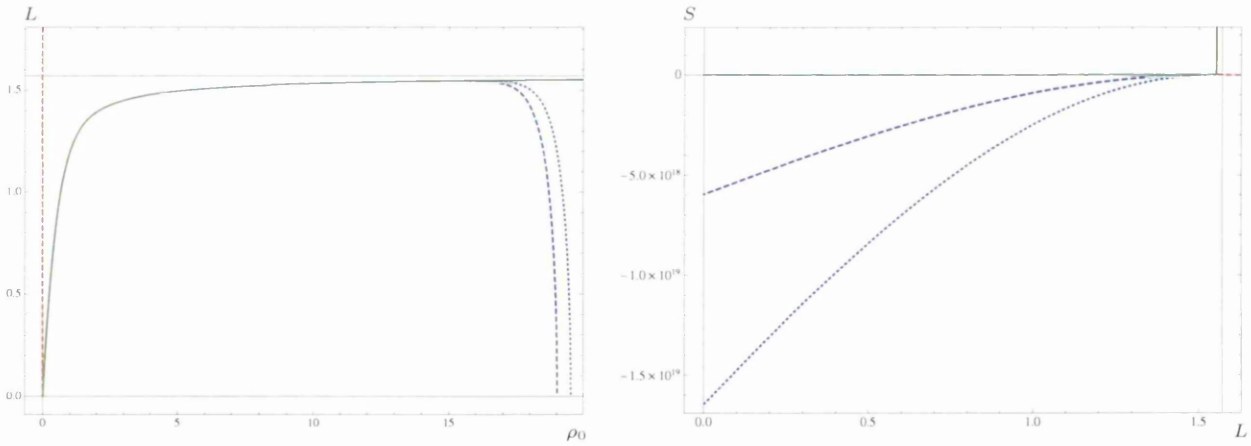

Figure 4.8: The system of D5s on a two-cycle — Here we plot $L(\rho_0)$ and $S(L)$ again, but this time introducing a UV cutoff. The green line is the solution without UV cutoff, the dashed blue line is with the cutoff at $\rho_U = 19$, the dotted blue is with the cutoff at $\rho_U = 19.5$, and finally the dashed red line represents the disconnected solution. Notice that increasing the value of ρ_U leads to an increase in the gradient in the visible branch in the $S(L)$ plot in the right panel.

In Figure 4.8 we show the result of considering these short configurations at the UV-cutoff. We see that these are the *correct* configurations to consider as they avoid the instability issue. The phase transition in $S(L)$ is recovered, as it corresponds to a confining model.

[*]As an aside, it should be noted that the 'finite size' effect reflected in the non-zero value of $L(\rho_0 \to \infty)$, was observed also for the Wilson loop when calculated in this sort of backgrounds in [36], [33], [43].

4.2.1 More on Non-Locality

To make the point of the 'non-locality' clearer, we will consider another solution describing D5 branes compactified on the two-cycle of the resolved conifold (the field theory has different operators driving the dynamics). Namely, the solution connecting the UV expansion (2.0.14) with the IR expansion (2.0.15). This second solution is well described in the papers [37, 39] — see Section 4 of the paper [29] for a good summary.

It was shown that this type of solution that has these two expansions, corresponds to the addition of a an irrelevant operator which in turn requires a UV completion of the field theory.

The field theory dual to the background obtained with the solution $P = 2N_c\rho$ is afflicted by *less severe non-localities* than the field theory dual to the second semi-analytical solution. What we mean by this here is a subtle point rather than some precise quantification of non-locality severity. Its is known that the baryonic branch is spanned by a one parameter family of solutions. See the paragraph just before Section 2.1. We used h_1 as the parameter as the actual calculations in these backgrounds make it a natural choice. But it could be characterised by equivalent but physically more relevant variables. For example, the scale at which the dilaton becomes constant. $h_1 = 2N_c$ is the limit as the scale becomes ∞. Thus the dilaton does not become constant at a finite scale and this causes problems as discussed previously, especially Chapter 2. So calculations of quantities in the UV changes for the background $P = 2N_c\rho$, but not as severe as for the backgrounds discussed in this section, where the dilaton actually does change behaviour at a finite scale, but adopts an unhealthy exponential behaviour instead.

We can see how the entanglement entropy reflects this. We recalculate the numerics for the entanglement entropy $S(\rho_0)$ and separation $L(\rho_0)$ (we do this for a sample numerical solution of the form given by eq.(2.0.14) and (2.0.15), where the irrelevant operator is inserted with a small coefficient $h_1 = 2N_c + \epsilon$). The result is described in Figure 4.9, showing that $L(\rho_0)$ deviates even more from the needed double valuedness. The saddle point solution does exist for all values of L and there is not any other connected solution. Note that whilst $L(\rho_0)$ vanishes linearly for small values of ρ_0, it grows exponentially in the UV, $L(\rho_0 \to \infty) \sim e^{2\rho_0/3}$. Of course, this departs even more from the Heisenberg-like scaling $L \sim \rho_0^{-1}$ characteristic of local field theories. All these results can be obtained from eq.(4.2.2) with the solution in eq.(2.0.14) and are reflected by Figure 4.9.

As described above, even when the string dual shows a confining Wilson loop or area law behaviour [*], the system is not showing a phase transition in the entanglement entropy. All this

[*] A subtle point is that the Wilson loop cannot be strictly calculated with the semi-analytical solution. This

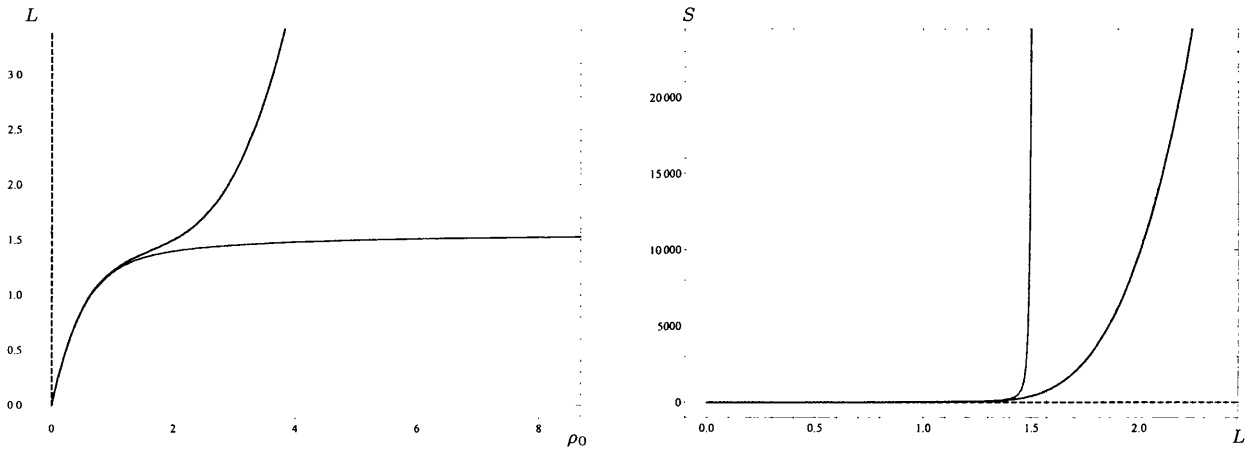

Figure 4.9: The system of D5s on a two-cycle but with exponential behaviour in P ($h_1 = \frac{203}{100}N_c$) — Here we plot $L(\rho_0)$ and $S(L)$. The grey line is the linear P solution ($h_1 = 2N_c$) for comparison.

relies on the UV properties of the field theory. The same phenomena can be displayed in other systems with qualitative similar field theoretic high energy behaviour, see Section 4.6.

One may wonder if all hope for observing a phase transition in the entanglement entropy (without appealing to the above discussed regulating cutoff and short solutions) is lost. In the next section, we will discuss a possible UV completion of the field theory on the compactified D5 branes. This completion, in terms of an inverse Higgs mechanism is discussed in the papers [39–41]. To this we turn now.

4.3 Recovering the Phase Transition: The Baryonic Branch

As we discussed above, the non-local UV-properties of the field theory dual to a stack of N_c D5 branes compactified on the two-cycle of the resolved conifold, needs of the introduction of a UV-cutoff (and associated effects) for the existence of a phase transition for the entanglement entropy (even when the Wilson loop displays an area law). A cleaner way of recovering the phase transition that the Klebanov-Strassler system displays [23], will be to appeal to the connection between both systems. This connection is well understood and discussed in the papers [39–41]. It is given by the U-duality described in Chapter 2. It connects both backgrounds and this constitutes the string/geometric version of an inverse Higgs mechanism; see the discussion in the paper [40].

is due to the boundary condition for the strings at infinity, that cannot be satisfied. See [56]. We will return to this point in Chapter 5

The string frame metric is,

$$ds^2_{str} = \alpha' g_s \sum_{i=1}^{10} (e^{\frac{\Phi}{4}} e^i)^2 \,, \tag{4.3.1}$$

where the vielbeins are given by (2.0.17).

The quantities needed for the calculation of the entanglement entropy are,

$$\alpha = e^{\Phi} \hat{h}^{-1/2}, \quad \beta = g_s \alpha' e^{2k} \hat{h}, \quad V^2_{int} = (2\pi)^6 (\alpha' g_s)^5 e^{4h+4g+5\Phi+2k} \hat{h}^{5/2},$$
$$H = (2\pi)^6 (\alpha' g_s)^5 e^{4\Phi+4g+4h+2k} \hat{h}. \tag{4.3.2}$$

We see that the difference to eq.(4.2.1) is the presence of the factor $\hat{h}$ defined in eq.(2.0.19). This warp factor has a large radius asymptotic given by — see Section 4 of [29],

$$\hat{h} \sim \frac{3N_c^2}{8c^2} e^{-8\rho/3}(8\rho - 1) + ... \tag{4.3.3}$$

and it is precisely this decaying behaviour that will bring back our phase transition. Indeed, we can calculate using eq.(4.1.4), that the small and large asymptotics of the function $L(\rho_0)$ vanish,

$$L(\rho) \sim \mathcal{Y}(\rho) = 2\pi \sqrt{\alpha' g_s} \frac{e^k \sqrt{\hat{h}}}{(4\Phi' + 4g' + 4h' + 2k') + \frac{\hat{h}'}{\hat{h}}}, \tag{4.3.4}$$
$$L(\rho_0 \to 0) \sim \rho_0, \quad L(\rho_0 \to \infty) \sim e^{-2\rho_0/3}.$$

As anticipated, the IR behaviour for $L(\rho_0)$ is the same as the one for the analytic solution $P = 2N_c\rho$ or the semi-analytical one connecting (2.0.14) and (2.0.15); this is because the warp factor $\hat{h}$ is constant for small radial coordinate. The UV behaviour instead, is quite different and driven by the factors of $\hat{h}$ in eq.(4.3.2). Notice also, that in a convenient radial variable $r = e^{2\rho/3}$, we have

$$L(r_0 \to \infty) \sim \frac{1}{r_0}. \tag{4.3.5}$$

This is a signal of 'locality' according to [49]. The UV-completion provided by the baryonic branch field theory has recovered locality. What about the phase transition in the EE?

Calculating with the expressions of eq.(4.3.2), the entanglement entropy associated with the Baryonic Branch of the KS-field theory gives the result displayed in Figure 4.10.

As one can see, here we get the nice phase transition behaviour, also expected from the calculation in the paper [23]. The intuitive description of what is going in terms of a Van der

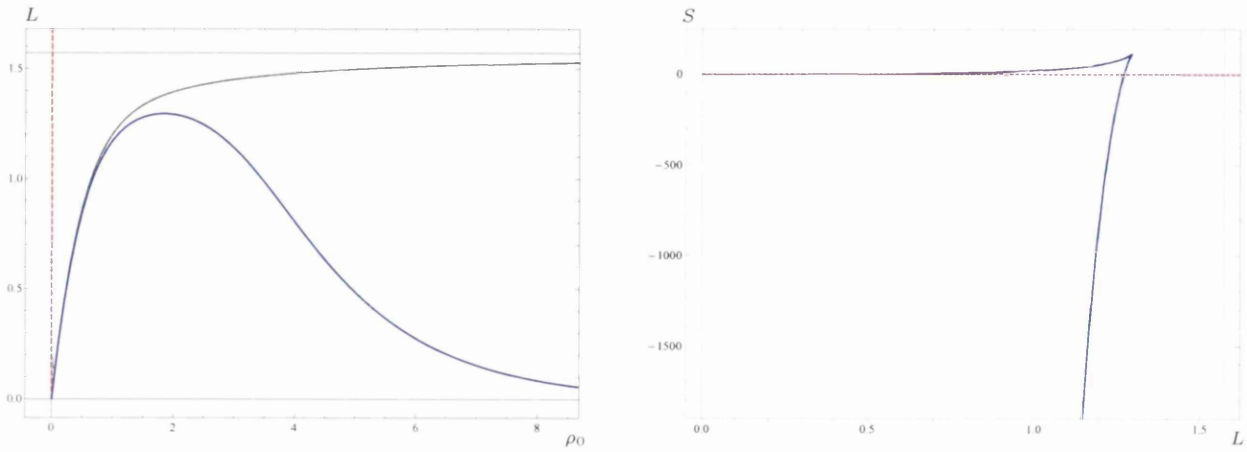

Figure 4.10: A typical solution on the Baryonic Branch of Klebanov-Strassler ($h_1 = \frac{203}{100}N_c$) — Here we plot $L(\rho_0)$ and $S(L)$. The grey line is the linear P solution ($h_1 = 2N_c$) for comparison.

Waals gas analogy* is consistent with this result as well. Figure 4.11 serves as a good summary of the discussion in the previous and the present sections.

We have settled the problem of recovering the phase transition. We would like now to do a couple of calculations that will lead to an improved understanding of the Klebanov-Strassler system (in nice agreement with the ideas presented in [57]). We will move our field theory to a mesonic branch. We will do this first in a way, that as was argued in [39], implies that towards high energies the evolution of the QFT is described in terms of Seiberg dualities, but more importantly successive Higgsings that change the matter content very fast. This quick growth of the matter content is equivalent to the addition of another irrelevant operator (of dimension-six in this case, different from the dimension-eight one we have discussed above). This was discussed in detail in [39] and [29] and presented in section 2.1.

As a consequence of the insertion of this new irrelevant operator, with the added non-localities to the QFT, we will loose the phase transition achieved (in nice agreement with the discussion of the previous section). We will then explain how to get the phase transition back, with a precise way of switching off that irrelevant operator. We turn to that now.

4.3.1 Losing our Phase Transition: Adding Sources

As described above, we now study our Klebanov-Strassler QFT in the mesonic branch.

We have seen in Chapter 2 that eq. (2.1.8) implies the insertion of a dimension 6 operator, making the QFT lose its $4 - d$ character.

*Please see Section 5.3 for more details.

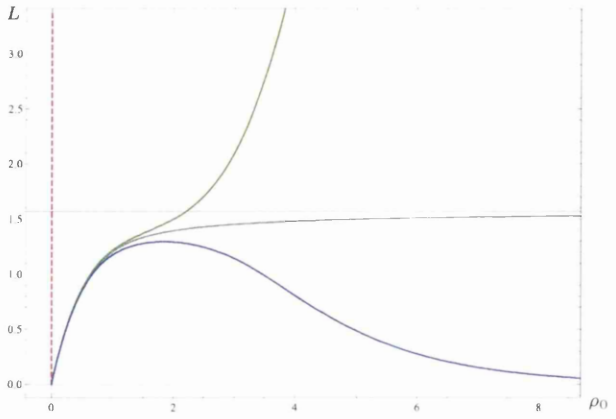

Figure 4.11: These are various plots of $L(\rho_0)$ for comparison. The grey graph is the solution $P = 2N_c\rho$ with linear dilaton. The green and blue lines represent numerical solutions before and after the U-duality respectively (solved for the same value of $h_1 = \frac{203}{100}N_c$ with asymptotically constant dilaton.

Aside from this, the calculation of the Wilson loop in the solution mentioned above will produce an area-law behaviour, indicating confinement, see Section 5.2. Following the logic of the previous sections, we should expect that in spite of the confining behaviour, a phase transition in the entanglement entropy is wiped-off by the irrelevant operator (the presence of this irrelevant can also be associated with finite-size effects in computing the Wilson loop).

This is indeed the case as one can explicitly calculate. While the small radius asymptotics for $L(\rho_0 \to 0) \sim \rho_0$ is unchanged, we obtain that

$$L(\rho_0 \to \infty) = \mathcal{Y}(\rho \to \infty) \sim \frac{3\pi\sqrt{\alpha' g_s N_f}}{8}.$$

Figure 4.12 illustrates this point, with $\rho_* = 0$, so no phase transition, unless of course a UV-cutoff is introduced and the study of 'short configurations' sorts out the problem as in the examples above.

This brings us to the conclusion that the field theory may be in a mesonic branch with good IR properties, but that we should look to somewhat 'localise' the sources to avoid this 'too-fast growth of degrees of freedom' expressed in eq.(2.1.9), if we wish to recover the high energy 4-d behaviour the baryonic branch was displaying (which is UV completing the system). We discuss this in the next section.

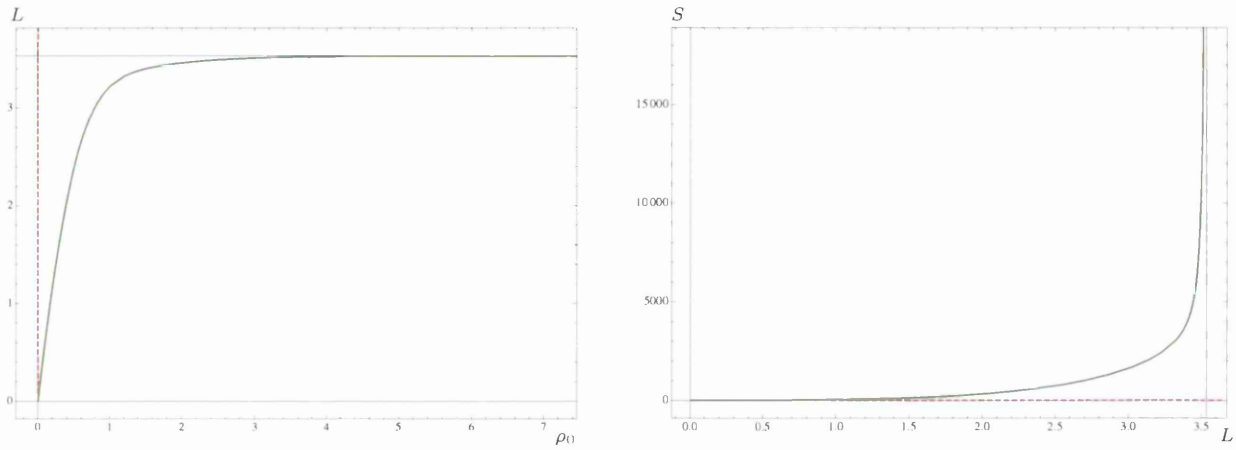

Figure 4.12: Plots of $L(\rho_0)$ and $S(L)$ for a solution with $\mathcal{S} \to N_f$ in the UV and $N_c = 4$, $N_f = 9$. No phase transition is present. Note that we have chosen a value of h_1 such that we have hardly any linear behaviour in P.

4.4 Getting Back the Phase Transition(s): Sources with a Decaying Profile

In the solution with source profile $\mathcal{S} \sim \tanh(2\rho)^4$, the rate of Higgsing becomes too fast at high energies, the UV of the field theory does not behave like a 4-d QFT. This is reflected in the entanglement entropy, which does not display the nice phase transition achieved in Section 4.3.

The profile we will adopt, following [29] is,

$$\mathcal{S}(\rho) = N_f \tanh(2\rho)^4 e^{-4\rho/3}. \tag{4.4.1}$$

Notice that now, one can find a new background solution, where the sources are somewhat 'localised'. The dual QFT is in a mesonic branch as explained in [29], where the background solution was explicitly written.

The relevant functions for the calculation of the entanglement entropy are those in eq.(4.3.2). The explicit expressions for the asymptotics (and numerical solutions) of all the participating functions are described in Section 4 of [29]. In particular

$$\hat{h}(\rho \to \infty) \sim \frac{3}{8c^2} e^{-8\rho/3}\Big[N_c^2(8\rho - 1) + 2cN_f - 4N_c N_f \mathcal{S}_\infty\Big] + ...$$
$$\mathcal{S}_\infty = \int_0^\infty d\rho\, \mathcal{S} \tanh(2\rho)^2.$$

Comparing this with eq.(4.3.3) we observe that the functional decay of the warp factor is the

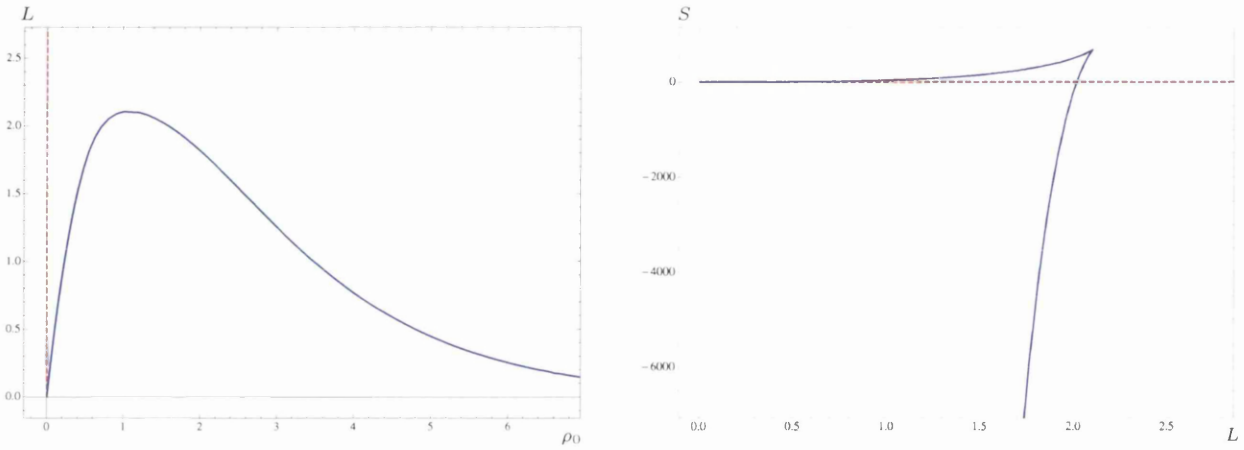

Figure 4.13: Plots of $L(\rho_0)$ and $S(L)$ for a solutions with $\mathcal{S} \to 0$ in the UV and $N_c = 4$, $N_f = 9$. A single first order phase transition is present. Note that we have chosen a value of h_1 such that we have hardly any linear behaviour in P.

same. The cascade of Seiberg dualities is still present (in this radial coordinate is represented by the term $N_c^2\rho$). The constant terms represent the effects of the sources, that even when they are very suppressed at large values of ρ still contribute. Indeed, using the radial coordinate $r \sim e^{2\rho/3}$, they contribute to the warp factor as $\hat{h} \sim \frac{N_f}{r^4}$, which was expected for a localised stack $N_f \sim n_f$ D3 branes.

It is not hard to believe that if we follow the full numerical calculation with the expressions of eq.(4.3.2), we will find a phase transition in the entanglement entropy. This is indeed the case, the plots of Figure 4.13, make this point concrete.

The function $L(\rho_0)$ is well approximated by the function $\mathcal{Y}(\rho_0)$ and satisfies a Heisenberg-like relation, as shown in eq.(4.3.5), with the numerical differences of the case induced by the factors of N_f and $\mathcal{S}_\infty$ in the warp factor $\hat{h}$, and in the other background functions. Still, we have $L(r_0 \to \infty) \sim 1/r_0$, in agreement with the 'locality criteria' proposed in [49].

An interesting observation is that since the sources can be translated at a given point ρ_* as discussed above

$$\mathcal{S}(\rho) = N_f\, \Theta(\rho - \rho_*) \tanh(2\rho - 2\rho_*)^4 e^{-4\rho/3}\,, \tag{4.4.2}$$

we can introduce another scale to the system, represented by ρ_*, the point where the source become 'activated'. Numerical solutions (that are a bit more time-expensive to find) can now show a double phase transition, as can be seen in Figure 4.14 (for further discussion — see Section 4.6).

This is a phenomena that probably was observed in other contexts, but we are unaware of them in the bibliography. There might be gas, generalisation of Van der Waals' one which includes two different interactions of similar strength between the particles composing the gas. This could lead to a double or even multiple first order transitions. The Figure 4.14, illustrate

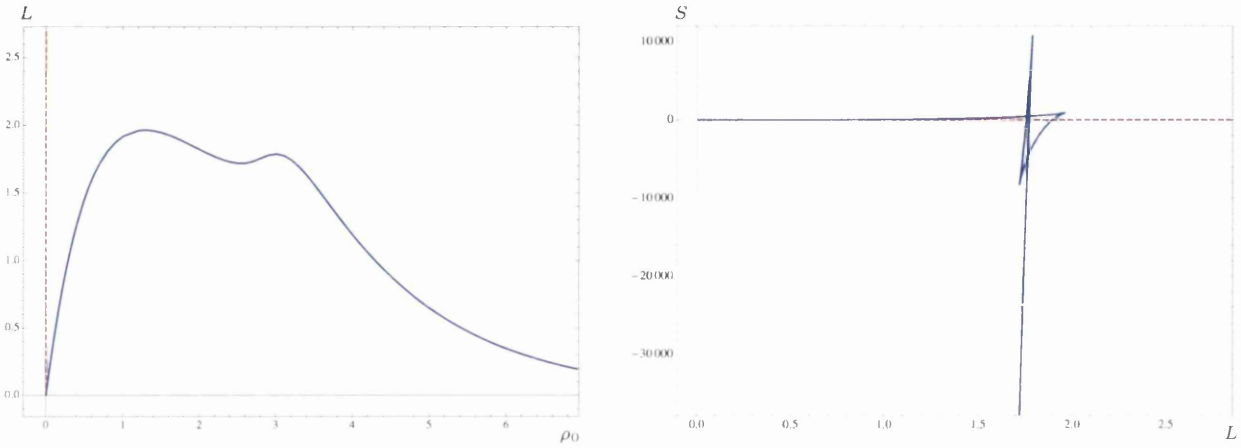

Figure 4.14: Plots of $L(\rho_0)$ and $S(L)$ for a solutions with $\mathcal{S} \to 0$ in the UV and $N_c = 4$, $N_f = 9$ but $\rho_* = \frac{25}{10}$. Two first order phase transitions are present. Note that we have chosen a value of h_1 such that we have hardly any linear behaviour in P.

our results for the entanglement entropy, $L(\rho_0)$ and $S(L)$, when calculated in the mesonic branch of the KS field theory in the presence of a localised bunch of matter represented by a D3-D5 bound state.

We wish to close this section by emphasizing that our findings are clearly making the point of KKM [23]: a phase transition in the EE is a sign of a confining QFT. But one should be careful about the UV behaviour of this field theory. If non-local, either cutoff effects or a UV completion will recover the phase transition. We can also think our findings for the EE as a diagnostic to decide if a QFT is showing or not the high energy behaviour expected from a four-dimensional (or lower) QFT, free of non-localities.

4.5 A Taxonomy of Behaviours for Systems with Sources

Adding sources to the D5 wrapped on a two-cycle as discussed in Sections 4.3.1 and 4.4, creates a rich and complex family of backgrounds, with many free parameters which influence the behaviour of the Entanglement Entropy of the dual QFT. In this section we will systematically

categorize the different cases the parameter space allows.* The behaviour of the Entanglement Entropy is most severely influenced by the following choices:

Rotation - The U-duality/rotation of the $SU(3)$-structure described in Chapter 2, that we will refer to as "rotation" for brevity, will only be applicable to cases where the solution to the 'master' equation exhibits exponential behaviour in the UV—see eq. (2.0.14). However, even after the addition of sources, solutions that are linear in the UV can still be found. In what follows we will make a clear distinction between the linear (and thus unrotated) and rotated exponential behaviour of $P(\rho)$. Note that here we shall not study unrotated exponentially growing solutions, representing QFTs coupled to gravity and string modes, as they are known to require a non-trivial UV completion and in these cases the Entanglement Entropy $S(L)$ will always diverge as in Figure 4.9.

Profile - The second important choice is the type of profile to be used. In what follows we will focus on two types of profile, those profiles in which $\lim_{\rho\to\infty} \mathcal{S}(\rho) = 1$, or those that instead have $\lim_{\rho\to\infty} \mathcal{S}(\rho) = 0$. The first type are given by eq.(2.1.6) and we will refer to profiles of this type as "sigmoid" profiles. The profiles we will adopt for the second case are given by eq.(4.4.1) and will be referred to as "bump-like" profiles.

Thus we will divide this section into 4 subsections, each discussing one possible combination of the above choices. The analysis in each subsection involves the study of the interplay of the three relevant scales in the background:

- ρ_* - The scale at which the source profile $\mathcal{S}(\rho)$ becomes non-zero
- $\bar{\rho}$ - The scale at which P changes from having linear behaviour (when $\rho < \bar{\rho}$) to having exponential asymptotic behaviour (when $\rho > \bar{\rho}$)†
- $x = \frac{N_f}{N_c}$ - the ratio of source branes to color branes present

In each subsection, the discussion will usually start with the case where $\rho_* = 0$, to see what effect the addition of sources has. Once this case is understood, predicting the behaviour of the system with non-zero ρ_* becomes trivial. For $\rho < \rho_*$, the system will behave like the corresponding solution on the Baryonic Branch, and then at ρ_* will smoothly switch to the associated behaviour of the sourced system.

*It should be noted that we will focus here on the connected solution of the EE. In all cases, we chose a renormalisation scheme such that the disconnected case will be a horizontal line at $S = 0$ in the $S(L)$ plots

†Note this only applies in cases with UV asymptotes $P \sim e^{4\rho/3}$ but not in cases with $P \sim \rho$

Further, note that the scale $\bar{\rho}$ is only finite in the rotated case. Thus, in a similar fashion to the discussion in the last paragraph, we know that for $\rho < \bar{\rho}$ the system will behave like its corresponding linear case (with or without the addition of sources). Thus it makes sense to study the linear P solutions with added sources first.

Finally, although we do not always discuss them here directly, the 'short configurations' play an important role in the examples below that exhibit non-locality in the corresponding QFT, in a similar way to the cases presented in the main body of the chapter.

4.5.1 Linear P Sourced Systems with Sigmoid Profiles

All the solutions of this form are such that $L \to \text{const} \neq 0$ from below with no phase transition in $S(L)$ as we move toward the UV. That said, there exists an interesting dependence on $x = \frac{N_f}{N_c}$, with $x = 2$ playing an important role. For $x < 2$ and setting $\alpha' = g_s = 1$ we have,

$$L(\rho_0 \to \infty) = \frac{\pi}{2}\sqrt{N_c}\left(1 - \frac{1}{4\rho_0}\right) + \mathcal{O}\left(\frac{1}{\rho_0^2}\right), \tag{4.5.1}$$

which is while for $x > 2$ we get

$$L(\rho_0 \to \infty) = \frac{\pi}{2}\sqrt{N_f - N_c}\left(1 - \frac{1}{4\rho_0}\right) + \mathcal{O}\left(\frac{1}{\rho_0^2}\right). \tag{4.5.2}$$

For $x = 2$ we get precisely

$$L(\rho_0 \to \infty) = \frac{\pi}{2}\sqrt{N_c}. \tag{4.5.3}$$

We see that for $x < 2$, L approaches $\frac{\pi}{2}\sqrt{N_c}$ (as in the sourceless case), while for $x > 2$, L approaches $\frac{\pi}{2}\sqrt{N_f - N_c}$. In the case of $x = 2$, the UV expansion is exact, indicating that L reaches its bound at a finite value of ρ. Taking into account the analysis of this class of solutions found in [45], this behaviour can be explained through a Seiberg Duality picture, which involves taking the function $Q \to -Q$ and $N_c \to N_f - N_c$, relating solutions below and above $x = 2$. For $x = 2$, we have an invariance under the aforementioned duality transformation, and this effectively freezes the entanglement entropy in place (away from the IR), causing the $S(L)$ plot of this solution (see Figure 4.15) to stop at a finite value and not grow without bound as $S(L)$ for all other solutions of this class.

If we now consider profiles with non-zero ρ_*, for $\rho_0 < \rho_*$, the solution will follow the sourceless case, whose limit is $L \to \frac{\pi}{2}\sqrt{N_c}$, and thus smaller than or equal to the limit of the equivalent solution with sources. This, and the fact that adding sources leads to the solution approaching its UV limit faster than the sourceless solution, guarantees that adding sources at

ρ_* will always cause an increase in L (as shown in Figure 4.15). Hence, it is not possible to produce a phase transition, due to the addition of sources, for these kinds of solutions.

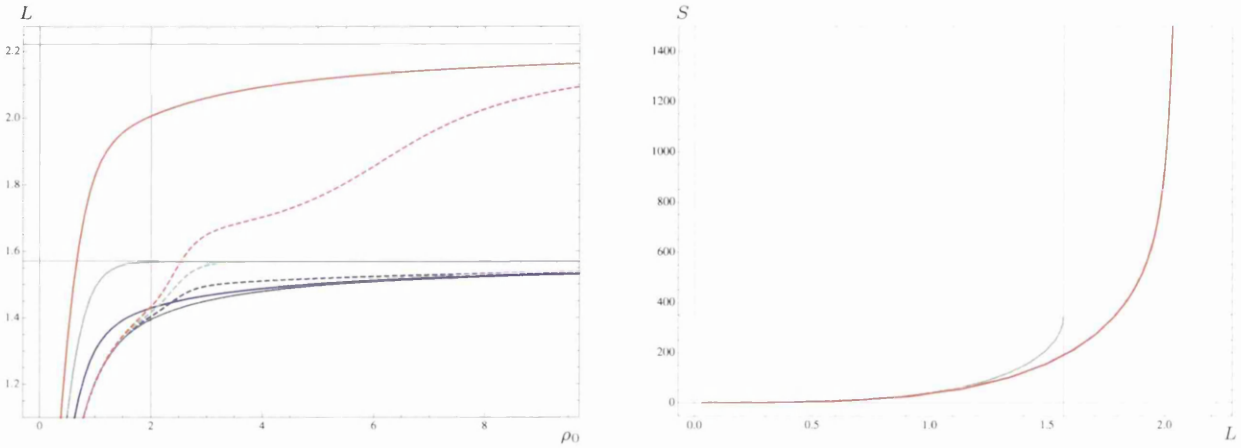

Figure 4.15: Various Plots of $L(\rho_0)$ and $S(L)$ in linear backgrounds with sigmoid source profiles. Continuous lines represent solutions for $\rho_* = 0$, while dashed lines represent $\rho_* = 2$. The colouring is such that the solutions with $x = \{1, 2, 3\}$ are given by {purple, green, red} respectively. The grey line represents the sourceless $P = 2N_c\rho$ solution.

4.5.2 Linear P Sourced Systems with Bump-like Profiles

The most important difference between this and the previous subsection is that the source profile is suppressed in the UV. Thus we expect the deviation from the sourceless case to diminish for large ρ. Nevertheless, the profile still introduces an interesting dynamic into the system, especially when we look at non-zero ρ_*. Although so far we have described this as the scale at which the sources become 'active' (forcing the system to deviate from the sourceless case), it now further dictates the point at which the sources effectively become 'inactive', thus bringing the system back in line with the corresponding sourceless case.

A simple check agrees with the above analysis: in all cases we have $L \to \frac{\pi}{2}\sqrt{N_c}$ in the UV, as expected. As in the previous subsection, the behaviour has an interesting dependence on x. For low x, we see no phase transition, only a small deformation on L around ρ_* is noticeable. But for large enough x, this deformation becomes sharp enough such that a local maximum forms in L, and thus a we have a phase transition in $S(L)$. The critical value x_c at which a phase transition forms is a monotonically decreasing positive-definite function of ρ_*. This is logical as a deformation in L means a change in L'. As we can see from Figure 4.7, L' is a monotonically decreasing positive-definite function, so at larger ρ any effect in L is more pronounced. It is

possible to estimate the value at which a phase transition is introduced. For $\rho_* = 0$, the critical value is $x_c \approx 5.3$, while for $\rho_* = 2$, $x_c \approx 2.3$ already.

Further, it should be noted that while we are able to form a phase transition via the addition of sources, the fact that L in the UV approaches a finite limit from below (which we term L_{UV}), guarantees that for every first order phase transition, from the disconnected to the connected solution, would be accompanied by a discontinuous jump, from the continuous solution back to the discontinuous solution. Thus, here we again require the introduction of the branch of solutions living close to the boundary (that we termed 'short configurations'), which will remove the problem, as it is the preferred branch for $L < L_{UV}$.

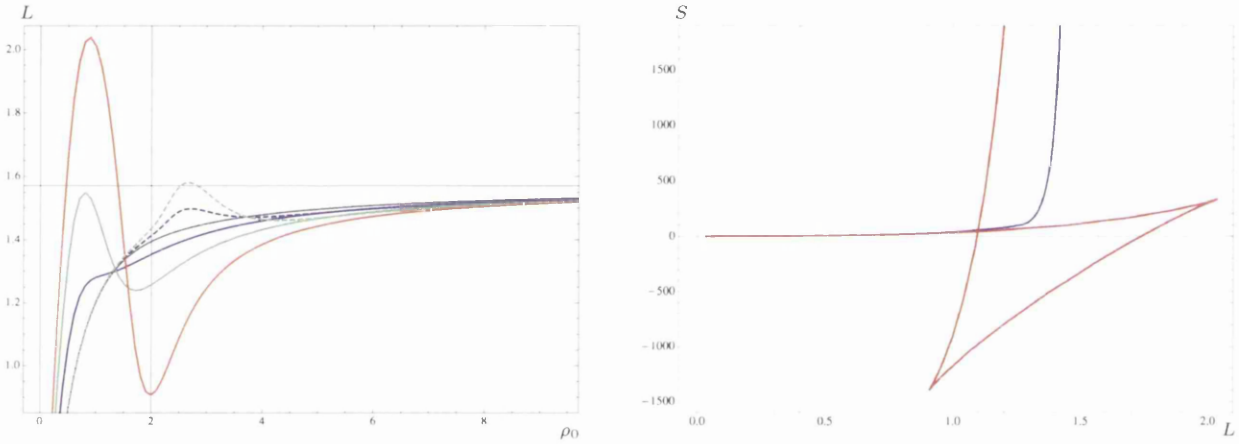

Figure 4.16: Various Plots of $L(\rho_0)$ and $S(L)$ in linear P backgrounds with bump-like source profiles. Continuous lines represent solutions for $\rho_* = 0$, while dashed lines represent $\rho_* = 2$. The colouring is such that the solutions with $x = \{5, 10, 15\}$ is given by {purple, green, red} respectively. The grey line represents the sourceless $P = 2N_c\rho$ solution.

4.5.3 Rotated Sourced Systems with Sigmoid Profiles

All solutions of this class share the following UV asymptotics for L:

$$L(\rho_0 \to \infty) = \frac{3\pi}{8}\sqrt{N_f}\left(1 - \frac{(N_f - 2N_c)^2}{4cN_f}\rho_0\, e^{-4\rho_0/3}\right) + \mathcal{O}\left(e^{-4\rho_0/3}\right). \tag{4.5.4}$$

From this we can immediately see that L will always eventually approach $\frac{3\pi}{8}\sqrt{N_f}$ from below. This means there are only the two possibilities (depicted in Figure 4.16): either we will have a phase transition (connected - disconnected) coupled with a discontinuity, or there will be no phase transition at all (disconnected always preferred). Again, bear in mind, that we would

employ the branch of solutions near the boundary to resolve any issues with the stability of the configuration and the above discontinuity, or lack of phase transition.

Let us study in detail which case occurs for different values in the parameter space.* As expected from the van der Waals gas analogy†, we will never find a phase transition when the two scales ρ_* and $\bar{\rho}$ are too close together. Thus we will assume that there always is a large enough separation between the two scales in the following.

First let us assume $0 \leq \rho_* < \bar{\rho}$. We know from our previous analysis that we cannot have a phase transition before $\rho < \bar{\rho}$. We also know that $\lim_{\rho\to\infty} L = \{\frac{\pi\sqrt{N_c}}{2}, \frac{\pi\sqrt{N_f - N_c}}{2}\}$ for $\{x \leq 2, x > 2\}$ respectively and beyond $\bar{\rho}$, L tends to $\frac{3\pi}{8}\sqrt{N_f}$. Thus we can see that L will (for almost all values of x) first approach a larger value than its UV limit, guaranteeing a phase transition. The exception is the range $\frac{16}{9} \leq x \leq \frac{16}{7}$, for which a phase transition does not occur, no matter the separation between ρ_* and $\bar{\rho}$, making the region around $x = 2$ quite special.

Let us study the case $0 \leq \bar{\rho} < \rho_*$. We know that before ρ_* the solution will behave like its corresponding (rotated) sourceless solution. Thus the Entanglement Entropy will behave as depicted in Figure 4.10 in this region. Thus, as long as we push ρ_* sufficiently far away to make sure we pick up the maximum in L, we will always produce a phase transition.

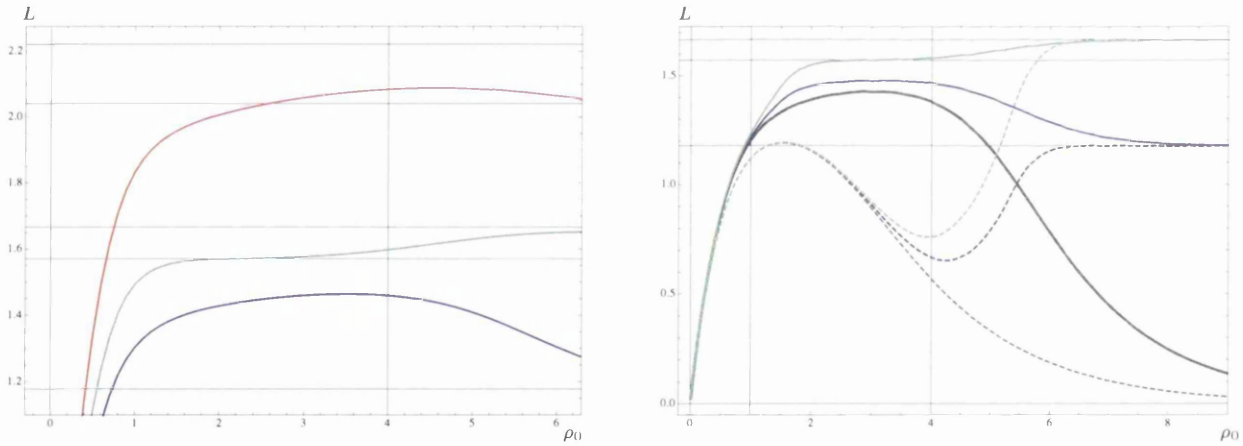

Figure 4.17: Various Plots of $L(\rho_0)$ in rotated backgrounds with sigmoid source profiles. The left-hand panel shows solutions for $\rho_* = 0$, $\bar{\rho} = 4$. In the right-hand panel, continuous lines are for solutions with $\rho_* = 4$, $\bar{\rho} = 1$, while dashed lines represent $\rho_* = 1$, $\bar{\rho} = 4$. The colouring is such that the solutions with $x = \{1, 2, 3\}$ is given by {purple, green, red} respectively. The grey graphs represent the corresponding rotated sourceless solutions.

*Keep in mind that as mentioned, for $\rho < \rho_*$ the solution will follow its corresponding (rotated) sourceless case, and for $\rho < \bar{\rho}$ the solution will behave exactly as the solutions discussed so far in this appendix.

†Which we will explain in more detail in Section 5.3

4.5.4 Rotated Sourced Systems with Bump-like Profiles

For all rotated systems with bump-like profile we have $L \to 0$ in the UV. This guarantees that we have at least one phase transition in every case. It turns out, one can construct solutions with two phase transitions, one between the disconnected solution and the connected, and one between two different branches of the connected solution.

As we know for $\rho < \bar{\rho}$ the solution will behave exactly as in Subsection 4.5.2. Thus we know, that we can pick up a phase transition for large x, that is produced through the interplay of the scales where the sources become relevant and are suppressed. Further, now that we have a finite $\bar{\rho}$, we effectively introduce a third scale, and it is exactly this scale that gives us the second phase transition. The phase transition due to $\bar{\rho}$ is always present.

Thus we know that we will always have two phase transitions for $x > x_c$. If we choose a non-zero ρ_*, we additionally need the condition $|\bar{\rho} - \rho_*| \gg 0$. However, there is a third, more subtle condition. It follows from the fact, that while the above conditions are sufficient to produce two phase transitions, it is possible for the system to "overshoot", leading to one of the phase transitions being in the unphysical branches of the Entanglement Entropy. A case like this is presented in Figure 4.18 in the middle-left panel. It is easy to see, that the physical branch of the Entanglement Entropy will contain two phase transitions if the second maximum of L is noticeably lower than the first maximum. Armed with this knowledge we deduce that the third condition is:

- $0 \leq \rho_* < \bar{\rho}$ - x must be very large. The critical value x_{cc} above which we have two phase transition is always larger than x_c. Thus, here, this condition is always strictly stronger than the first one.

- $\bar{\rho} < \rho_*$ - x increases the size of the second bump, so we know that we will have two physical phase transitions only for a bounded range of values of x, namely $x_c < x < x_{cc}$.

Last, but not least it should be noted, that we can increase the number of phase transitions by introducing additional scales. For example, we could use source profiles such as [33]:

$$\hat{s}(\rho) = \begin{cases} \tanh^4(2(\rho-\rho_{*1}))e^{\frac{-4(\rho-\rho_{*1})}{3}} + \tanh^4(2(\rho-\rho_{*2}))e^{\frac{-4(\rho-\rho_{*2})}{3}} & \text{if } \rho \geq \rho_{*2} \\ \tanh^4(2(\rho-\rho_{*1}))e^{\frac{-4(\rho-\rho_{*1})}{3}} & \text{otherwise.} \end{cases} \tag{4.5.5}$$

We will discuss these kinds of profiles also with regard to the Wilson loop, see Section 5.4. Each time we let the sources become relevant again, we will introduce additional phase transitions that can be tuned to lie on the physical branch.

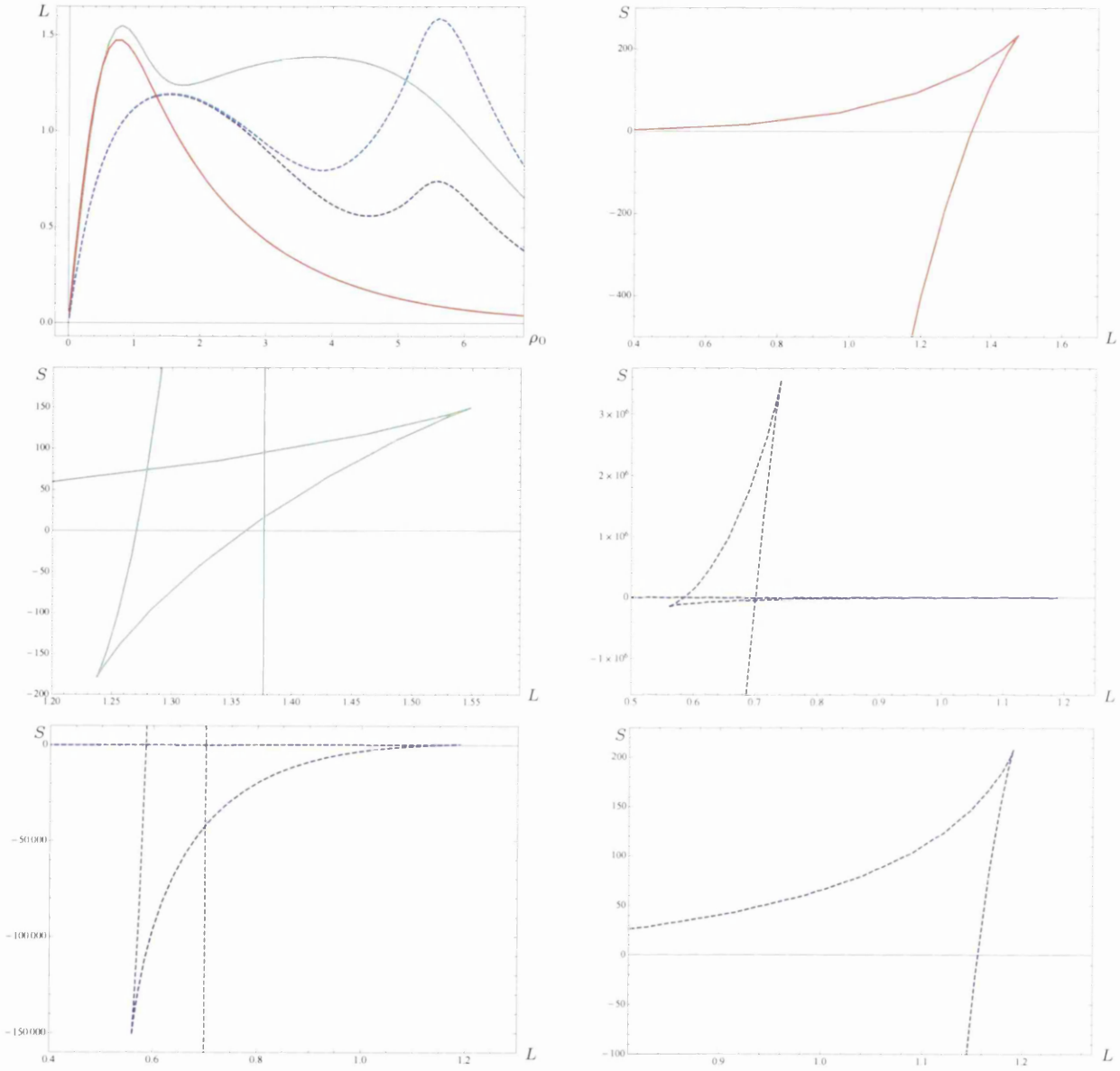

Figure 4.18: In all figures above: continuous graphs have $\rho_* = 0$ and $x = 10$ and dashed ones have $\rho_* = 5$ and $\bar{\rho} = 2$. For the continuous lines, the red line has $\bar{\rho} = 0$, while the green line has $\bar{\rho} = 4$. For the dashed lines, blue indicates $x = 10$ and purple $x = 2$. In all of the panels involving $S(L)$, the disconnected solution lies at $S = 0$, but is not shown. As we can see in the top-right panel, the continuous red solution has a first order phase transition. The left-hand panel in the middle row is an example of overshooting - the branch that is relevant in the dashed purple case between the transitions, is above the disconnected solution and is thus unphysical. The right-hand figure in the middle row represents a solution that has been tuned to have 2 physical phase transitions. The graph has been enhanced in the two panels in the bottom row to clearly show each of the phase transitions.

Notice that in this thesis, we have used the word 'source' branes instead of 'flavour' branes. We made this distinction because in many cases studied here, the fluctuations on the branes (the 'mesons') are non-normalisable, and hence non-dynamical. The connection with studies and ideas presented by the authors in [58] is worth pursuing and is left for future work.

4.6 Other Models without Phase Transitions

Here we will summarise the situation in other known confining models that do not produce a phase transition in the EE, unless of course, a cutoff is introduced as explained in the main body of this chapter.

We will start off by discussing the cases of D5 branes wrapped on a three-cycle and see how it is similar to that of the D5 branes wrapped on two-cycle. We shall then go on to look at the backgrounds discussed in KKM, but modified by changing the warp factor in such a way that can be thought of as adding a relevant operator that changes the UV, but leaves the IR unaffected. We then finally go on to discuss D6 branes wrapped on three-cycle, discuss the similarities, and make a comment about hard cut-offs.

We will notice, that making a more natural choice of the radial coordinate implies, that when $\lim_{\rho_0\to\infty} L(\rho_0) = \infty$, L diverges linearly. This is true for many of the 'divergent' cases we have studied in this thesis. For example, in systems generated by D5 branes, a closer analysis reveals that a coordinate transformation $e^{\frac{2\rho}{3}} = r$ is needed to properly compare those cases to the ones presented below. It is easy to check that this will recover the linear behaviour for $L(\rho_0)$.

4.6.1 D5 on Wrapped on a Three-Cycle

Here we look at the backgrounds presented in [59], and generalised in [60],[61]. We start by defining the ansatz: there are two sets of $SU(2)$ left-invariant 1-forms, σ^i and $\tilde{w}^i$ $(i = 1, 2, 3)$, which obey

$$d\sigma^i = -\frac{1}{2}\epsilon_{ijk}\sigma^j \wedge \sigma^k, \qquad d\tilde{w}^i = -\frac{1}{2}\epsilon_{ijk}\tilde{w}^j \wedge \tilde{w}^k. \tag{4.6.1}$$

Each parametrises a three-sphere, and can be represented by three angles, (θ, φ, ψ),

$$\sigma^1 = \cos\psi d\theta + \sin\psi \sin\theta d\varphi, \quad \sigma^2 = -\sin\psi d\theta + \cos\psi \sin\theta d\varphi, \quad \sigma^3 = d\psi + \cos\theta d\varphi, \tag{4.6.2}$$

and similarly, three angles $(\tilde{\theta}, \tilde{\phi}, \tilde{\psi})$ for $\tilde{w}$, which take a similar explicit form*. Our spheres will also be fibered with a one-form A^i. The A^i take the form

$$A^i = \frac{1}{2}(1+w)\,\sigma^i\,, \tag{4.6.3}$$

where w is a function of the radial coordinate. We can then write down our Type IIB metric ansatz (in Einstein Frame), in terms of the following vielbeins,

$$\begin{aligned} &E^{x_i} = e^f dx_i, \quad E^\rho = e^{f+g}d\rho, \quad E^\theta = \frac{e^{f+h}}{2}\sigma^1, \quad E^\varphi = \frac{e^{f+h}}{2}\sigma^2, \quad E^\psi = \frac{e^{f+h}}{2}\sigma^3, \\ &E^1 = \frac{e^{f+g}}{2}(\tilde{w}^1 - A^1), \quad E^2 = \frac{e^{f+g}}{2}(\tilde{w}^2 - A^2), \quad E^3 = \frac{e^{f+g}}{2}(\tilde{w}^3 - A^3)\,, \end{aligned} \tag{4.6.4}$$

where x_i represents the Minkowski metric in $2+1$ dimensions, ρ is the radial coordinate, and $\{f, g, h\}$ are only functions of ρ. This means we can write the metric compactly as

$$ds_E^2 = \sum_i (E^i)^2\,. \tag{4.6.5}$$

The theory also contain a non-trivial dilaton Φ. There is also a RR three-form F_3 but we shall not require its expression here. From the usual SUSY requirements we find $\Phi = 4f$.

There is a solution generating procedure [62] (similar to the one discussed in the case of D5 branes wrapped on a two-cycle in the main text) which takes us from this solution to one of Type IIA (with extra fluxes). Here we write the relevant parts: we can write our metric in the string frame using $ds_s^2 = e^{\Phi/2}ds^2$, then use an S-duality. The S-duality takes

$$ds_s^2 \to e^{-\Phi}ds_s^2 = ds_{str}^2, \qquad F_3 \to H_3, \qquad \Phi \to -\Phi, \tag{4.6.6}$$

leaving us in the common Type II NS-sector. Then after applying the dualities we generate the following Type IIA solution

$$d\hat{s}_{str}^2 = \hat{h}^{-1/2}dx_i^2 + \hat{h}^{1/2}ds_7^2, \qquad e^{2\hat{\Phi}} = \hat{h}^{1/2}e^{-2\Phi}, \qquad \hat{h} = \frac{1}{\cosh^2\beta}\left(1 - \tanh^2\beta\, e^{2(\Phi-\Phi_\infty)}\right), \tag{4.6.7}$$

where hatted quantities denote the new rotated solution and the unhatted are the original Type IIB functions. Again, we shall not require the explicit forms of F_4 and H_3 for what follows. We can recover the original string frame metric by taking $\hat{h} \to 1$.

*The range of the angles here is $0 \le \theta, \tilde{\theta} < \pi$, $0 \le \varphi, \tilde{\varphi} < 2\pi$ and $0 \le \psi, \tilde{\psi} < 4\pi$.

We again read off the relevant quantities to calculate the EE as

$$V_{\text{int}} = 4\pi^4 \times \hat{h}^{3/2} e^{3g+3h}, \qquad H(\rho) = e^{-4\hat{\Phi}} V_{\text{int}}^2 \alpha^2, \qquad \alpha(\rho) = \hat{h}^{-1/2}, \qquad \beta(\rho) = \hat{h} e^{2g}, \quad (4.6.8)$$

and making the appropriate substitutions we find that

$$\sqrt{H(\rho)} = 2\pi^2 \times \hat{h}^{1/2} e^{3g+3h+2\Phi}, \qquad \sqrt{\beta} = \hat{h}^{1/2} e^{g}. \quad (4.6.9)$$

We can now discuss the behaviour of the EE in each case. For the Maldacena-Nastase (MNa) case, we find the same as in the D5 wrapped on a two-cycle (with linear $P = 2N_c\rho$), such that the separation L grows with ρ_0, and finds a maximum at $L_\infty = \pi/2$. The 'unrotated' case initially follows the MNa behaviour in the IR, but then blows up, whereas the 'rotated' result (which again follows the MNa result up to around the same scale as the 'unrotated'), goes to zero for larger ρ_0. This can all be seen in Figure 4.19.

If you have read this far, congratulations and thank you for showing interest. Email me saying I Know, and next time I see you I will buy you a beverage or send you a card if that is not possible. Have fun!

This means that for the EE, in both the MNa and unrotated case, the disconnected branch is always the lower than the connected branch and thus we require the 'short configurations'. This is not true in the rotated case, where we find a behaviour like that of a first order phase transition (thanks to the presence of the function $\hat{h}$), akin to what happened with the D5 branes wrapped on a two-cycle, after completing the system into the Baryonic Branch solution.

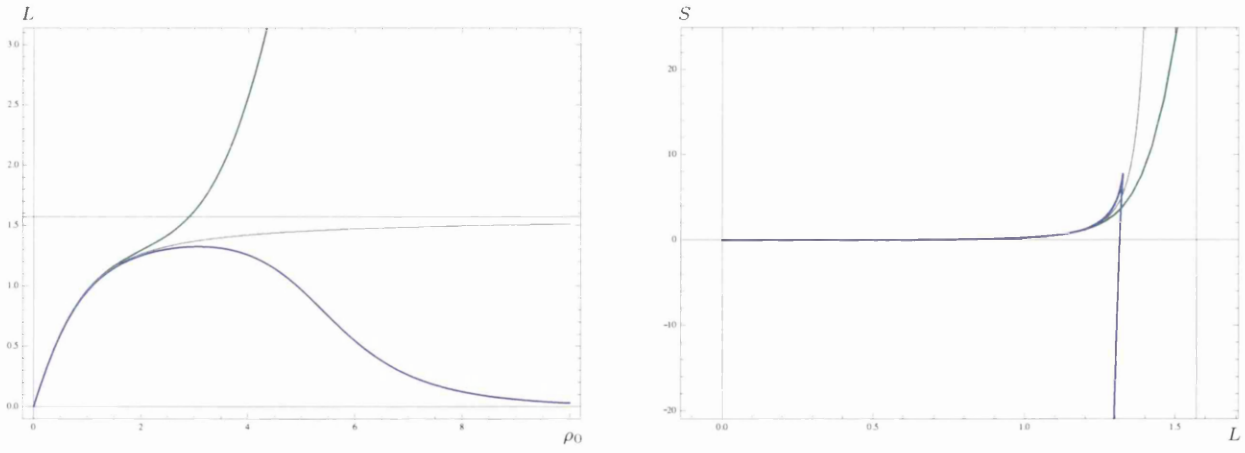

Figure 4.19: Here we have plots of the separation $L(\rho_0)$ on the left and the entanglement entropy $S(L)$ on the right. The MNa background is in grey ($g_0 = 1$), the unrotated in green and rotated in blue (both have $g_0 = 1 + 10^{-2}$).

4.6.2 Deformed D4 on a S^1, D3 on a S^1 and $AdS_5 \times S^5$

Initially, we start with the deformation of the D4 branes on S^1, where we write the metric as

$$ds^2 = \hat{h}(\rho)^{-\frac{1}{2}}\left[dx^\mu dx_\mu + f(\rho)(dx_4)^2\right] + \hat{h}(\rho)^{\frac{1}{2}}\left[\frac{d\rho^2}{f(\rho)} + \rho^2 d\Omega_4^2\right], \quad e^{-4\phi} = \hat{h}(\rho). \tag{4.6.10}$$

We then get as usual

$$\alpha(\rho) = \hat{h}(\rho)^{-1/2}, \qquad \beta(\rho) = \frac{\hat{h}(\rho)}{f(\rho)}, \qquad V_{int}(\rho) = \frac{32\pi^3 R^{\frac{3}{2}}}{9\sqrt{\rho_\Lambda}}\hat{h}(\rho)^{\frac{3}{4}}\rho^4\sqrt{f(\rho)}. \tag{4.6.11}$$

It is easy to check that if we instead choose the warp factor as (this choice emphasizes the 'non-locality' discussed in the main body of the thesis),

$$\hat{h} = 1 + \left(\frac{R}{\rho}\right)^3 \tag{4.6.12}$$

we find

$$\beta(\rho) = \frac{\rho^3 + R^3}{\rho^3 - {\rho_\Lambda}^3}, \qquad H(\rho) = \frac{1024\pi^6\rho^2 R^3\left(\rho^3 + R^3\right)\left(\rho^3 - {\rho_\Lambda}^3\right)}{81\rho_\Lambda}, \tag{4.6.13}$$

where ρ_Λ is the beginning of space. This leads to the behaviour presented in the left-hand panel of Figure 4.20. Note that now, L grows linearly in the UV. This is easy to see if we look at L in the UV as

$$L_{dD4}(\rho_0 \to \infty) = \frac{2\pi\rho_0\left(\rho_0^3 + R^3\right)^{3/2}\sqrt{\rho_0^3 - {\rho_\Lambda}^3}}{8\rho_0^6 + 5\rho_0^3\left(R^3 - {\rho_\Lambda}^3\right) - 2R^3{\rho_\Lambda}^3} \sim \rho_0. \tag{4.6.14}$$

Similarly for the deformed D3, with

$$ds^2 = \hat{h}(\rho)^{-\frac{1}{2}}\left[dx^\mu dx_\mu + f(\rho)(dx_3)^2\right] + \hat{h}(\rho)^{\frac{1}{2}}\left[\frac{d\rho^2}{f(\rho)} + \rho^2 d\omega_5^2\right], \quad e^{-4\phi} = \text{const}, \tag{4.6.15}$$

and $\alpha(\rho)$ and $\beta(\rho)$ as in (4.6.11), but with the warp factor modified as

$$\hat{h}(\rho) = 1 + \left(\frac{R}{\rho}\right)^4, \tag{4.6.16}$$

$$V_{int}(\rho) = \frac{\pi^4 R^2}{\rho_\Lambda}\hat{h}(\rho)\rho^5\sqrt{f(\rho)}, \tag{4.6.17}$$

and thus

$$\beta(\rho) = \frac{\rho^4 + R^4}{\rho^4 - {\rho_\Lambda}^4}, \qquad H(\rho) = \frac{\pi^8\rho^4 R^8\sqrt{R^4 + \rho^4}\left(\rho^4 - {\rho_\Lambda}^3\right)}{{\rho_\Lambda}^2}. \tag{4.6.18}$$

For deformed $AdS_5 \times S^5$, we simply neglected the standard periodic association of the x_3 coordinate (be aware that this leaves a conical singularity at ρ_Λ). As x_3 is not compact, it no longer is a part of V_{int} but of $dx^\mu dx_\mu$. Note that the metric is no longer of the form of (4.0.2). But this can trivially be dealt with by modifying the equation of $H(\rho)$ to

$$H(\rho) = e^{-4\phi} V_{\text{int}}^2 \alpha^d f(\rho) \ . \tag{4.6.19}$$

We get

$$V_{int}(\rho) = \pi^3 \hat{h}(\rho)^{\frac{5}{4}} \rho^5, \qquad H(\rho) = \pi^6 \rho^2 \left(\rho^4 + R^4\right) \left(\rho^4 - {\rho_\Lambda}^4\right) \ . \tag{4.6.20}$$

The results are qualitatively equal to what we found for the deformed D4 on S^1. Choosing the warp factor as we did, causes L to grow linearly in the UV, preventing the phase transition. The UV expansion for L yield the following

$$L_{dD3}(\rho_0 \to \infty) = \frac{\pi \rho_0 \sqrt{\left(\rho_0^4 + R^4\right)^3 \rho_0^4 - {\rho_\Lambda}^4}}{5\rho_0^8 - 2R^4 \left({\rho_\Lambda}^4 - 2\rho_0^4\right) - 3\rho_0^4 {\rho_\Lambda}^4} \sim \rho_0, \tag{4.6.21}$$

$$L_{dAdS}(\rho_0 \to \infty) = \frac{\pi \rho_0 \sqrt{\left(\rho_0^4 + R^4\right)^3 \left(\rho_0^4 - {\rho_\Lambda}^4\right)}}{5\rho_0^8 + 3\rho_0^4 \left(R^4 - {\rho_\Lambda}^4\right) - R^4 {\rho_\Lambda}^4} \sim \rho_0. \tag{4.6.22}$$

The right-hand panel of Figure 4.20 shows the deformed D3 result and the deformed $AdS_5 \times S^5$ behaviour is very similar.

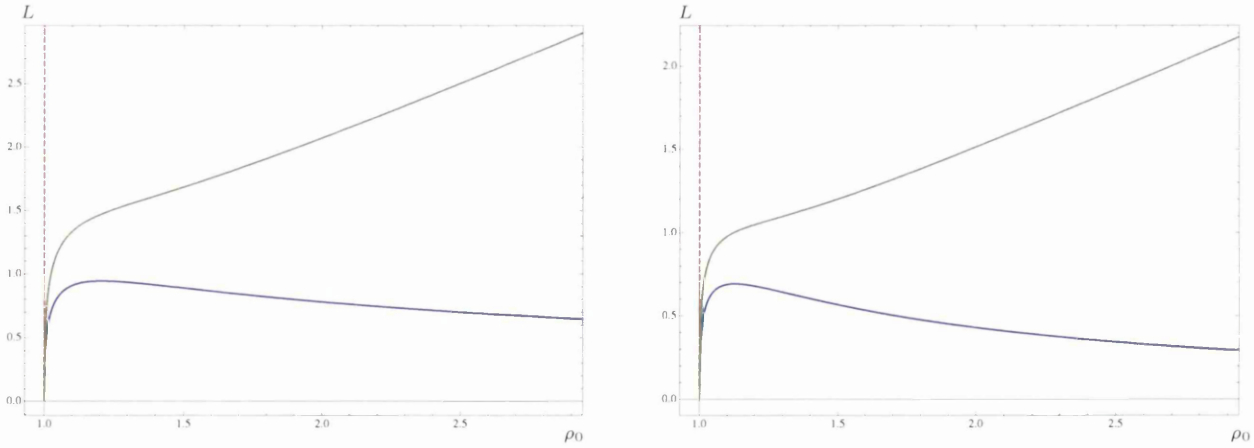

Figure 4.20: In the left panel we have $L(\rho_0)$ for the deformed D4 on S^1 and in the right panel we have $L(\rho_0)$ for the deformed D3 on S^1. The blue lines represented the undeformed solutions compared with those with the deformation in green.

4.6.3 D6 Wrapped on a Three-Cycle

Here we look at the behaviour of the solutions recently discussed in [63]. The full metric and dilaton are given by [64],

$$\begin{aligned} ds^2_{IIA,st} &= Ne^{2\phi/3}\Big[\tfrac{dx^2_{1,3}}{N} + dr^2 + b^2(d\theta^2 + \sin^2\theta d\varphi^2) + \\ &\qquad a^2(\tilde{\omega}^1 + g d\theta)^2 + a^2(\tilde{\omega}^2 + g\sin\theta d\varphi)^2 + h^2(\tilde{\omega}^3 - \cos\theta d\varphi)^2\Big], \qquad (4.6.23) \\ h^2 &= \tfrac{c^2 f^2}{f^2 + c^2(1+g_3)^2}, \\ e^{4/3\phi} &= \tfrac{c^2 f^2}{4Nh^2}. \end{aligned}$$

The background functions a, b, c, f, g and g_3 are determined through the BPS equations

$$\begin{aligned} \dot{a} &= -\frac{c}{2a} + \frac{a^5 f^2}{8b^4 c^3}, \qquad \dot{b} = -\frac{c}{2b} - \frac{a^2(a^2 - 3c^2)f^2}{8b^3 c^3}, \\ \dot{c} &= -1 + \frac{c^2}{2a^2} + \frac{c^2}{2b^2} - \frac{3a^2 f^2}{8b^4}, \qquad \dot{f} = -\frac{a^4 f^3}{4b^4 c^3}, \end{aligned} \qquad (4.6.24)$$

as well as the relations

$$g(r) = \frac{-a(r)f(r)}{2b(r)c(r)}, \quad g_3(r) = -1 + 2g(r)^2. \qquad (4.6.25)$$

The forms of the functions required for the calculation of the Entanglement Entropy are given by

$$\begin{aligned} V_{int} &= \int d^{8-d}y\sqrt{\det[g_{ij}]} = (4\pi)^3 b^2 a^2 h(\alpha' g_s N)^{5/2} e^{5\phi/3}, \\ \alpha &= \mu e^{2\phi/3}, \quad \beta = \frac{\alpha' g_s N}{\mu}, \quad , d = 3, \\ H &= e^{-4\phi} V^2_{int}\alpha^d = (4\pi)^6 \mu^3 b^4 a^4 h^2 (\alpha' g_s N)^5 e^{4\phi/3}, \\ ds^2_5 &= \kappa[dx^2_{1,3} + dr^2], \quad \kappa^3 = H. \end{aligned} \qquad (4.6.26)$$

The solutions in which the dilaton stabilises are interesting because the associated backgrounds do not need an M-theory completion, so we will focus on them. We will re-express the expansion parameters used in [63] as follows*,

$$q_0 = \frac{2}{\frac{1}{2} + c}, \qquad R_0 = \frac{1}{2} + c. \qquad (4.6.27)$$

*keeping $q_0 R_0 = 0$ fixes the normalisation of the dilaton in the IR.

So the parameter space is then defined through c thus we choose to explore the following values for c:

$$c = \frac{3}{2}, \frac{3}{2} + 10^{-5}, \frac{3}{2} + 10^{-1}, \frac{3}{2} + 10^{3}, \frac{3}{2} + 10^{5}. \tag{4.6.28}$$

It appears that $c = \frac{3}{2}$ is a limiting case and the dilaton diverges, while for $c > \frac{3}{2}$ it eventually stabilises. The results are presented in Figure 4.21. Note that in all the cases, L grows without

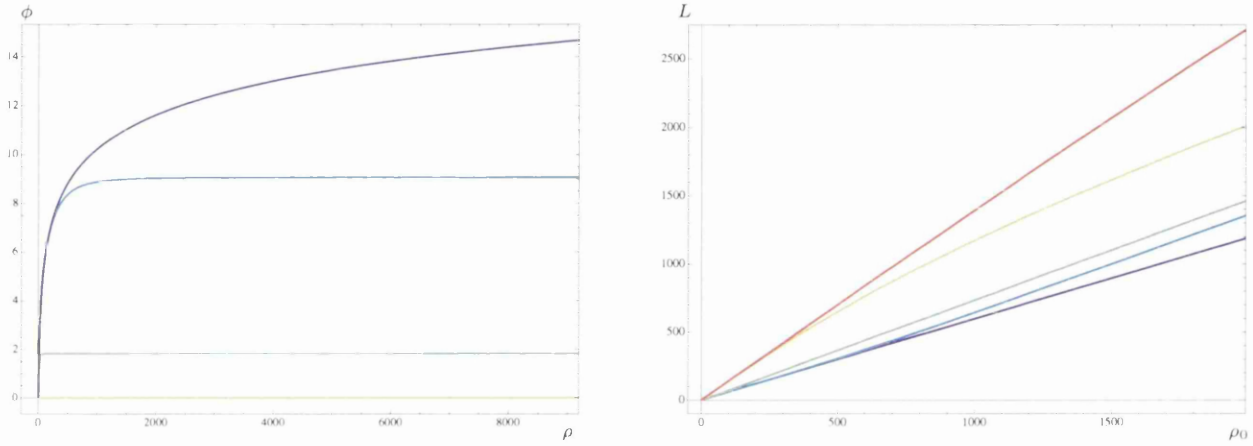

Figure 4.21: Here we have plots of the dilaton in the left panel and the separation $L(\rho_0)$ in the right panel in the backgrounds based on the D6 branes wrapped on a three-cycle. The range of c is given in the text, with $c = \frac{3}{2}$ in purple and larger values c in the range of colours to up to red.

bound for large ρ_0. This agrees with the UV expansion of L which is given by

$$L(\rho_0 \to \infty) = \frac{\pi}{5}\rho_0 - \frac{3}{5}(\pi q_1 R_1) + \mathcal{O}\left(\frac{1}{\rho_0}\right). \tag{4.6.29}$$

In these solutions we find initially that L will shoot off at different gradients depending on c, but eventually curves down to approach a line with the same gradient, but shifted by a constant.

4.6.3.1 Illustrating the Dependence on the UV Cutoff

The equations (4.6.24) also have a known analytical solution [65], that reads

$$\begin{aligned} a(r) &= -\frac{r}{3}\left(1 - \frac{r_\Lambda^3}{r^3}\right), & b(r) &= \frac{r}{2\sqrt{3}}, \\ c(r) &= -\frac{r}{3}\left(1 - \frac{r_\Lambda^3}{r^3}\right), & f(r) &= \frac{r}{2\sqrt{3}}. \end{aligned} \tag{4.6.30}$$

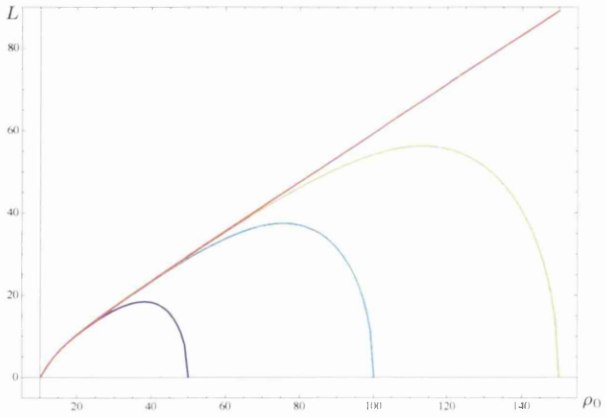

Figure 4.22: These are various plots of $L(\rho_0)$ in the D6 wrapped on a three-cycle solution with $r_\Lambda = 10$. The linear graph is the solution without cutoff, while the other three are numerical solutions with cutoff $50, 100, 150$ respectively.

From this form, one can work out the relevant functions and find that

$$L(\rho_0 \to \infty) = -\frac{2\sqrt{\pi}\Gamma(\frac{5}{12})}{\Gamma(-\frac{1}{12})}\rho_0. \tag{4.6.31}$$

Note that here L also grows linearly into the UV. In the main body of the chapter we discuss the need for additional solutions, especially in backgrounds that have some form of non-locality. We found that these solutions are given by 'short configurations' that never go far from the boundary. In Section 4.1.2, we explicitly mention that one can find these solution by studying the behaviour of the system close to the UV cutoff.

In the cases discussed where L diverges, if we look at the 'short configurations', we find that they change as we vary the UV cutoff. Thus, we may want to think of this as viewing a system with strong IR/UV mixing, which causes the divergence, as discussed in [53],[54] (see to Figure 4.22).

One could easily conclude that this solution has a phase transition, at a particular separation L, for a particular value of the cutoff, when in fact it is entirely cutoff dependent. Another case where the cutoff has caused similar effects was presented in [66].

4.7 Hints at Invariances of the Entanglement Entropy

When calculating the Holographic Entanglement Entropy Density, we always seem to be able to reduce the problem to a one-dimensional system such that

$$\frac{S_A}{V_{d-1}} = \int d\rho \mathcal{L}(\rho, \dot{\rho}) \,. \tag{4.7.1}$$

For backgrounds of the form given in eq.(4.0.2) this is a trivial observation. However, as we will show in the two examples examples, this remains true even for more complicated backgrounds, with warp factors depending on the coordinates of the internal space and various fibrations.

4.7.1 The D4-D8 System

Let us look at the system presented by Brandhuber and Oz in [67], the D4-D8 system. Here the ten dimensional space is a fibration of AdS_6 over S^4. Let us study if this causes complications with the entanglement entropy calculation. The metric can be written as

$$ds^2_{str} = M(\omega) \left[U^2 dx^2_{1,4} + \frac{9Q}{4} \frac{dU^2}{U^2} + Q\, d\Omega_4^2 \right], \tag{4.7.2}$$

where

$$M(\omega) = \alpha' Q^{-1/2} \left[\frac{3}{4\pi} C(8 - N_f) \sin\omega \right]^{-1/3}, \qquad d\Omega_4^2 = d\omega^2 + \cos^2\omega\, d\Omega_3^2, \tag{4.7.3}$$

and the dilaton has a profile given by

$$e^{\Phi} = Q^{-1/4} C \left[\frac{3}{4\pi} C(8 - N_f) \sin\omega \right]^{-5/6}. \tag{4.7.4}$$

Choosing the appropriate 8-dimensional surface $\Sigma_8 = \{\omega, \theta_1, \theta_2, \theta_3, x_2, x_3, x_4, \sigma\}$ and allowing the radial coordinate to be $U = U(x_1)$ and for fixed t we find that the induced metric takes the form

$$ds^2_{\Sigma_8} = M(\omega) \left[U^2 (dx_2^2 + dx_3^2 + dx_4^2) + U^2 dx_1^2 \left[1 + \frac{9Q}{4} \frac{(U')^2}{U^4} \right] + Q \left(d\omega^2 + \cos^2\omega\, d\Omega_3^2 \right) \right]. \tag{4.7.5}$$

We can then write

$$\sqrt{\det g_8} = \sin^2\theta_1 \sin\theta_2\, M(\omega)^4\, \cos^3\omega\, U^4 \left(1 + \frac{9Q}{4} \frac{(U')^2}{U^4} \right)^{1/2}. \tag{4.7.6}$$

From here it is easy to see that we can perform the integrals in the action for the entanglement entropy and the result will be of the form

$$S = 2\pi^2(\alpha')^4 \left[\frac{3}{4\pi}C(8-N_f)\right]^{1/3} \frac{Q^{1/2}}{C^2} \times \frac{9}{20}\int \mathrm{d}\sigma\, U^4 \sqrt{1+\frac{9Q}{4}\frac{(U')^2}{U^4}}\,, \tag{4.7.7}$$

where the last part which is now in the usual form (the factor of $\frac{9}{20}$ comes from the ω integral) and is the standard result for AdS_6. Thus the D4-D8 system can be solved using the method we have employed previously.

4.7.2 A Background with a Cyclic RG Flow

We now turn our attention to the setup described by Balasubramanian in [68]. In this paper they construct non-singular solutions of a six dimensional theory which is a warped product of AdS_5 and a circle. These solutions have very non-trivial warp factors which break the symmetries of AdS_5 to discrete scale invariance and also break the translational symmetry along the circle. Let us study if these causes troubles in our calculation of the entanglement entropy of a strip. The metric takes the form

$$ds_6^2 = e^{2C[\omega,\theta]}\left[e^{2\omega/L}(-dt^2+dx_i^2)+d\omega^2\right] + e^{2B[\omega,\theta]}(d\theta+\mathcal{A}[\omega,\theta]d\omega)^2\,, \tag{4.7.8}$$

where the functions B, C and $\mathcal{A}$ are non-trivial functions of the Jacobi Elliptic functions $\mathfrak{sn}$, $\mathfrak{cn}$ and $\mathfrak{dn}$, that are defined in Appendix A of [68]. Their exact form will not be important in what follows. We are interested in whether the mixing in the metric due to the fibration represented by $\mathcal{A}$ causes any issue in the calculation of the EE. If we calculate the form of the corresponding pullback of the metric onto the now 4-dimensional surface $\Sigma_4 = \{x_2, x_3, x_1, \theta\}$, and setting the radial coordinate $\omega = \omega(x_1)$ we find that when we take the determinant it gives

$$\sqrt{\det g_4} = e^{B[\omega,\theta]+3C[\omega,\theta]+\frac{3\omega}{L}}\sqrt{1+e^{-\frac{2\omega}{L}}(\omega')^2}. \tag{4.7.9}$$

From this we see that there are no terms involving the function $\mathcal{A}$ and that this again falls into the simple form and we can again use the standard procedure.

Chapter 5

Wilson Loops

So far we have used entanglement entropy in the study of confinement in holographic field theories. Another important operator in the study of confinement is the Wilson Loop [25]. It has first been introduced to help with the study of confinement in QCD. It has been known — see [69] — that if the Wilson loop shows an "Area Law" behaviour, we have confinement. In the setup of the rectangular Wilson loop, see Figure 5.1, we expect $E(L) \sim L$ for large L in a confining theory. We will compute the Wilson loop for the family of backgrounds introduced in Chapter 2. We will confirm the confining nature of the dual field theories, as discussed in Chapter 4. We will also comment on the 'sicknesses' of certain solutions and how they are affecting the Wilson Loop. Finally, we will notice the existence of first order phase transitions and discuss why they are occurring. We will use this knowledge to construct multiple phase transitions, which gives evidence to the validity of our interpretation and opens up possible avenues into future research.

5.1 General Theory

Here, I will discuss how to compute Wilson loops, as well as the potential energy of the $q\bar{q}$-pair using the ideas from above for holographic theories. The following is based on [24]. Consider a 10d spacetime of the form:

$$ds^2 = -g_{\mu\mu}(\rho)(dx^\mu)^2 + g_{\rho\rho}(\rho)(d\rho)^2 + g_{\theta\psi}(\rho)dx^\theta dx^\psi, \tag{5.1.1}$$

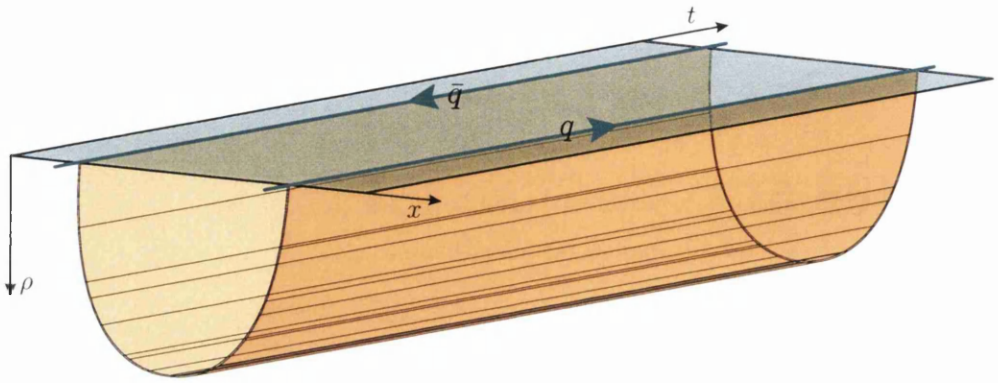

Figure 5.1: A representation of the square Wilson Loop. It involves a quark and an antiquark a distance L apart from each other. We chose a frame such that the separation is along the $x_1 = x$ direction of spacetime. Since we have to take $t \to \infty$ the rectangle, which is comprised of the path of the $q\bar{q}$ pair and their separation, the rectangle will look like a strip. In the Gauge/Gravity correspondence, the Wilson is calculated by the string attached to the $q\bar{q}$ pair. This string will explore the bulk but we restrict it to not explore the compactified internal dimensions. The shape of the string is determined by the extremal to the Nambu-Goto action with appropriate boundary conditions. The worldsheet of the string will create a surface. The area of this surface gives the value of the Wilson loops, and thus the potential of the $q\bar{q}$ pair.

as well as the Nambu-Goto Action

$$S_{NG} = \int d\sigma d\tau \sqrt{\det[\partial_\alpha x^\mu \partial_\beta x^\nu g_{\mu\nu}]}. \tag{5.1.2}$$

Now, since we will be talking about static configuration, we will choose a reference frame that is sometimes referred to as the 'string gauge' [69]

$$\tau = t\,, \qquad \sigma = x. \tag{5.1.3}$$

Using this and disallowing the string to explore then internal space, we can transform (5.1.2) to

$$S_{NG} = T \int dx \sqrt{f^2(\rho(x)) + g^2(\rho(x))(\partial_x \rho)^2}\,. \tag{5.1.4}$$

Where

$$f^2(\rho(x)) = g_{tt} g_{xx}\,, \qquad g^2(\rho(x)) = g_{tt} g_{\rho\rho}\,. \tag{5.1.5}$$

Now, one can either solve the Euler-Lagrange equations of this system or transfer to the Hamiltonian picture and note that the Hamiltonian in the x direction is a constant of motion as the Lagrangian is independent of t. Either way, one will derive the following equation of motion

for the string:

$$\frac{d\rho}{dx} = \pm \frac{f(\rho)}{g(\rho)} \frac{\sqrt{f^2(\rho) - f^2(\rho_0)}}{f(\rho_0)} \,. \tag{5.1.6}$$

From here one can calculate that the length L of the static string configuration connecting two quarks is

$$L(\rho_0) = \int dx = 2 \int_{\rho_0}^{\infty} \frac{g(\rho)}{f(\rho)} \frac{f(\rho_0)}{\sqrt{f^2(\rho) - f^2(\rho_0)}} \, d\rho \,. \tag{5.1.7}$$

Now that we have all the ingredients we need, we can use equation (1.0.12) to obtain $E(L)$, the potential energy of the quark-antiquark pair as a function of their separation. This result is generally divergent, as we have to assume infinite quark masses in order to make the $q\bar{q}$-pair static, which in turn allows us to obtain the rectangular Wilson loops needed. The infinite potential energy can be renormalized by subtracting the mass of the quarks $m_q = \int_0^{\infty} g(\rho) d\rho$. The renormalized result is

$$E(\rho_0) = f(\rho_0) L(\rho_0) + 2 \int_{\rho_0}^{\infty} \frac{g(\rho)}{f(\rho)} (\sqrt{f^2(\rho) - f^2(\rho_0)} - f(\rho)) \, d\rho - 2 \int_0^{\rho 0} g(\rho) \, d\rho \,. \tag{5.1.8}$$

Please note that we can make contact with the formalism of Chapter 4 if we define

$$g(\rho) \equiv \alpha(\rho) \sqrt{\beta(\rho)} \,, \qquad\qquad f(\rho) = \alpha(\rho). \tag{5.1.9}$$

Following this formalism we can follow the same analysis leading to

$$E_{WL}(\rho_0) = 2 \int_{\rho_0}^{\infty} \frac{g(\rho)}{\alpha(\rho)} \sqrt{\frac{\alpha^2(\rho)}{1 - \frac{\alpha^2(\rho_0)}{\alpha^2(\rho)}}} - 2 \int_{\rho_\Lambda}^{\infty} d\rho g(\rho). \tag{5.1.10}$$

The authors of [24] found that the background admits linear confinement if one of the following conditions is satisfied;

$$\begin{aligned} &1. \quad \alpha\,(\rho) \text{ has a minimum} \\ &2. \quad g\,(\rho) \text{ diverges} \end{aligned} \tag{5.1.11}$$

and the corresponding string tension is $\alpha(\rho_\Lambda) \neq 0$, where ρ_Λ is either the point where α minimizes or where g diverges.

Now that we have introduced the formalism, we will apply to the confining field theories dual to $D5$ on S^2. We will start with the analytic solution given by $P = 2N_c\rho$ and then study its generalisation, closely following Chapter 2. At every stage we will evaluate equations (5.1.7) and (5.1.8) to illustrate the behaviour of Wilson loops discussed. Afterwards we will construct cases, where the change of E(L) to linear behaviour is started off by a phase

transition. This is then generalised to obtain solutions that produce several phase transitions.

5.2 Wrapped-D5

We study the rectangular Wilson loop for (2.0.11), as well as for rotated* and unrotated numerical solutions connecting (2.0.15) with (2.0.14). In the numerical case, we first solve the master equation using (2.0.15) and its derivative as initial conditions to generate the background. We then obtain the background functions using the relations (2.0.8). We then solve the Nambu-Goto Action, as outlined in Section 5.1 to obtain $L(\rho_0)$ and $E(\rho_0)$ given by (5.1.7) and (5.1.8). These two functions can be combined to give us $E(L)$. This leads to the plots of Figure 5.2.

For the analytical solution $P = 2N_c\rho$ we can see that there is a minimum separation length beyond which the quarks cannot be forced closer to each other. $E(L)$ asymptotes the vertical line $L = \pi$ for small L. In fact, we can easily calculate that

$$L(\rho_0 \to \infty) = \pi \lim_{\rho_0 \to \infty} \frac{g(\rho_0)}{\partial_{\rho_0} f(\rho_0)} = \pi. \tag{5.2.1}$$

This seems to indicate that the quarks are not point-like objects, but have a finite size. This is not very surprising as it is well known that the analytical solution is not dual to a Field Theory, but rather a Little String Theory [35]. This is one way to make sense of the nonlocalities that occur. If the fundamental particles of the theories are now strings and not dots, the nonlocality is due to the fact if something happens to one part of the string, the whole string knows about it instantly.

The dynamics of the numerical solutions mirror $P = 2N_c\rho$ in the IR. This is expected, as P is always linear below the confinement scale. Thus for large L, $E(L) \sim L$ and all cases are dual to confining theories. For the numerical solutions it then changes its behaviour to become exponential, in the order to match the UV expansions (2.0.14). At this point $L(\rho_0)$ starts to increase exponentially for the unrotated case. This is due to the aforementioned irrelevant dimension 8 operator, coupling to gravity and thus causing the unphysical behaviour observed in the UV, where $E(L)$ gets a second solution for large L which grows exponentially. The 'Coulomb like' behaviour that $E(L)$ displays in a healthy theory below the confinement scale is completely absent. After a UV completion given by the rotation, we see that $L(\rho_0) \to 0$ when $\rho_0 \to \infty$ and we recover the Coulomb like behaviour that describes $E(L)$ all the way down to $L = 0$.

*This is how we will refer to the U-duality procedure that acts as a UV-completion, please see Chapter 2 for details.

The analysis in this subsection has been very similar to [40]. However, in that paper, solutions to the master equation (2.0.10) were studied, for which it was assumed that $P \gg Q$. This leads to an IR behaviour of P that is constant to first order and not linear [70]*. This has led to some interesting effects like phase transitions, which for our IR expansion (2.0.15) we have not been able to find. However, their Wilson Loops feature cusps in the string configuration in some regimes of the parameter space that would break down the steepest descent approximation. This is not present in our backgrounds.

Now let us study the background given by equation (2.1.1). The result are given by Figure 5.3. We see that this background is unphysical. As described in Chapter 2, the high density stacking of source branes at $\rho = 0$ cause the IR of the field theory to be singular. The Wilson loop does not even want to explore this region, $E(L)$ has no solutions for large L due to this singularity. Interestingly, $E(L)$ gets a butterfly shape as we have observed for the entanglement entropy for confining theories.

We now have a visual indication of the fact that the way we introduced sources gives us problems. The solution is provided distributing the density of sources according to a profile $\mathcal{S}(\rho)$ so that not all source branes can reach 0. Using the nomenclature of Section 4.5, we know of one profile proven to be allowed by kappa-symmetry, the Sigmoid profile of eq. (2.1.4). The result of the Wilson loop calculations in this background is displayed in Figure 5.4

As one can see, $E(L)$ is defined and linear again for large L. From the perspective of the Wilson Loop, the profile successfully fulfilled its purpose of curing the IR of the field theory. Let us define h_{1c} to be the value of h_1 for which P remains linear in the UV. Note that $h_1 \approx h_{1c}$ here, thus P remains linear for quite some time, resulting in $L(\rho_0)$ plateauing before approaching 0. Nevertheless, for large ρ_0 we have $L(\rho_0) \to 0$. In fact using the UV asymptotics listed in Chapter 4 of [29] we can calculate that $L \sim e^{\frac{-4\rho}{3}}$. Thus the Wilson Loop seems to be oblivious to the UV nonlocalities, unlike the EE.

We move on to our phenomenological bump-profiles that make the theory local again. We have observed that the results obtained from using the profiles (2.1.10) and (2.1.11) are virtually the same. However, using the profile of (2.1.11) is far more taxing for the numerics. Thus, we will concentrate on (2.1.10) for the rest of the chapter. We observe that we get a very similar picture to the previous analysis, see Figure 5.5.

As we can see, the behaviour of the Wilson loop is as expected for a confining theory, and no area of concern can be found due to the study of this observable in this background. Note

*Recall from Chapter 2 that we focus on solutions for which $c_0 = 0$. Their limit requires $c_0 > 0$

that, as described in [29] and Section 2.1, all profiles used in this paper lack a rigorous proof of existence, as the profiles are not derived from a kappa-symmetric embedding. However, the healthy behaviour of the backgrounds found in this and other works on these backgrounds suggests that they are nonetheless physically relevant.

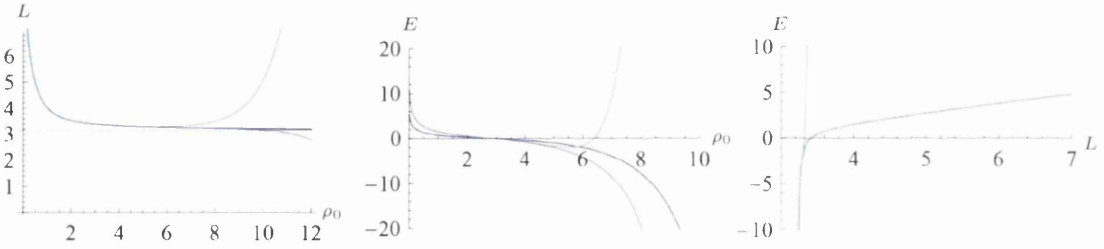

Figure 5.2: Purple represents $P = 2N_c\rho$, while green and blue are unrotated/rotated numerical solutions respectively. For the constants we chose $N_c = 1$, $\Phi_0 = 0$ and $h_1 = 2 + 10^{-10}$

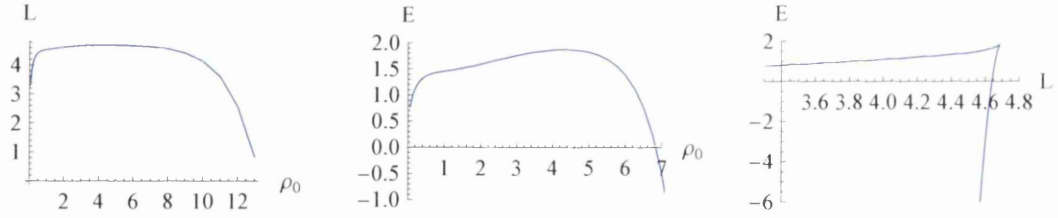

Figure 5.3: $\Phi_0 = 0$, $N_c = 1$, $N_f = 1$ and $h_1 = 4$

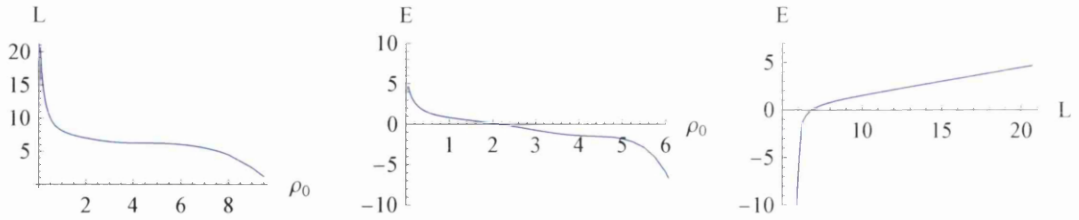

Figure 5.4: $\Phi_0 = 0$, $N_c = 5$, $N_f = 2$ and $h_1 = 11$

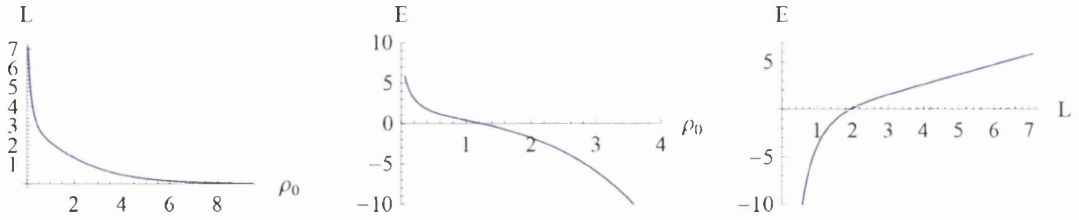

Figure 5.5: $\Phi_0 = 0$, $N_c = 1$, $N_f = 1$ and $h_1 = 3.12932$

5.3 Phase Transition

An interesting observable phenomenon that can be found is a phase transition. This was first observed for SQCD-like field theories in [71]. The interpretation of such a phenomena is similar to the phase transition of a boiling Van-der-Waals gas. Several other papers have found such a phenomena in similar cases since. See for example [43, 56, 72–74]

In order to find them for the theory discussed here, the parameter space of varying h_1 was explored. We remind again that not all values of h_1 are valid. There always exists a critical value for h_1, for which P grows linearly. For $h_1 > h_{1c}$, P grows exponentially in the UV and for $h_1 < h_{1c}$, P dies down to a singularity. Note Figure 5.6.

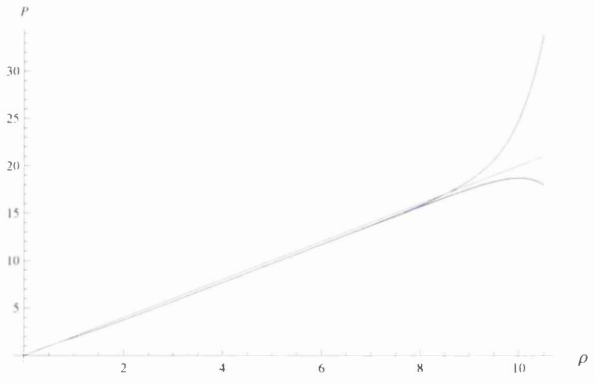

Figure 5.6: The green line represents P for h_{1c}, red $h_{1c} + \epsilon$ and blue $h_{1c} - \epsilon$

Our requirement for Φ to be bounded only allows exponentially growing solutions like the red curve. Thus a shooting procedure was used to find h_{1c}, which was used as starting value for our exploration into ever increasing values of h_1. Exploring this parameter space did not

yield any phase transitions for the three profiles (2.1.4), (2.1.10) and (2.1.11) mentioned above.

To see how to proceed from here, let us analyse that Van-der-Waals gas analogy from the beginning of the section more closely. Such a gas follows an equation of state of the form

$$P = \frac{NRT}{V - bN} - \frac{N^2 a}{V^2}\,, \tag{5.3.1}$$

where R, b, a are constants. Look at the diagrams 5.7*

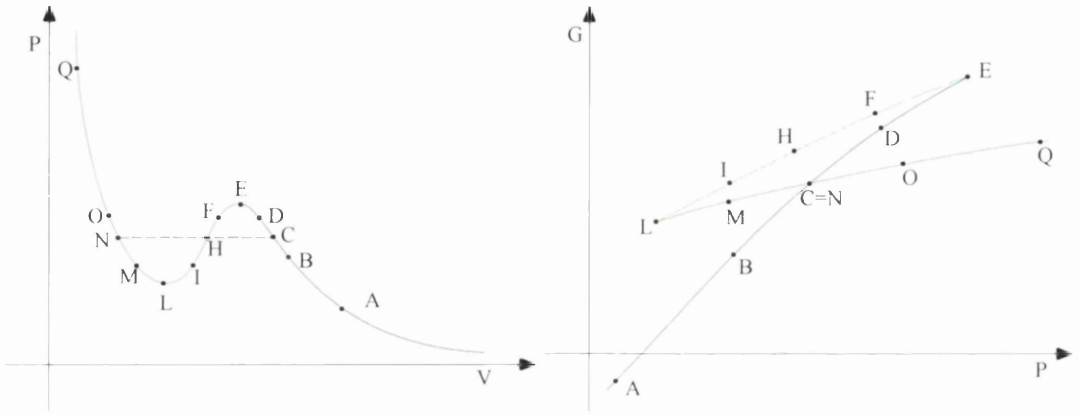

Figure 5.7: The pressure P as a function of the volume V (left panel) and the Gibbs free energy G as a function of the pressure P(right panel) for the same isotherm curve.

Clearly this analogy works by linking $L(\rho_0)$ to $P(V)$ as well as $E(L)$ to $G(P)$, such that $L \leftrightarrow P$, $\rho_0 \leftrightarrow V$ and $E \leftrightarrow G$. On the VdW side, it is clear that a phase transition will be observed, if $P(V)$ has a local maximum. This can be achieved by tuning two scales, dictated by the constants a and b, representing the interaction between the VdW gas particles and their non-zero size respectively. We have so far only explored a 1-dimensional parameter space. We will need to find another scale to adjust.

One thing one can try is to let the source branes not quite reach 0 but only start at some point ρ_*. This is easily achieved by multiplying the profile with a step function $\Theta(\rho - \rho_*)$ and performing the coordinate transformation $\rho \to \rho - \rho_*$. So, for example, our bump profile becomes $\mathcal{S}(\rho) = \Theta(\rho - \rho_*)\tanh(2\rho - 2\rho_*)^4 e^{-4(\rho-\rho_*)/3}$. This shift still preserves SUSY.

Numerically, one can simply solve the unflavoured system between 0 and ρ_* and then connect the system by using $P_{\text{unfl}}(\rho_*) = P(\rho_*)$ and $P'_{\text{unfl}}(\rho_*) = P'(\rho_*)$ as initial conditions for the flavoured system. As shown in [43] this is justified if $\mathcal{S}'(\rho_*) = \mathcal{S}''(\rho_*) = 0$ which is true in our cases.

*The authors of [56] graciously allowed the use of these figures in this work.

Here, a phase transition can be found regardless of which profile has been used. When we studied the parameter space in detail, we found that as we increased h_1, $L(\rho_0)$ began to flatten in the region just below ρ_* until a peak appeared that kept getting more pronounced. See Figure 5.10. This behaviour was so typical that we conjecture that given any acceptable profile and $\rho_* > 0$ a phase transition can be found for this system. As an example look at the Figure 5.8.

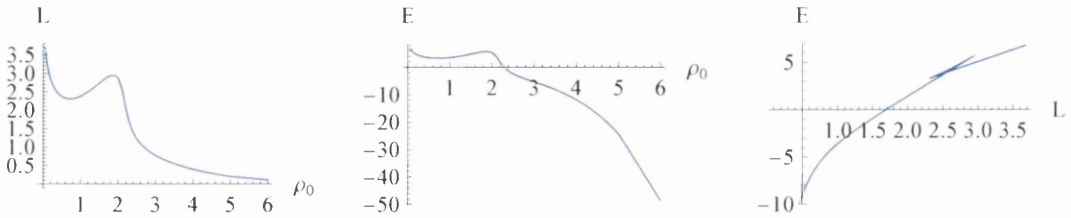

Figure 5.8: Here, $S(\rho) = \frac{\tanh^4(2(\rho-\rho_*))}{(\sinh(4(\rho-\rho_*))-4(\rho-\rho_*))^{\frac{1}{3}}}$, $\Phi_0 = 0$, $N_c = 1$, $N_f = 1$, $h_1 = 27$ and $\rho_* = 2$.

The position of the phase transition is not random and has a nice physical interpretation. Before the phase transition the string explores only the sourceful region, while afterwards a majority of the string is located in the sourceless region $\rho < \rho_*$. Thus the phase transition appears as more and more of the string enters the sourceless part. With an analogy to the Van-der-Waals phase transition, which occurs because first energy has to be exerted to break the intermolecular bonds of the liquid, before heating can continue, now 'energy' has to be exerted to push more and more of the string into the sourceful region, before the string can continue exploring the space below. This changes the geometry of the string. Please see Figure 5.9. It is exactly this change in geometry that causes the phase transition. Please note that all phase transition discovered in this chapter are first order phase transitions.

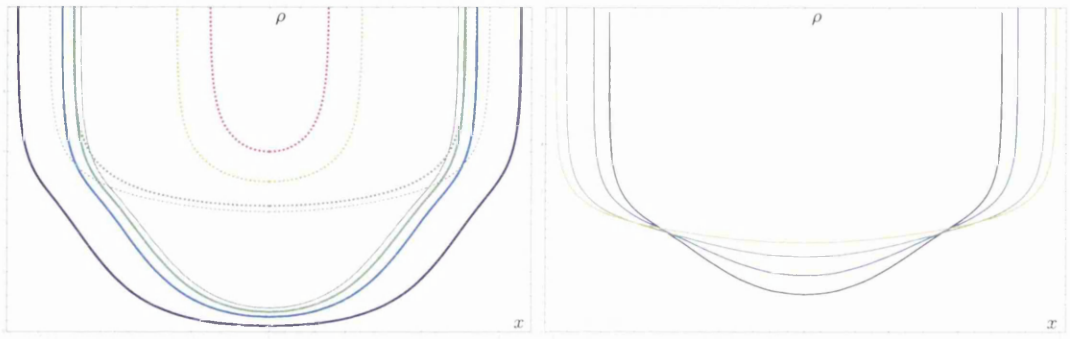

Figure 5.9: The diagrams shows the string for the exact system described in Figure 5.8. The left diagram shows the geometries before the confinement scale as dashed lines. The geometry after the confinement scale is given by solid lines. We chose colours such that when we increase the width L of the $q\bar{q}$ pair, we will follow the colour wheel. We start with the red string, move over yellow to green. The green configuration lies at the phase transition. The dashed green configuration transforms into the solid green one. If we seperate the quarks further we observe configuration blue then purple. Two gray graphs show configurations in the superheated/supercooled branches of the transition. On the right we see configuration that lie on the unphysical branch of the phase transition ($E \to L$ of Figure 5.7). While these configurations are not realised in practise, they can serve as an illustration of the change in geometry happening at the transition point.

For a given ρ_*, the value of h_1 that produces a phase transition is only bound below. This also has a nice physical picture associated to it. h_1 is directly related to $c+$, the expansion parameter of the UV asymptotes of P (2.0.14). $c+$ in turn is related to the scale at which P stops being linear and starts growing exponential. Please note that in Chapter 4 this scale was referred to as $\bar{\rho}$. This in turn effects the gradient of $E(L)$ and thus the "speed" with which the string hits the sourceless region. For a more pictorial description, the reader may imagine a light ray getting refracted on a block of glass due to the fact that it is slowed down by the medium. The higher h_1, the sooner P becomes exponential, and the "faster" the string hits the sourceless region. Above a certain threshold, which we will refer to as h_{1t}, we observe phase transitions.

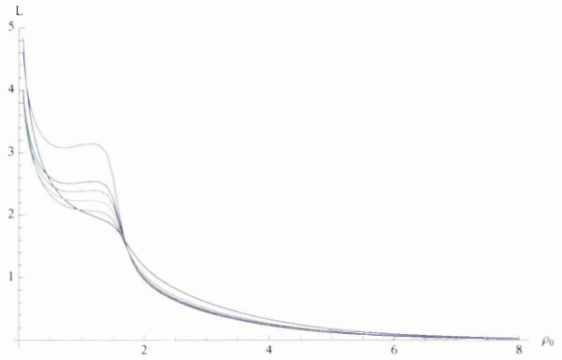

Figure 5.10: $L(\rho_0)$ for the exact same system for $h_1 = h_{1c} + 5$ at the bottom, till $h_1 = h_{1c} + 45$ in increments of 10 and then at the top for $h_1 = h_{1c} + 100$.

As the gradient of $L(\rho_0)$ grows to ∞ as $\rho_0 \to 0$, it is clear that the threshold for producing phase transitions, h_{1t}, also grows to ∞ as $\rho_* \to 0$. This relationship between $\frac{dL(\rho_0)}{d\rho_0}$ and h_{1t} exists as h_1 represents how much $L(\rho_*)$ is lifted compared to close by points, and a steeper gradient requires more lift. See the Figure 5.10. For large ρ_0, L is already quite flat, so even small values of h_1 will cause a bump to appear. For small ρ_0, L is quite steep, so the initial increase in h_1 only flattens the profile. This is why we have not observed phase transitions just varying h_1 and effectively leaving $\rho_* = 0$. Of course other parameters in the theory will also influence the development of phase transitions.

We would also like to point out that the authors of [24] believed that in confining backgrounds $L(\rho_0)$ is a monotonically decreasing function. The existence of phase transitions in such backgrounds shows that this assumption is outdated and that even in confining backgrounds, $L(\rho_0)$ is allowed to have local maxima.

5.4 Double phase transition

In the last section we have described several ways to achieve phase transitions. This can be best understood through the variation of two scales, dictated by h_1, giving the "speed" of the increase of the potential with respect to separation length, and ρ_*, the scale at which the N_f sources kick in. In particular, a general characteristic of profiles has been identified that is key in producing phase transitions. We need a region where the source density rapidly changes to be able to observe them. This appears to be a universal requirement. Our interpretation of the reason for the occurrence of the phase transitions actually enables us to provide a testable prediction, that can be exploited to produce new phenomena.

The possibility for double phase transition might have been mentioned in the literature [75], but has never been explicitly shown. With the knowledge gained in the previous section, we know have the possibility to find solutions with more than one phase transition. Below we list several types of profiles that allow us to generate these.

In this chapter, we will restrict ourselves to profiles producing two phase transitions as proof of concept. In general though, these procedures seem to be able to produce an arbitrarily large amount of phase transitions if one so wishes.

5.4.1 Double Bump and Tumbling profiles

The first idea is to add several profiles of the form of eq. (2.1.4) or (2.1.10). This leads to

$$S(\rho) = \begin{cases} \frac{1}{2}(\tanh^4(2(\rho-\rho_{*1})) + \tanh^4(2(\rho-\rho_{*2}))) & \text{if } \rho \geq \rho_{*2} \\ \frac{1}{2}\tanh^4(2(\rho-\rho_{*1})) & \text{otherwise,} \end{cases} \tag{5.4.1}$$

$$\hat{S}(\rho) = \begin{cases} \tanh^4(2(\rho-\rho_{*1}))e^{\frac{-4(\rho-\rho_{*1})}{3}} + \tanh^4(2(\rho-\rho_{*2}))e^{\frac{-4(\rho-\rho_{*2})}{3}} & \text{if } \rho \geq \rho_{*2} \\ \tanh^4(2(\rho-\rho_{*1}))e^{\frac{-4(\rho-\rho_{*1})}{3}} & \text{otherwise.} \end{cases} \tag{5.4.2}$$

giving us the following source profiles:

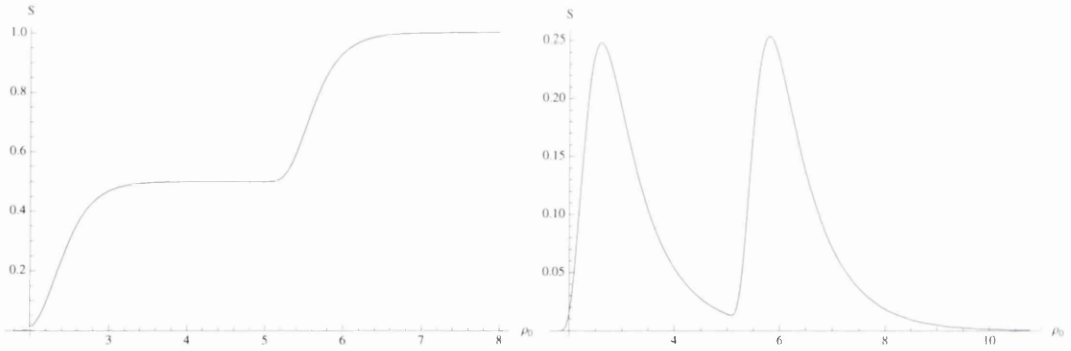

Figure 5.11: The left panel shows $S(\rho)$, while the right panel gives $\hat{S}(\rho)$. For both graphs we chose $\rho_{*1} = 1.8$ and $\rho_{*2} = 5$.

We shall refer in this subsection to $S(\rho)$ as the Tumbling case and to the background with $\hat{S}(\rho)$ as the Double Bump. Both of these profiles will also serve to refine our understanding of the phase transition. The double bump lets us confirm that the phase transition actually has something to do with the source density and not some underlying hidden occurrences. The Tumbling profile lets us study whether it really is the change in source density that is responsible for the source density. It might be that the phase transition is triggered by the source density crossing some threshold instead.

The results are displayed in Figure 5.12.

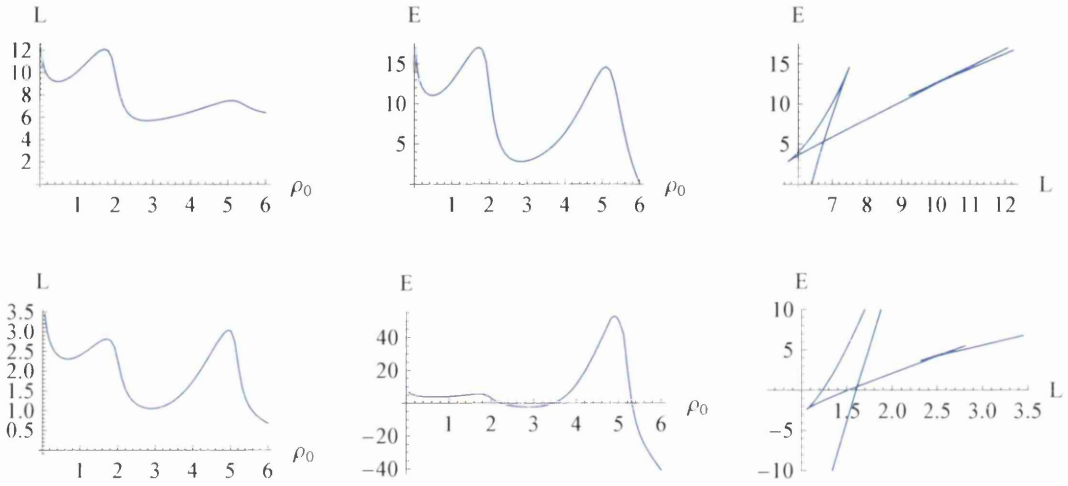

Figure 5.12: The Tumbling case is presented in the top row, while the Double Bump is the bottom row. In both cases $h_1 = 47$.

We see, that it really is the change in source density that causes the phase transition. Each bump in the source profile is a region of high source density and each high density region leads to a phase transition. The Tumbling profile shows that the phase transition is independent of the actual value of the source density. It is only the difference in density that counts.

Also the Tumbling profile in particular can be very interesting for Holographic Technicolor theories with Higgsing cascades. Here, each of the steps in the profile would correspond to a particular generation of quarks. Thus cases like [76] might profit from the use of such profiles.

5.4.2 Plateau profiles

So far all the phase transitions observed come from the string moving from regions of high source density to regions of lower density. It would be interesting to see if this also works if we move from low to high density. Thus we would like to engineer profiles that quickly rise from 0 to 1, stay at 1 for some time before quickly decreasing back to 0. It is a major challenge to find such functions and so far none have been found that have a continuous first derivative. We have made sure that the discontinuity is well away from the regions of interest at the middle of the plateau.

The easiest way to obtain profiles as described, is to use a profile that behaves like $\mathcal{S}(\rho)$ from eq. 2.1.4 and then mirror it around the axis $\rho = c$, where $\mathcal{S}(c) \approx 1$ and then forcing $\mathcal{S}$ to be 0 after it reached that value again. As an example we used

$$\mathcal{S}(\rho) = \begin{cases} 0 & \text{if } \rho \geq \rho_* + 4 \\ \tanh^4(2(\rho - \rho_* - 4)) & \text{if } \rho_* + 4 \geq \rho \geq \rho_* + 2 \\ \tanh^4(2(\rho - \rho_*)) & \text{otherwise,} \end{cases}$$

resulting in

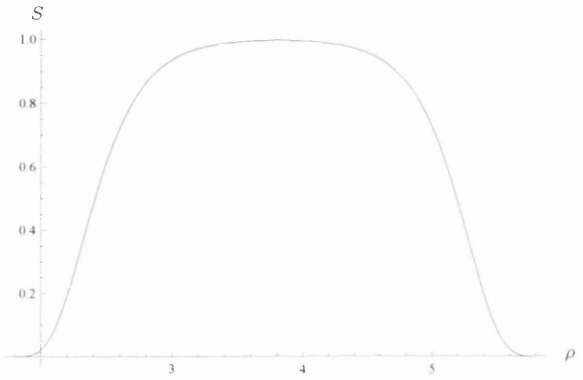

Figure 5.13: Here, $\rho_* = 1.8$.

This leads to the following situation.

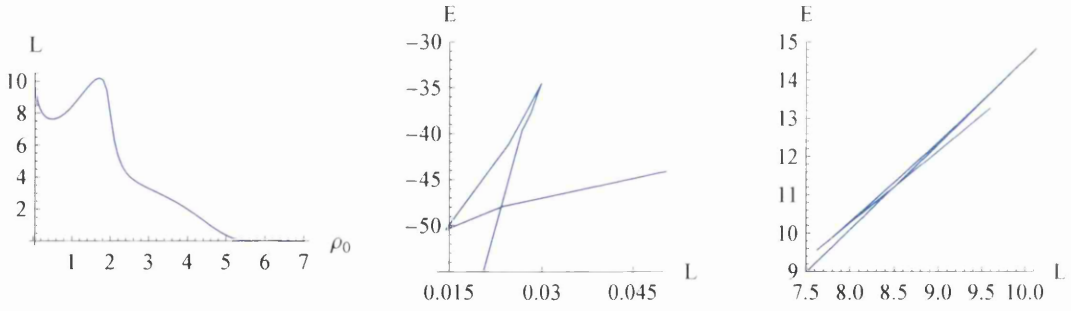

Figure 5.14: $L(\rho_0)$ and $E(L)$ at both phase transitions. $N_f = N_c = 1$ and $h_1 = 47$.

Thus we have strong evidence that phase transitions also occur when entering region of higher source density. This leads us to believe, that every bump profile could actually produce two phase transitions per bump. However we believe that they merge into another through an

effect that is analogous to the effect that limits the angular resolution of lenses. Both bumps in $L(\rho_0)$ or $E(\rho_0)$ of, for example, figure 5.8 are so close together that there is only one local maximum.

We again would like to point out that already the bump profile was a phenomenological profile. With the complications added to the profiles in this section we move further away from analyticity. However, we still believe the reason why we we believe the bump profile to be physically relevant, see Section 2.1, to still hold. For example, encouragingly, the central charge of the solutions of all profiles in this section, including plateau profiles of Section 5.4.2 are monotonically increasing and thus show no sign of unphysical behaviour. We know from [29], that the central charge in the backgrounds discussed is given by

$$c(\rho) = \frac{\hat{h}^2 e^{2\Phi+2h+2g+4k}}{8(\partial_\rho \log[\sqrt{\hat{h}} e^{2\Phi+2h+2g+k}])^3} \,. \tag{5.4.3}$$

This leads to graphs of the following shape:

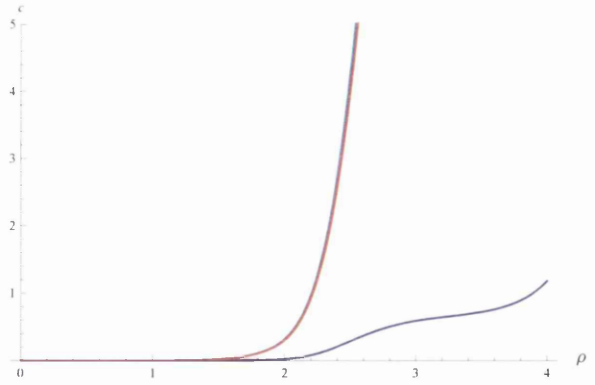

Figure 5.15: This is a plot of $c(\rho)$ for the various cases; the Double Bump is purple, the Tumbling case is teal, and the central charge for solution generated through the plateau profiles is depicted in red.

5.5 Powers of Tanh and x

Of course other variables do also have an effect on the Wilson loop and the associated phase transition.

For example, we can generalise the tanh component in the profiles discussed above from, $\tanh^4(2\rho)$ to $\tanh^{2n}(2\rho)$ where $n \geq 2$ is an integer. This has the conceptual imperfection

though, that it pushes the flavour correction in the IR expansion of P to higher orders of ρ and thus effectively diminishes the effect of the flavour branes on the system more and more.

Also $x = \frac{N_f}{N_c}$ being a variable that affects many aspects of this system, also plays a role for how easily phase transitions can be found. As an example, here is $E(L)$ for systems equal to figure 5.8.

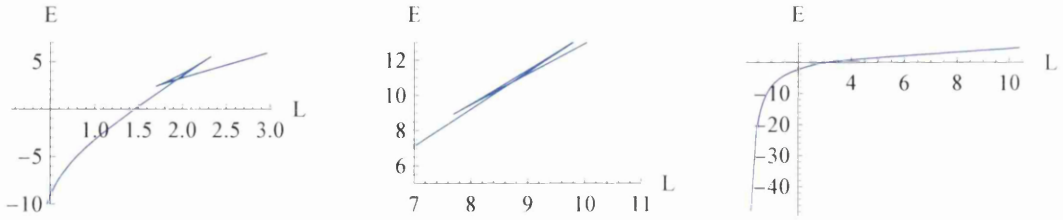

Figure 5.16: On the left $n = 5$, in the middle $x = 5$ and on the right $x = \frac{1}{5}$

Please note, that we can also find phase transitions for $x < 1$ but higher values of h_1 have to be used. As we can see the higher x the easier it is to find a phase transition. By this we mean that h_{1t} will be closer to h_{1c}. The greater the power of tanh in the profile, the harder it is to find a phase transition, as expected. However, we must note that the effect of n is very subtle, much less pronounced than one would expect from the expansion argument given above.

5.5.1 Different profiles

The problem of finding a source profile with the right UV asymptotes remains an open problem. So far we have taken the simplest analytic solution known, eq. (2.1.4), and forced it to have the right asymptotes. It would be helpful if one could simply take a whole other class of analytic profiles and repeat this process, while getting the same results. For example, we could start with

$$\mathcal{S}(\rho) = \begin{cases} 1 - \left(\frac{\cosh(4\rho_{q_1}) + \cosh(4\rho_q)}{2} - 1\right)e^{-4\rho} & \text{if } \rho \geq 4 \\ \frac{2}{3} \frac{(\cosh(4\rho) - \cosh(4\rho_q))^{\frac{3}{2}}}{(\cosh(4\rho_{q_1}) - \cosh(4\rho_q))\sqrt{\cosh(4\rho) - 1}} & \text{if } \rho \leq \rho_{q_1} \\ \frac{2}{3} \frac{(\cosh(4\rho) - \cosh(4\rho_q))^{\frac{3}{2}} - (\cosh(4\rho) - \cosh(4\rho_{q_1}))^{\frac{3}{2}}}{(\cosh(4\rho_{q_1}) - \cosh(4\rho_q))\sqrt{\cosh(4\rho) - 1}} & \text{otherwise,} \end{cases}$$

based on the Flat Measure described in [43]. ρ_{q_1} is related to ρ_q via

$$\rho_{q_1} = \frac{1}{4}\text{arcosh}(\delta + \cosh(4\rho_q))\,. \tag{5.5.1}$$

Here, analytical conditions are found, that the profile must fulfil, to produce desirable back reactions. These are then solved in a lengthy but logical procedure whose details are mentioned

in the paper cited. If one wishes to have a decaying profile one could use $\hat{\mathcal{S}}(\rho) = \mathcal{S}(\rho)e^{-\frac{4}{3}\rho}$.

These profiles have the following form

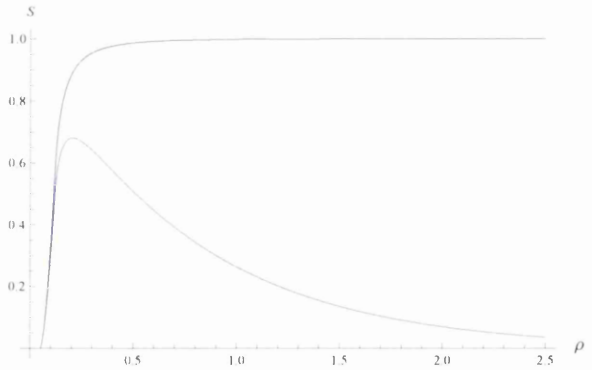

Figure 5.17: $\mathcal{S}(\rho)$ is blue while $\hat{\mathcal{S}}(\rho)$ is red.

Both profiles lead to a phase transition:

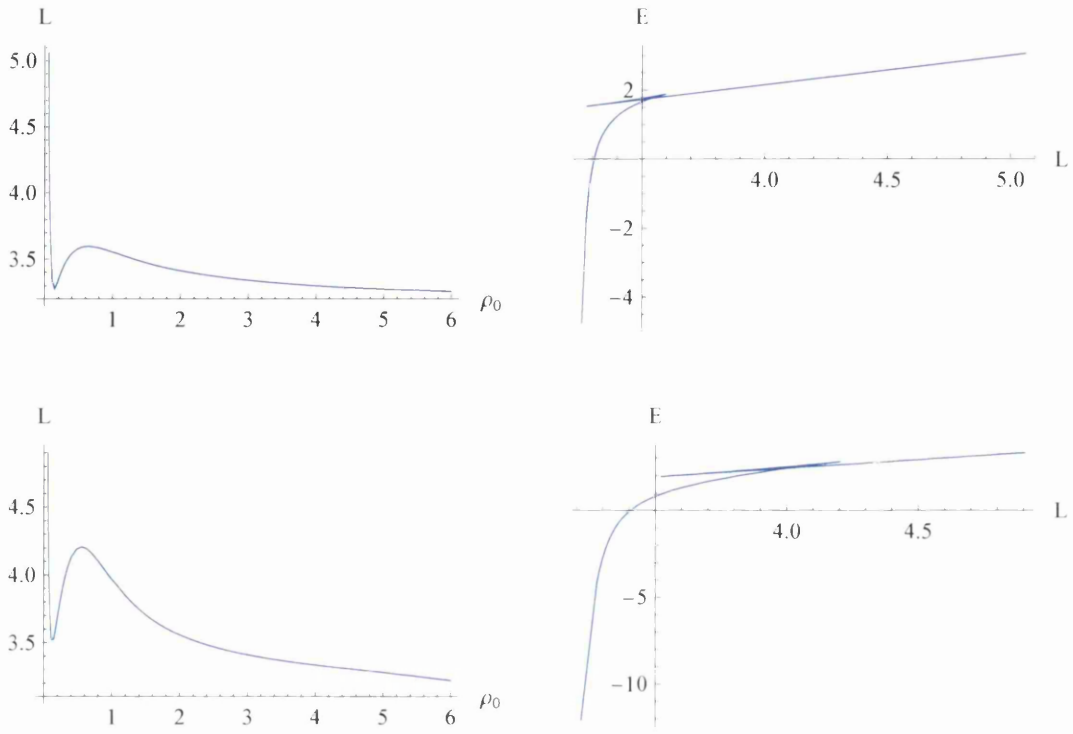

Figure 5.18: The background generated with $\mathcal{S}(\rho)$ is in the top row. We used $N_c = N_f = 1$ and $h_1 = 3.9581$. On the bottom row we have the $\hat{\mathcal{S}}(\rho)$ case with $N_c = N_f = 1$ and $h_1 = 3.25291$.

As δ decreases, the width of the brane distribution becomes smaller, The mass of the heaviest quark decreases and phase transitions are produced. Despite the large amount of control such types of profiles offer, one should be aware, that their realization is not completely clean, in the sense that S' is not continuous everywhere. Also note, that while now we did not have to introduce ρ_* to produce phase transitions, this profile already uses the two scales δ and q to produce the dynamics described above.

We see that also in this case, adding a factor $e^{\frac{-4}{3}\rho}$ did not produce any unphysicalities.

5.5.2 Curiosities

To finish this chapter, we will present some odd findings that have been discovered during the analysis of the Wilson loops of the various CVMN solutions.

Firstly, it might be worth mentioning that, after the addition of flavor sources without a source profile as done in Section 5.2 during the analysis leading to Figure 5.3, we can produce

a phase transition like behaviour in the lower, physical branch of $E(L)$ plot when $x = \frac{N_f}{N_c} < \frac{1}{2}$ and $h_1 \gg h_{1c}$:

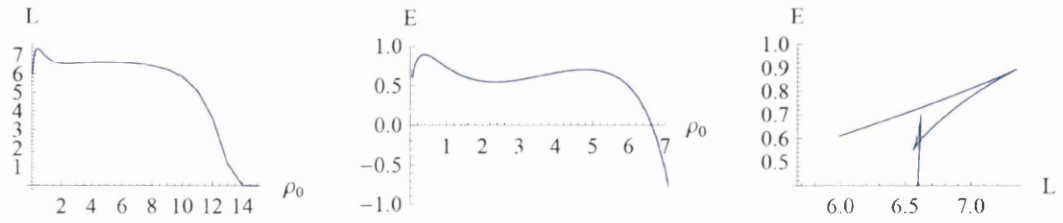

Figure 5.19: $\Phi_0 = 0$, $N_c = 5$, $N_f = 2$ and $h_1 = 29$.

Another quite surprising fact that was discovered during the search for phase transitions is that while most profiles require $h_1 \gg h_{1c}$ to show a transition, profiles of the type $\mathcal{S}(\rho) = \tanh^4(2(\rho - \rho_*))$ do not. For $h_1 \approx h_{1c}$, $P(\rho)$ will stay linear for quite some time before exhibiting exponential behaviour. This can be seen in Figure 5.6. In such cases, $L(\rho_0)$ will not immediately approach 0, but first approach a non-zero value α before, and β after the transition of P's behaviour. Depending on several factors, such as the power of tanh, we can force $\beta > \alpha$, leading to a very curious phase transition as shown in the following diagram.

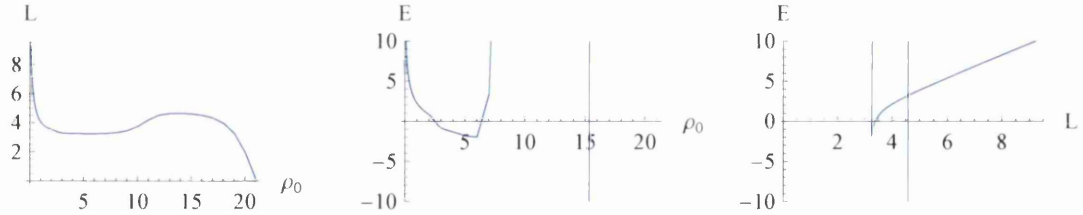

Figure 5.20: Here, $\mathcal{S}(\rho) = \tanh^4(2(\rho - \rho*))$, $N_c = N_f = 1$, $h_1 = \frac{1000519}{500000}$, $\rho_* = 2$.

Please note that beside the phase transition the overall shape of $E(L)$ is equivalent to the expected, but one would have to plot it approximately between -10^7 and 10 to see it. The unnatural curvature at the end of the linear confining branch of $E(L)$ is due to a numerical error in the interpolation during the numerical calculation as we zoomed in too far in the rightmost plot of Figure 5.20, than the machine precision allows.

Chapter 6

Entanglement Entropy and Wilson Loops

So far we have discussed entanglement entropy and the Wilson loop in confining backgrounds separately. *A priori*, these two quantities are not related to each other, and indeed, they show very different behaviours - the first presents a phase transition in the form of a "butterfly" shape, while the later is monotonic, at least when it comes towards identifying confinement. However, the fact that both are probes of confinement suggests that there maybe some deeper relation between them. Moreover, as we will discuss below, the functional form of both quantities is very similar.

The length of the entangling strip (4.0.6) and the length of the Wilson loop (5.1.7) can both be written in the form

$$L(\rho_0) = 2\int_{\rho_0}^{\infty} d\rho \sqrt{\frac{\beta(\rho)}{\frac{M(\rho)}{M(\rho_0)} - 1}}, \tag{6.0.1}$$

where $M(\rho)$ is different for the two cases and is given by

$$M_{EE}(\rho) = H(\rho), \tag{6.0.2}$$

$$M_{WL}(\rho) = \alpha^2(\rho). \tag{6.0.3}$$

The entropy of the strip (4.0.8) and the energy of the Wilson loop (5.1.8) can also be written in a similar way as

$$\begin{pmatrix} \frac{4G_N^{(10)}}{V_{d-1}} S \\ E_{WL} \end{pmatrix} = 2\int_{\rho_0}^{\infty} d\rho \sqrt{\frac{\beta(\rho)M(\rho)}{1 - \frac{M(\rho_0)}{M(\rho)}}} - 2\int_{\rho_\Lambda}^{\infty} d\rho \sqrt{\beta(\rho)M(\rho)}\,. \tag{6.0.4}$$

The expression (6.0.4) can also be written in the following form

$$\begin{pmatrix} \frac{4G_N^{(10)}}{V_{d-1}} S \\ E_{WL} \end{pmatrix} = \sqrt{M(\rho_0)} L(\rho_0) - 2K(\rho_0)\,, \tag{6.0.5}$$

$$K(\rho_0) \equiv \int_{\rho_\Lambda}^{\infty} d\rho \sqrt{\beta(\rho) M(\rho)} - \int_{\rho_0}^{\infty} d\rho \sqrt{\beta(\rho)\left(M(\rho) - M(\rho_0)\right)}\,. \tag{6.0.6}$$

The form (6.0.5) emphasizes the linear nature of E_{WL} at long distances. In both cases, $M(\rho)$ is a monotonically increasing function. Therefore, the functional form of the EE and the Wilson loop is very similar. Of course, these mathematical similarities in equations (6.0.1) and (6.0.4) are based on the fact that both observables are solutions to a minimization problem.

The question arises as to what is the difference between them. We claim that the qualitative difference between these two observables (at least in the case of confining QFTs) is due to the behaviour of the function $M(\rho)$ close to the origin. For both cases $M(\rho)$ is a monotonically increasing function, but the behaviour close to the origin is different. While in most of the thesis we were free to set the origin at 0, for generality we now let it be at $\rho = \rho_\Lambda$. For the entanglement entropy $M(\rho) = H(\rho)$ shrinks to zero close to ρ_Λ, since $H(\rho)$ includes a factor of the internal volume — see (4.0.4) — which always goes to zero at the end of the geometry*. On the other hand, for the Wilson loop in confining backgrounds $M(\rho_\Lambda) = \alpha^2(\rho_\Lambda) \neq 0$ since this quantity is related to the confining-string tension. Therefore $M(\rho_\Lambda)$ behaves very differently for the two observables, when calculated in a generic confining background. This is the source for the qualitative difference between these two quantities.

To be concrete, let us focus on Dp branes compactified on a circle. These backgrounds are dual to confining field theories in p space-time dimension. The background metric and dilaton are a generalisation of those written by Witten, as a dual to a Yang-Mills-like four dimensional QFT [52, 77] (with $\alpha' = g_s = 1$),

$$\begin{aligned} ds^2 &= \left(\frac{\rho}{R}\right)^{\frac{7-p}{2}} \left[\left(\frac{R}{\rho}\right)^{7-p} \frac{d\rho^2}{h(\rho)} + dx_{1,p-1}^2\right] + h(\rho)\left(\frac{\rho}{R}\right)^{\frac{7-p}{2}} d\varphi_c^2 + \left(\frac{\rho}{R}\right)^{\frac{p-3}{2}} R^2 d\Omega_{8-p}^2, \\ h(\rho) &= 1 - \left(\frac{\rho_\Lambda}{\rho}\right)^{7-p}, \quad e^{-4\phi} = \left(\frac{\rho}{R}\right)^{(3-p)(7-p)}, \\ \alpha^2(\rho) &= \left(\frac{\rho}{R}\right)^{7-p}, \quad g^2(\rho) = \frac{1}{1 - \left(\frac{\rho_\Lambda}{\rho}\right)^{7-p}}, \end{aligned} \tag{6.0.7}$$

*The vanishing of the internal volume is in agreement with the vanishing of the central charge at zero energies. This is characteristic of confining field theories.

which implies that,

$$M_{EE}(\rho) = (S_{7-p} \times 2\pi R_c)^2 R^{7-p} \rho^{9-p} h(\rho), \;\; M_{WL}(\rho) = \left(\frac{\rho}{R}\right)^{7-p}. \tag{6.0.8}$$

R_c is the radius of the compact cycle (see for example [78]),

$$R_c = \frac{2}{7-p}\left(\frac{R}{\rho_\Lambda}\right)^{\frac{7-p}{2}} \rho_\Lambda \tag{6.0.9}$$

and $S_{n-1} = \frac{2\pi^{\frac{n}{2}}}{\Gamma\left(\frac{n}{2}\right)}$ is the surface area of the n-sphere. Therefore $M_{WL}(\rho_\Lambda) \sim {\rho_\Lambda}^{7-p} \neq 0$, while $M_{EE}(\rho_\Lambda) = 0$. This difference of behaviour in the function $M(\rho)$, creates a "butterfly" shape (and a phase transition) in $S(L)$, whereas it gives place to a monotonic behaviour and a long-separation linear law in $E_{WL}(L_{WL})$.

6.1 Sufficient Conditions for Phase Transitions

The conditions a background must satisfy so that the Wilson loop shows a confining behaviour (5.1.11), were derived in [24]. The difference in behaviour, of the Wilson loop and the Entanglement Entropy as probes of the phenomenon of confinement, leads to the following question:

- *Question:* What are the conditions on the background to present a phase transition in the EE?

Using a similar logic to that of [24], in the following we will derive sufficient conditions on the background to present a phase transition in the Entanglement Entropy. More explicitly, we will derive the conditions on the background such that $L(\rho_0)$ (the length of the entangled strip as a function of the minimal radial position) will increase for ρ_0 close to ρ_Λ (the IR of the dual QFT) and decrease for asymptotically large value of ρ_0 (the UV of the dual QFT). Hence, the quantity L will present (at least) a maximum and the required double valuedness needed for a phase transition.

We start by deriving the conditions on the background such that $L(\rho_0)$ is an increasing function close to $\rho_0 = \rho_\Lambda$. Let us assume that the functions $H(\rho)$ and $\beta(\rho)$ have the following expansions around $\rho_0 = \rho_\Lambda$

$$H(\rho) = h_r(\rho - \rho_\Lambda)^r + \mathcal{O}(\rho - \rho_\Lambda)^{r+1}, \quad \beta(\rho) = \beta_t(\rho - \rho_\Lambda)^{-t} + \mathcal{O}(\rho - \rho_\Lambda)^{-t+1}, \tag{6.1.1}$$

with $r, t > 0$. Then, the integrand corresponding to L in (4.0.6) is divergent close to $\rho = \rho_\Lambda$, and therefore the integral gets most of its contribution from this region. That allows us to approximate the integrand using eq.(6.1.1),

$$\lim_{\rho_0 \to \rho_\Lambda} L(\rho_0) = 2\sqrt{\beta_t} \int_{\rho_0}^{\infty} d\rho (\rho - \rho_\Lambda)^{-\frac{t}{2}} \left[\left(\frac{\rho - \rho_\Lambda}{\rho_0 - \rho_\Lambda} \right)^r - 1 \right]^{-\frac{1}{2}} \tag{6.1.2}$$
$$= (\rho_0 - \rho_\Lambda)^{1-\frac{t}{2}} \frac{2\sqrt{\beta_t}}{r} \int_1^{\infty} dz (z-1)^{-\frac{1}{2}} z^{-\frac{t+2r-2}{2r}} = (\rho_0 - \rho_\Lambda)^{1-\frac{t}{2}} \frac{2\sqrt{\pi\beta_t}\Gamma\left(\frac{t+r-2}{2r}\right)}{r\Gamma\left(\frac{t+2r-2}{2r}\right)}.$$

We have changed variables to $z \equiv \left(\frac{\rho-\rho_\Lambda}{\rho_0-\rho_\Lambda}\right)^r$. We find that $L(\rho_0)$ is monotonically increasing when

$$t < 2. \tag{6.1.3}$$

This means that $\beta(\rho)$ should not diverge faster than $\frac{1}{(\rho-\rho_\Lambda)^2}$ close to ρ_Λ.

Next, we derive the conditions on the background such that $L(\rho_0)$ is a decreasing function at asymptotically large value of ρ. Close to the boundary $\rho = \infty$ we can expand

$$H(\rho) = h_k \rho^k + \mathcal{O}(\rho^{k-1}), \quad \beta(\rho) = \beta_j \rho^{-j} + \mathcal{O}(\rho^{-j+1}). \tag{6.1.4}$$

Plugging these expansions in (4.0.6) we find,

$$L(\rho_0) = 2\sqrt{\beta_j} \int_{\rho_0}^{\infty} d\rho \rho^{-\frac{j}{2}} \left[\left(\frac{\rho}{\rho_0} \right)^k - 1 \right]^{-\frac{1}{2}}. \tag{6.1.5}$$

Changing variables to $z \equiv \frac{\rho}{\rho_0}$ we find the asymptotic behaviour of $L(\rho_0)$ near the boundary

$$L(\rho_0) = 2\sqrt{\beta_j} {\rho_0}^{1-\frac{j}{2}} \int_1^{\infty} dz \frac{z^{-\frac{j}{2}}}{\sqrt{z^k - 1}} = \frac{2\sqrt{\pi\beta_j}\Gamma\left(\frac{k+j-2}{2k}\right)}{k\Gamma\left(\frac{2k+j-2}{2k}\right)} {\rho_0}^{1-\frac{j}{2}}. \tag{6.1.6}$$

We see that for

$$j > 2 \tag{6.1.7}$$

the length L will go to zero as $\rho_0 \to \infty$. There is a maximum somewhere in the middle, hence a double valuedness for $\rho_0(L)$ and the possibility of a phase transition in the quantity $S(\rho_0[L])$. On the other hand, for $j \leq 2$, the quantity L will either diverge, or saturate at a constant value, in the same limit and in this case we do not expect to have a phase transition.It should be noted however, that the above condition do lead to phase transitions, we do know of examples where the above conditions do not hold while we still have phase transitions. Apart from short

configurations, Section 4.5 has many other curious examples. We have documented background, where L will either diverge or approach a non-zero constant in the UV and still has a maximum.

For now, let us present some examples of absence or presence of phase transitions in the EE, in agreement with the criteria of this section.

6.2 Examples of the Criteria for Phase Transitions

As anticipated, we will study here different non-confining and confining models to illustrate our criteria above. $AdS_5 \times S^5$, Dp branes compactified on a circle, hard and soft walls and the Klebanov-Strassler model [30] will serve as confirmation of our treatment.

6.2.1 $AdS_5 \times S^5$

As a first example we discuss the EE of $N = 4$ Super-Yang-Mills, to demonstrate that it does not present a phase transition. The metric is given by (4.1.1). Notice that in this case $t = 4$ and the condition (6.1.3) is not attained. The calculations of the EE where previously shown in Figure 4.2. We see that $L(\rho_0)$ is a monotonically decreasing function which diverges at the origin and goes to zero at the boundary. The EE shows two possible phases: in the first, it monotonically grows with L while in the second (the disconnected phase) it is constant. The second phase is not favoured, since the EE in this phase is always larger than the EE in the 'connected' phase. Therefore there is no phase transition, as appropriate for a conformal field theory. Incidentally, also notice that the concavity of the $S(L)$ is such that the correct condition, see eq.(4.1.2), is achieved.

6.2.2 Dp brane on a Circle

Next we consider the background generated by Dp brane compactified on a circle described in eq.(6.0.7). The functions $\alpha(\rho)$ and $\beta(\rho)$ are,

$$\alpha(\rho) = \left(\frac{\rho}{R}\right)^{\frac{7-p}{2}}, \quad \beta(\rho) = \frac{1}{1-\left(\frac{\rho_\Lambda}{\rho}\right)^{7-p}} \left(\frac{R}{\rho}\right)^{7-p}. \tag{6.2.1}$$

Close to the horizon $\rho = \rho_\Lambda$, we can expand

$$\beta(\rho) = \frac{\rho_\Lambda}{7-p} \left(\frac{R}{\rho_\Lambda}\right)^{7-p} \frac{1}{\rho - \rho_\Lambda} + \dots \tag{6.2.2}$$

where "..." stands for subleading (finite) terms.

Comparing with (6.1.1) we find that in this case $t = 1$. This means that for this background, and for any value of p, the condition (6.1.3) will be satisfied and $L(\rho_0)$ will always go to zero at the horizon. Close to the boundary $\beta(\rho_0) \sim {\rho_0}^{-(7-p)}$ and therefore in this case, comparing with eq.(6.1.4), we have $j = 7 - p$. Hence, for $p \leq 4$, the condition (6.1.7) will be satisfied and $L(\rho_0)$ will decrease to zero close to the boundary. However, for $p = 5$, $L(\rho_0)$ will saturate to a finite value and for $p \geq 6$ it will increase towards the boundary.

We conclude that for $p \leq 4$ there will be a phase transition since $L(\rho_0)$ is a non-monotonic function, but for $p > 4$ $L(\rho_0)$ is monotonic and there will be no phase transition. In Figure 6.1 we draw the functions $L(\rho_0)$ and $S(L)$ for the cases $p = 3, 4, 5, 6$. We observe a crossing (and hence a phase transition) between the connected and disconnected solutions for the EE, in the case $p < 5$. We also see that the concavity of S is the correct one for $p \leq 4$, but does not satisfy eq.(4.1.2) for $p > 4$.

6.2.3 Hard and Soft Walls

The Hard Wall model was proposed in [79] as a holographic description of low-energy properties of QCD. It is described by the AdS metric with the radial coordinate cut at some value $\rho = \rho_\Lambda$. The results for the entanglement entropy are shown in Figure 6.2.

The authors of [80] have improved the Hard Wall model by cutting of the AdS space smoothly, instead of a hard-wall cutoff in the IR. The metric of the Soft Wall model is the same as the AdS metric but there is a non-trivial dilaton

$$e^{\phi} = e^{\frac{1}{\rho^2}} . \tag{6.2.3}$$

Then we have

$$\beta(\rho) = \frac{R^4}{\rho^4} , \tag{6.2.4}$$

$$H(\rho) = \left(\frac{8\pi^2}{3}\right)^2 R^4 \rho^6 e^{-\frac{4}{\rho^2}} . \tag{6.2.5}$$

The results are shown in Figure 6.2. We see that the soft wall model admits a similar behaviour to the D3 and D4 branes with a phase transition.

We cannot check the conditions for confinement in these examples. The Hard Wall background is just a cut AdS. The Soft Wall background does not admit the expansion (6.1.1) for the function $H(\rho)$ in the IR since it includes an exponential factor. Therefore, even though

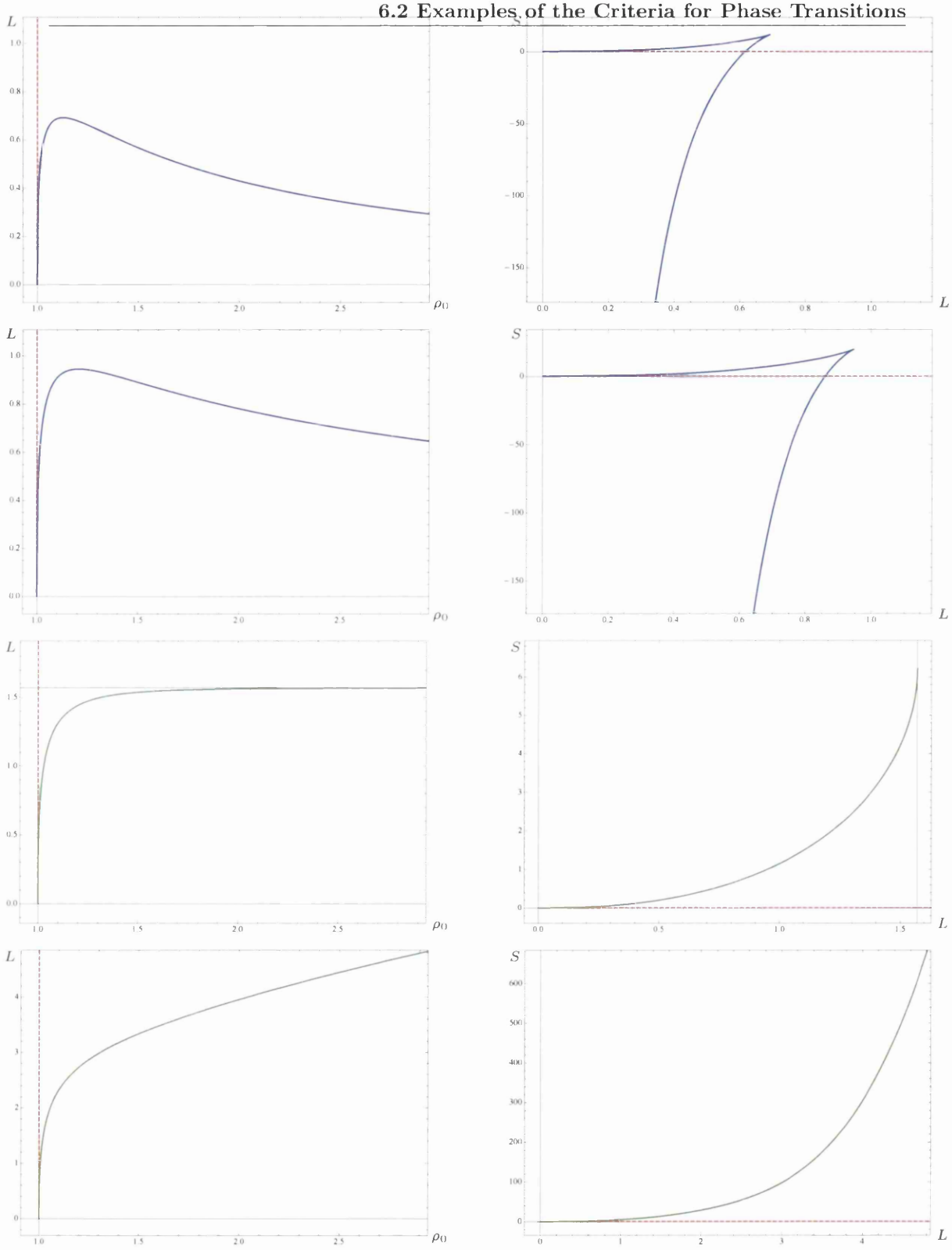

Figure 6.1: The function $L(\rho_0)$ and $S(L)$ in the near extremal Dp brane backgrounds for $p = 3, 4, 5, 6$ moving down the page. The location of the horizon was set to $\rho_\Lambda = 1$ in the figures. The dashed red line is the disconnected solution. The D3 and D4 branes shows a phase transition behaviour while in the D5 and D6 branes there is no phase transition.

$\beta(\rho)$ diverges strongly, we still have a phase transition since the exponential decay of $H(\rho)$ takes-over the divergence of $\beta(\rho)$.

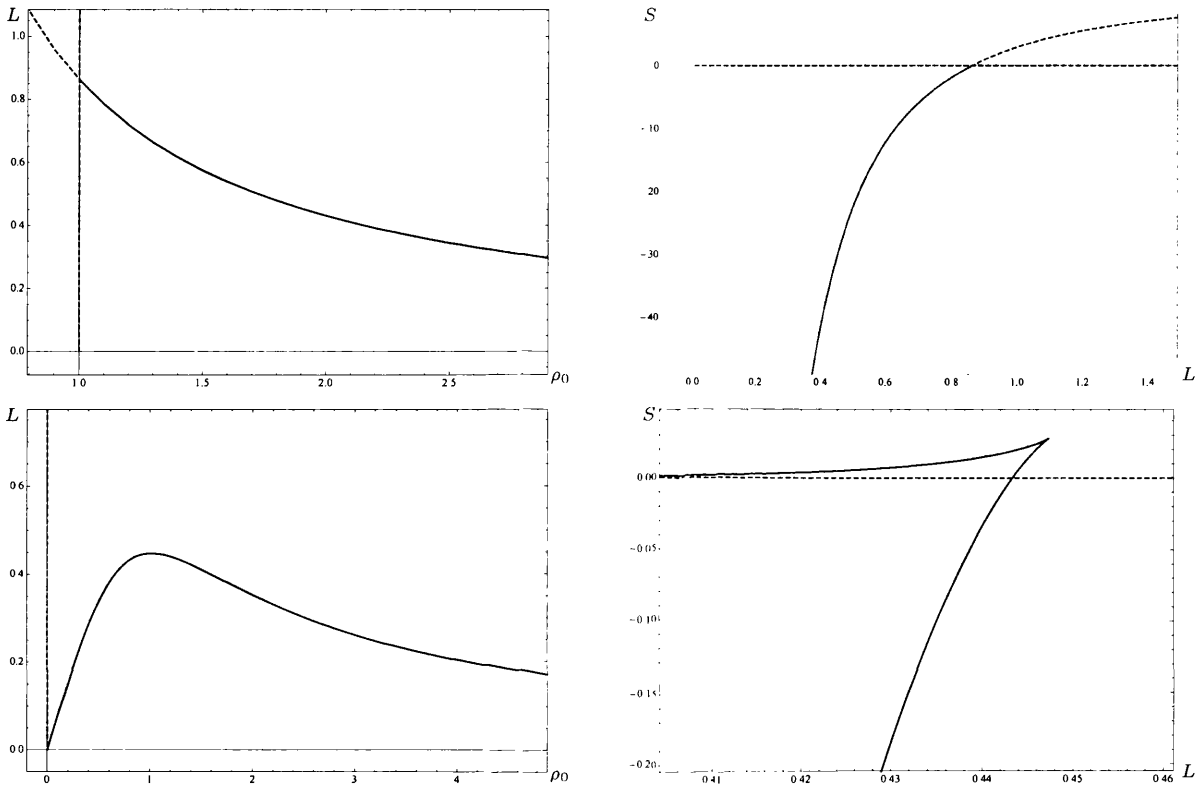

Figure 6.2: The function $L(\rho_0)$ and $S(L)$ in the Hard (top row) and Soft Wall (bottom row) models. The location of the hard wall was set to $\rho_\Lambda = 1$ in the figures. The dashed red line is the disconnected solution and the dashed blue line represents the continuation of the AdS solution beyond the hard wall.

6.2.4 Klebanov-Strassler

The entanglement entropy of the background dual to a cascading supersymmetric gauge theory, the deformed conifold [30], was analysed in details in [23]. The authors of [23] have shown that in this case there is a phase transition of the same form as in the D3 and D4 branes, as expected in a confining theory. We would like to demonstrate how this background follows the conditions for phase transition, which we derived above.

The supergravity solution of the deformed conifold is of the following form [30, 81]

$$ds^2 = h^{-\frac{1}{2}}(\tau)\, dx_{1,3}^2 + h^{\frac{1}{2}}(\tau)\, ds_6^2\,, \tag{6.2.6}$$

where ds_6^2 is the metric of the deformed conifold

$$ds_6^2 = \frac{\epsilon^{4/3}}{2} K(\tau) \left(\frac{1}{3K^3(\tau)} \left[d\tau^2 + \left(g^5\right)^2 \right] + \cosh^2\left(\frac{\tau}{2}\right) \left[\left(g^3\right)^2 + \left(g^4\right)^2 \right] + \sinh^2\left(\frac{\tau}{2}\right) \left[\left(g^1\right)^2 + \left(g^2\right)^2 \right] \right). \quad (6.2.7)$$

ϵ is the energy scale and the functions $h(\tau)$ and $K(\tau)$ are given by

$$h(\tau) = (g_s M \alpha')^2 2^{2/3} \epsilon^{-8/3} I(\tau), \quad (6.2.8)$$

$$I(\tau) \equiv \int_\tau^\infty dx \frac{x \coth x - 1}{\sinh^2 x} (\sinh 2x - 2x)^{\frac{1}{3}}, \quad (6.2.9)$$

$$K(\tau) = \frac{(\sinh(2\tau) - 2\tau)^{\frac{1}{3}}}{2^{\frac{1}{3}} \sinh \tau}, \quad (6.2.10)$$

where τ is a dimensionless radial coordinate running from zero to infinity on the boundary. Then we have,

$$\alpha = h^{-\frac{1}{2}}(\tau), \qquad \beta(\tau) = \frac{h(\tau)\epsilon^{4/3}}{6K^2(\tau)}, \quad (6.2.11)$$

$$V_{int} = \frac{4\pi^3}{\sqrt{6}} h^{5/4} \epsilon^{10/3} K(\tau) \sinh^2(\tau), \quad (6.2.12)$$

$$H(\tau) = e^{-4\phi} V_{int}^2 \alpha^3 = \frac{8\pi^6}{3} \epsilon^{20/3} h(\tau) K^2(\tau) \sinh^4(\tau). \quad (6.2.13)$$

The function $\beta(\tau)$ approaches a finite value in the far IR $\tau = 0$, and therefore we have in this case $t = 0$, corresponding to a monotonically increasing $L(\tau_0)$ in the IR, in accordance with (6.1.3). Near the boundary, i.e. at large τ, the $h(\tau)$ and $K(\tau)$ function takes the form

$$H(\tau \ll 1) = \epsilon^4 (g_s M \alpha')^2 \pi^6 \tau e^{2\tau}, \quad (6.2.14)$$

$$\beta(\tau) = \epsilon^{-\frac{4}{3}} (g_s M \alpha')^2 2^{-\frac{4}{3}} \tau e^{-\frac{2}{3}\tau}. \quad (6.2.15)$$

In this region the functions does not admit the power expansion we have assumed in (6.1.4) and therefore we cannot directly check the conditions we have found, but a direct computation [23] shows that $L(\tau_0)$ indeed goes to zero close to the boundary and therefore there is a phase transition. The intuition is that $\beta(\tau)$ decays exponentially fast close to the boundary, and therefore meets the requirement for sufficiently strong decay ($j > 2$) of eq. (6.1.7).

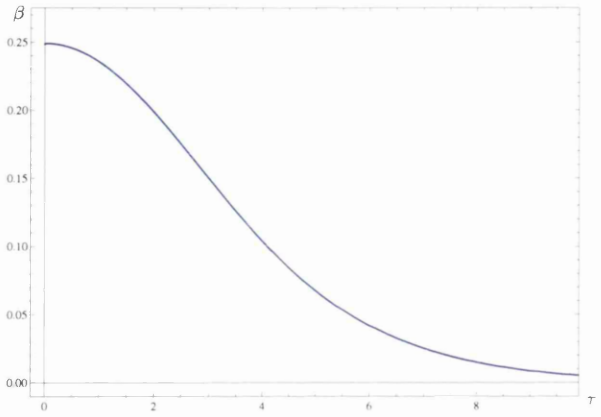

Figure 6.3: The function $\beta(\tau)$ in the Klebanov-Strassler background. $\beta(\tau)$ saturates to a finite value at the origin $\tau = 0$ and therefore meets the condition for a phase transition.

6.3 Confinement and Phase Transitions

We are now in a position to compare the conditions for confinement on the Wilson loop, see eq. (5.1.11) or the derivation in [24] and the conditions for a phase transition in the entanglement entropy as were suggested in [23] and further developed in the previous subsection. On physical grounds, since both observables are probes of confinement, we expect both conditions to coincide. We will not be able to prove the last statement, but we will give a flavour of why it should be true in some examples. On the other hand, we will emphasise a puzzle which arises in other cases. The solution for this puzzle was partly the aim of Chapter 4.

Let us start with the conditions in the IR. The conditions on the Wilson loop, eq. (5.1.11) are really a statement about the IR and therefore we will compare them to the condition we derived for the entanglement entropy in the IR, see eq.(6.1.3). The condition of eq.(6.1.3) means that $\beta(\rho)$ should diverge slower than $\frac{1}{(\rho-\rho_\Lambda)^2}$ in order to observe a phase transition in the EE. Using eq. (5.1.9) we relate the divergence of β to the divergence of g, which is one of the conditions for linear confinement in the Wilson loop, see eq. (5.1.11) (remember that since $\alpha(\rho_\Lambda)$ is the string tension it must be finite, and therefore does not play a role in the discussion about divergences). If we take the case of the Dp brane on S^1 — see eq.(6.0.7) — as an example, we see that close to $\rho = \rho_\Lambda$

$$g^2(\rho) = \left(\frac{\rho_\Lambda}{7-p}\right)\frac{1}{\rho-\rho_\Lambda} + \dots \tag{6.3.1}$$

where "..." stand for sub-leading finite corrections. This divergence is in agreement with

the condition on β in eq. (6.1.3), for any value of p. A possible violation of (6.1.3) would correspond to a stronger divergence of g. We are not aware of such examples. Based on the intuition of backgrounds with compact circles, such a case would correspond to a situation with two compact circles with a topology of a cigar, where the tip of both cigars located in the same radial position. It would be interesting to try to rule out that case (or alternatively find one such example), but we leave this for future work. When β approaches a finite value at $\rho = \rho_\Lambda$, the corresponding confinement-condition on the Wilson loop is the first among the two in eq. (5.1.11), which is that α has a minimum at $\rho = \rho_\Lambda$. In this case it seems that the maximum of $\beta(\rho)$ at $\rho = \rho_\Lambda$ (as in Figure 6.3) corresponds to the minimum of $\alpha(\rho)$, via the relation $\beta \sim \frac{1}{\alpha^2}$, see eq. (5.1.9).

While we have presented an intuition (but not a proof) of the equivalence between the conditions on the EE and the Wilson loop in the IR, there is a puzzle concerning the UV. First, we note that there are no UV conditions on the Wilson loop to obey confinement. As far as the Wilson loop is concerned, the only condition we demand is linearity at long distances (IR). On the other hand, in order to observe a phase transition in the EE, the background also has to satisfy the condition in the UV, eq.(6.1.7). This last condition is not satisfied in certain confining backgrounds — Dp branes on S^1 with $p > 4$ — as discussed in the previous subsection. The question that arises is

- *Question:* Why do certain cases show linear confinement in the Wilson loop but do *not* show a phase transition in the entanglement entropy?

The answer is provided in detail by the analysis in the first half of Chapter 4. Non-localities present in the QFT can mask the phase transition in the EE. These theories will have short configurations with a Volume Law divergence. A naive analysis will not lead to the discovery of them. One rather has to refer to the right ordering of the limits to produce them. Alternatively, the non-localities telltale the need for a suitable UV-completion that will make the QFT local for all energies. both the short configurations and the UV-completion will lead to a recovery of the phase transition. Since the short configurations defy the usual minimisation analysis, the conditions for confinement via EE will not capture them, and thus the conditions are incomplete. However, for fully local holographic field theories we conjecture them to be be both necessary and sufficient.

6.4 Wilson Loop-Entanglement Entropy Relation - An Exercise

The similarities between the EE and the Wilson loop, summarised in equations (6.0.1), (6.0.4) suggest an interesting small exercise. We can ask what are the conditions on a given background, so that the EE and the Wilson loop have the same L dependence. In order to solve this exercise, we will consider situations in which the EE behaves, for large separations, as $S \sim L^{-p}$, where p is some positive number. For example, in the case of conformal field theories in $d+1$ dimensions, one finds that $p = d-1$. This is referred to as an 'Area law' for the EE. In some other examples–characteristically in non-local (d+1)-dimensional theories — one finds $p = d$, in which case the name of 'Volume law' is used. We will first study, based on the similarities alluded to above and summarised by equations (6.0.1), (6.0.4) the characteristics that a background must have such that the Wilson loop behaves like the EE, namely $E_{WL} \sim L_{WL}^{-p}$. Let us start with an IR analysis.

6.4.1 Small Radius Expansion of the Wilson Loop

The functions $\alpha(\rho), g(\rho)$ characterising the Wilson loop computations, can be expanded around $\rho = \rho_\Lambda$ as follows

$$\begin{aligned} \alpha(\rho) &= \alpha(\rho_\Lambda) + a_k \rho^k + \mathcal{O}(\rho^{k+1}), \\ g(\rho) &= b_j \rho^j + \mathcal{O}(\rho^{j+1}). \end{aligned}$$

If $\alpha(\rho_\Lambda) \neq 0$ the Wilson loop exhibits linear confinement with $\alpha(\rho_\Lambda)$ the string tension. We are not interested in a linear law $E_{WL} \sim f(\rho_\Lambda) L_{WL}$ and therefore assume $\alpha(\rho_\Lambda) = 0$. Further assuming $k > 0$, $j > -1$ and a few other reasonable assumptions on the functions $\alpha(\rho), g(\rho)$, the authors of [24] found that

$$E \sim L^{-\frac{j+1}{k-j-1}},$$

for large L and for the case $k > j+1$ (the case $k \leq j+1$ will not result in a negative power of ℓ).

6.4.2 Large Radius Expansion of the Wilson Loop

On the other hand, the functions $\alpha(\rho), g(\rho)$ can be expanded around the boundary $\rho = \infty$ as follows

$$\begin{aligned} \alpha(\rho) &= c_n \rho^n + \mathcal{O}(\rho^{n-1}), \\ g(\rho) &= g(\infty) + d_m \rho^{-m} + \mathcal{O}(\rho^{-m+1}), \end{aligned}$$

with $n, m > 0$. In the region close to the boundary, i.e. small distances, the Wilson loop then behaves as [78]

$$E \sim L^{-\frac{1}{n-1}}. \tag{6.4.1}$$

The UV-behaviour of the Wilson loop will take the same functional form as the EE (for the case of a $d+1$ QFT with Area law) $S \sim L^{1-d}$, when

$$n = \frac{d}{d-1}.$$

For the Dp brane we then have $n = \frac{7-p}{2}$. The UV-behaviour of the Wilson loop in the p-dimensional QFT, coincides with the functional dependence of the EE, calculated for a strip of length L in d-space dimensions and with Area law, when

$$p = \frac{5d-7}{d-1}. \tag{6.4.2}$$

Chapter 7

Conclusions

We started by calculating the entanglement entropy of the photon with the electron. After detailing the mathematical machinery, we first applied to a toy model. This was a scalar field theory with a light and a heavy scalar. We calculated various vacuum and 1-particle entropies. We discovered divergences in the EE in regimes where the interaction vertex had an instability. We also detailed the differences that arise in different spacetime dimensions. With the insight that we have gained, we then went on to a phenomenologically very interesting case, QED. We discovered that in this case the entanglement entropy is divergent. We handled this the usual way, and looked at differences in EE. Now it is much better behaved, but a logarithmic divergence remains. Understanding or taming this divergence is an interesting avenue for future work. Furthermore it would be interesting to see the vacuum and the 1-electron entanglement entropies.

Chapter 4 started off by trying to answer the question: 'Why the relation between Confinement and the existence of a phase transition in the Entanglement Entropy breaks down, for models based on D($p > 4$) branes ?'

Section 4.1 answered this question, after a detour into non-local QFTs, QFT with a cutoff and the realisation that, when calculating with string duals to non-local QFTs, we are potentially missing a set of configurations that are very important in the calculation of the Entanglement Entropy. These configurations that become apparent when considering the non-local QFT with a cutoff, solve the Physics problem of having only a disconnected and an unstable solution. This is the material discussed in Section 4.1, together with the explicit solution for a simple confining model — D5's on S^1 — where the problem originally appears.

It may be unpleasant to some physicists that we need a UV-cutoff to resolve the problem of stability and to regain the phase transition argued to be present in confining models in [23]. Nevertheless, we want to point out that this UV cutoff is actually capturing the behaviour that the QFT, once UV-completed, will display. Indeed, this is the point made in Section 4.2. We studied a trademark model of confinement in four dimensions, the string background corresponding to D5 branes wrapping a two-cycle of the resolved conifold. We explained how this model would not display a phase transition if taken at face value. But upon the introduction of the cutoff at high energies, we observed the phase transition and the whole behaviour of a four dimensional confining field theory with a Hagedorn density of glueball-states. The effect of this cutoff is the same as the one found in the UV-completed QFT on the D5 branes. Indeed, an inverse Higgs mechanism takes place completing the non-local QFT into the Klebanov-Strassler field theory (in a generic point of its Baryonic Branch). This point is made clear, with calculations and plots of the $S(L)$ phase transition in Section 4.3. Further to this, in Section 4.3, we also pointed out that some backgrounds describing the Mesonic Branch of the Klebanov-Strassler field theory (these backgrounds include a large number of D5-D3 sources) are also afflicted by a non-locality, unless the sources are introduced with a particular profile proposed (using completely different arguments) in [29].

This completes a very pleasant picture advocated in Section 4.4, linking confining, non-local QFTs and their local UV-completed counterparts. Further a link between the Entanglement Entropy and its phase transition, that act as a measure of both locality and confinement. Numerous further calculations complement the presentation, and study a wide variety of other examples, to further illustrate our ideas above.

Lastly, another interpretation of our results could be that entanglement entropy associated with a region in spacetime is not well-defined in the UV phase of non-local theories. After all, the entanglement entropy seems to be unbounded below there, which looks very non-physical and one has to be careful how to define the degrees of freedom of such a theory in the first place. We, however believe different. First of all, note that like many other values in quantum field theory, the entanglement entropy is actually infinite. In order to make physical sense of these quantities we have to choose some scheme of renormalization, where we subtract out the infinite bit and only keep the finite bit. Unlike for local theories, where the phase transition is due to a change in this finite bit of the entanglement entropy, in non-local theories we have a change in the divergent part, where the leading order behaviour changes from an "Area Law" to a "Volume Law". Thus if we choose a scheme that successfully removes the divergent terms on

one side will necessarily fail to remove the divergent terms on the other. That the entanglement entropy seems unbounded below is an artefact of this. If we go one step further, we should note, that the divergent bit in the entanglement entropy comes from the following fact. When we define the entanglement entropy across two complementary regions A and $\bar{A}$, there is an infinity of higher and higher energy modes, closer and closer to the boundary ∂A. Thus it makes intuitive sense that the divergent part follows an area law, i.e. scales with ∂A. However for non-local theories where A is the size of non-local effects or smaller, these high energy modes are free to entangle and interact with modes all over A. So it also makes sense that in this regime the divergence follows a volume law, i.e. it scales with A. From this perspective, we believe our results to be in line with what is expected and presents non-trivial evidence that Ryu-Takayanagi also holds for non-local holographic theories.

Now, let us first summarise the contents and ideas explained in the chapter about Wilson Loops.

The basic idea of the study of the Wilson loops was to study the details of Wilson loops of a novel class of solutions [29], that generalise the KS [30] and baryonic branch [82] solutions, that, by the addition of sources, move the QFT to the mesonic branch..

This was done constructively, by starting from a relatively plain wrapped branes model and slowly adding all the necessary features, keeping track of the properties of the Wilson loops of the theory at each stage.

Afterwards we discussed the possibility of creating a phase transition by tuning two scales dictated by h_1 and ρ_*. This construction of phase transitions has been very successful and yielded a positive outcome in every case. We also explained why these transitions occur.

Lastly, to illustrate the reason behind the phase transitions, the possibility to create several phase transitions has been discussed. We identified which features a profile $\mathcal{S}(\rho)$ needs to produce these. We then constructed new source profiles exemplifying the ideas. Each new profile yielded a double phase transition in each case. Notably, a profile that might become useful for some extended holographic technicolor theories has been described. it in particular could be of interest for further study.

The procedures should also be applicable to the 2+1 d equivalent that has been discussed in [73].

We finished by observing the obvious analogy between the holographic calculation of Wilson loops and Entanglement Entropy. Indeed, being both minimisation problems for two- and eight-surfaces, they display very similar general solutions. In spite of the analogous formulas

derived when minimising surfaces, the two observables are such that when evaluated on particular backgrounds the results are quite different. For example, in confining backgrounds (the topic that mostly occupied us in this thesis) the Wilson loop holographic calculation gives a linear dependence between the quark-antiquark's Energy and separation $E_{QQ} \sim \sigma L_{QQ}$ (for large L_{QQ}), while for the Entanglement Entropy, we observe a very different behaviour, including a first order phase transition. Aside from these observations, either obvious or made previously in the bibliography, the first contribution of Chapter 6 was to develop a simple and operative criteria to test under which conditions the Entanglement Entropy would display a phase transition. Aside from the criteria for phase transitions, some examples were given and an interesting exercise was performed, calculating whether it is possible to find backgrounds where the EE will behave exactly like the Wilson Loop.

Let us describe a couple of ideas that this work suggests as possible extensions of what we have learnt here.

First of all, since we found that confining models typically imply a phase transition for the EE, it would be interesting to ask what happens to the EE when one considers a confining model that presents also a phase transition for the Wilson loop. Indeed, models with various scales have shown this behaviour — see for example [71], [40]. It may be, as we argued in Section 4.4, a multi-phase transition is present for the EE in these cases. It is also worth analysing if the confining behaviour implies that $H(\rho_\Lambda) = 0$, since the argument we gave involving the central charge of the field theory may be evaded. In this same line, the criteria for phase transitions in the EE, discussed in Section 6.1, may lead to interesting extensions. One could try to find out if confinement is actually *needed* for the EE to present a phase transition. Studying the invariances of the EE under different dualities seems like another small and nice project. We already know that S-duality and non-Abelian T-duality [83], [63], are invariances of the EE.

On more general grounds, an observation that this work suggests is the following: we know that black holes for Dp branes (with $p > 4$) turn out to have negative specific heat. We also know that the holographic renormalisation program can be successfully applied to backgrounds based on Dp branes with $p < 5$ [84]. We found that the connection between non-locality of the QFT and the absence of the phase transition in the EE, is there for solutions based on Dp branes with $p > 4$, and this signals that probably, as it happens with the EE, one may find a way to 'fix' the density of states of the finite Temperature QFT and also, with a UV-cutoff, or better with a suitable UV-completion, one may be able to implement the program of

holographic renormalisation. Sorting out which observables turn out to behave similarly with the cutoff, or the UV-completion, seems another interesting problem.

Last but not least, comparing the results of Chapter 3 with Chapter 4 raises the interesting question. 'Might the Ryu-Takayanagi (RT) formula (1.0.8) be wrong?' This is meant in the following sense. An assumption of the eq. (1.0.8) is that, when there are several extremal surfaces, the smallest of them is to be preferred. In Chapter 3 we found legitimate examples where the Entropy is an increasing unbounded function. For Holographic theories, the disconnected surface will always be a solution to RT. Thus with RT we could never have a solution that is unbounded and always increasing, as the value of the disconnected surface will always provide an upper bound. Thus, in some cases, the other non-minimal extremal surfaces might have some physical merit. Perhaps under a different interpretation, such as a different split of the Hilbert space.

References

[1] T. Hartman, "Lectures on Quantum Gravity and Black Holes," http://www.hartmanhep.net/topics2015/. 1, 32

[2] M. B. Hastings, "An area law for one-dimensional quantum systems," *Journal of Statistical Mechanics: Theory and Experiment* **8** (Aug., 2007) 24, arXiv:0705.2024 [quant-ph]. 1

[3] M. Srednicki, "Entropy and area," *Phys. Rev. Lett.* **71** (1993) 666–669, arXiv:hep-th/9303048 [hep-th]. 2

[4] L. Bombelli, R. K. Koul, J. Lee, and R. D. Sorkin, "A Quantum Source of Entropy for Black Holes," *Phys. Rev.* **D34** (1986) 373–383. 2

[5] H. Casini and M. Huerta, "A c-theorem for the entanglement entropy," *J. Phys.* **A40** (2007) 7031–7036, arXiv:cond-mat/0610375 [cond-mat]. 2

[6] H. Casini and M. Huerta, "On the RG running of the entanglement entropy of a circle," *Phys. Rev.* **D85** (2012) 125016, arXiv:1202.5650 [hep-th]. 2

[7] Z. Komargodski and A. Schwimmer, "On Renormalization Group Flows in Four Dimensions," *JHEP* **12** (2011) 099, arXiv:1107.3987 [hep-th]. 2

[8] T. Nishioka, S. Ryu, and T. Takayanagi, "Holographic Entanglement Entropy: An Overview," *J.Phys.* **A42** (2009) 504008, arXiv:0905.0932 [hep-th]. 2

[9] J. Eisert, M. Cramer, and M. Plenio, "Area laws for the entanglement entropy - a review," *Rev.Mod.Phys.* **82** (2010) 277–306, arXiv:0808.3773 [quant-ph].

[10] M. Headrick, "General properties of holographic entanglement entropy," *JHEP* **1403** (2014) 085, arXiv:1312.6717 [hep-th].

[11] H. Casini and M. Huerta, "Entanglement entropy in free quantum field theory," *J.Phys.* **A42** (2009) 504007, arXiv:0905.2562 [hep-th].

[12] P. Calabrese and J. Cardy, "Entanglement entropy and conformal field theory," *J.Phys.* **A42** (2009) 504005, arXiv:0905.4013 [cond-mat.stat-mech]. 2

[13] V. Balasubramanian, M. B. McDermott, and M. Van Raamsdonk, "Momentum-space entanglement and renormalization in quantum field theory," *Phys. Rev.* **D86** (2012) 045014, arXiv:1108.3568 [hep-th]. 2, 19

[14] J. M. Maldacena, "The Large N limit of superconformal field theories and supergravity," *Int.J.Theor.Phys.* **38** (1999) 1113–1133, arXiv:hep-th/9711200 [hep-th]. 2

[15] A. H. Chamseddine and M. S. Volkov, "Non-Abelian BPS monopoles in N=4 gauged supergravity," *Phys.Rev.Lett.* **79** (1997) 3343–3346, arXiv:hep-th/9707176 [hep-th]. 3

[16] J. M. Maldacena and C. Nunez, "Towards the large N limit of pure $N = 1$ superYang-Mills," *Phys.Rev.Lett.* **86** (2001) 588–591, arXiv:hep-th/0008001 [hep-th]. 3, 9, 49

[17] S. Ryu and T. Takayanagi, "Holographic derivation of entanglement entropy from AdS/CFT," *Phys.Rev.Lett.* **96** (2006) 181602, arXiv:hep-th/0603001 [hep-th]. 3, 4

[18] S. Ryu and T. Takayanagi, "Aspects of Holographic Entanglement Entropy," *JHEP* **0608** (2006) 045, arXiv:hep-th/0605073 [hep-th]. 3

[19] J. D. Bekenstein, "Black holes and entropy," *Phys. Rev.* **D7** (1973) 2333–2346. 3

[20] S. W. Hawking, "Particle Creation by Black Holes," *Commun. Math. Phys.* **43** (1975) 199–220. [,167(1975)]. 3

[21] T. Faulkner, A. Lewkowycz, and J. Maldacena, "Quantum corrections to holographic entanglement entropy," *JHEP* **11** (2013) 074, arXiv:1307.2892 [hep-th]. 4

[22] A. Lewkowycz and J. Maldacena, "Generalized gravitational entropy," *JHEP* **08** (2013) 090, arXiv:1304.4926 [hep-th]. 4

[23] I. R. Klebanov, D. Kutasov, and A. Murugan, "Entanglement as a probe of confinement," *Nucl.Phys.* **B796** (2008) 274–293, arXiv:0709.2140 [hep-th]. 4, 5, 31, 36, 49, 53, 54, 59, 104, 105, 106, 112

[24] Y. Kinar, E. Schreiber, and J. Sonnenschein, "Q anti-Q potential from strings in curved space-time: Classical results," *Nucl.Phys.* **B566** (2000) 103–125, arXiv:hep-th/9811192 [hep-th]. 5, 6, 77, 79, 87, 99, 106, 108

[25] K. G. Wilson, "Confinement of Quarks," *Phys.Rev.* **D10** (1974) 2445–2459. 5, 77

[26] S. A. Hartnoll and S. P. Kumar, "Higher rank Wilson loops from a matrix model," *JHEP* **0608** (2006) 026, arXiv:hep-th/0605027 [hep-th]. 5

[27] S.-J. Rey and J.-T. Yee, "Macroscopic strings as heavy quarks in large N gauge theory and anti-de Sitter supergravity," *Eur.Phys.J.* **C22** (2001) 379–394, arXiv:hep-th/9803001 [hep-th]. 6

[28] J. M. Maldacena, "Wilson loops in large N field theories," *Phys.Rev.Lett.* **80** (1998) 4859–4862, arXiv:hep-th/9803002 [hep-th]. 6

[29] E. Conde, J. Gaillard, C. Nunez, M. Piai, and A. V. Ramallo, "A Tale of Two Cascades: Higgsing and Seiberg-Duality Cascades from type IIB String Theory," *JHEP* **1202** (2012) 145, arXiv:1112.3350 [hep-th]. 6, 7, 9, 11, 13, 15, 16, 52, 54, 55, 57, 81, 82, 91, 112, 113

[30] I. R. Klebanov and M. J. Strassler, "Supergravity and a confining gauge theory: Duality cascades and chi SB resolution of naked singularities," *JHEP* **0008** (2000) 052, arXiv:hep-th/0007191 [hep-th]. 6, 13, 101, 104, 113

[31] T. J. Hollowood and M. Warschawski, "In preparation, to be published soon,". 6

[32] U. Kol, C. Nunez, D. Schofield, J. Sonnenschein, and M. Warschawski, "Confinement, Phase Transitions and non-Locality in the Entanglement Entropy," *JHEP* **1406** (2014) 005, arXiv:1403.2721 [hep-th]. 6

[33] M. Warschawski, "Wilson Loops of Klebanov-Strassler like Wrapped Brane Models," arXiv:1212.3472 [hep-th]. 6, 51, 65

[34] R. Andrews and N. Dorey, "Spherical deconstruction," *Phys.Lett.* **B631** (2005) 74–82, arXiv:hep-th/0505107 [hep-th]. 7

[35] R. Andrews and N. Dorey, "Deconstruction of the Maldacena-Nunez compactification," *Nucl.Phys.* **B751** (2006) 304–341, arXiv:hep-th/0601098 [hep-th]. 7, 49, 80

[36] R. Casero, C. Nunez, and A. Paredes, "Towards the string dual of $N = 1$ SQCD-like theories," *Phys.Rev.* **D73** (2006) 086005, arXiv:hep-th/0602027 [hep-th]. 9, 10, 51

[37] C. Hoyos-Badajoz, C. Nunez, and I. Papadimitriou, "Comments on the String dual to $N = 1$ SQCD," *Phys.Rev.* **D78** (2008) 086005, arXiv:0807.3039 [hep-th]. 9, 52

[38] R. Casero, C. Nunez, and A. Paredes, "Elaborations on the String Dual to $N = 1$ SQCD," *Phys.Rev.* **D77** (2008) 046003, arXiv:0709.3421 [hep-th]. 9

[39] J. Gaillard, D. Martelli, C. Nunez, and I. Papadimitriou, "The warped, resolved, deformed conifold gets flavoured," *Nucl.Phys.* **B843** (2011) 1–45, arXiv:1004.4638 [hep-th]. 9, 13, 14, 15, 52, 53, 55

[40] D. Elander, J. Gaillard, C. Nunez, and M. Piai, "Towards multi-scale dynamics on the baryonic branch of Klebanov-Strassler," *JHEP* **1107** (2011) 056, arXiv:1104.3963 [hep-th]. 11, 13, 53, 81, 114

[41] J. Maldacena and D. Martelli, "The Unwarped, resolved, deformed conifold: Fivebranes and the baryonic branch of the Klebanov-Strassler theory," *JHEP* **1001** (2010) 104, arXiv:0906.0591 [hep-th]. 11, 53

[42] C. Nunez, A. Paredes, and A. V. Ramallo, "Unquenched Flavor in the Gauge/Gravity Correspondence," *Adv.High Energy Phys.* **2010** (2010) 196714, arXiv:1002.1088 [hep-th]. 14

[43] E. Conde, J. Gaillard, and A. V. Ramallo, "On the holographic dual of $N = 1$ SQCD with massive flavors," *JHEP* **1110** (2011) 023, arXiv:1107.3803 [hep-th]. 14, 15, 17, 51, 83, 84, 92

[44] O. Aharony, "A Note on the holographic interpretation of string theory backgrounds with varying flux," *JHEP* **0103** (2001) 012, arXiv:hep-th/0101013 [hep-th]. 16

[45] A. Barranco, E. Pallante, and J. G. Russo, "$N = 1$ SQCD-like theories with N_f massive flavors from AdS/CFT and beta functions," *JHEP* **1109** (2011) 086, arXiv:1107.4002 [hep-th]. 17, 61

[46] A. F. Faedo, M. Piai, and D. Schofield, "Gauge/gravity dualities and bulk phase transitions," *Phys.Rev.* **D89** (2014) 106001, arXiv:1402.4141 [hep-th]. 36, 48

[47] C. Bachas, "Convexity of the Quarkonium Potential," *Phys.Rev.* **D33** (1986) 2723. 40

[48] A. Brandhuber and K. Sfetsos, "Wilson loops from multicenter and rotating branes, mass gaps and phase structure in gauge theories," *Adv.Theor.Math.Phys.* **3** (1999) 851–887, arXiv:hep-th/9906201 [hep-th]. 40

[49] J. L. Barbon and C. A. Fuertes, "Holographic entanglement entropy probes (non)locality," *JHEP* **0804** (2008) 096, arXiv:0803.1928 [hep-th]. 41, 43, 44, 45, 48, 54, 58

[50] A. F. Faedo, M. Piai, and D. Schofield, "On the stability of multiscale models of dynamical symmetry breaking from holography," *Nucl.Phys.* **B880** (2014) 504–527, arXiv:1312.2793 [hep-th]. 42

[51] S. D. Avramis, K. Sfetsos, and K. Siampos, "Stability of strings dual to flux tubes between static quarks in $N = 4$ SYM," *Nucl.Phys.* **B769** (2007) 44–78, arXiv:hep-th/0612139 [hep-th]. 42

[52] E. Witten, "Anti-de Sitter space, thermal phase transition, and confinement in gauge theories," *Adv.Theor.Math.Phys.* **2** (1998) 505–532, arXiv:hep-th/9803131 [hep-th]. 42, 98

[53] W. Fischler, A. Kundu, and S. Kundu, "Holographic Entanglement in a Noncommutative Gauge Theory," *JHEP* **1401** (2014) 137, arXiv:1307.2932 [hep-th]. 44, 45, 74

[54] J. L. Karczmarek and C. Rabideau, "Holographic entanglement entropy in nonlocal theories," *JHEP* **1310** (2013) 078, arXiv:1307.3517 [hep-th]. 45, 74

[55] N. Shiba and T. Takayanagi, "Volume Law for the Entanglement Entropy in Non-local QFTs," *JHEP* **1402** (2014) 033, arXiv:1311.1643 [hep-th]. 44

[56] C. Nunez, M. Piai, and A. Rago, "Wilson Loops in string duals of Walking and Flavored Systems," *Phys.Rev.* **D81** (2010) 086001, arXiv:0909.0748 [hep-th]. 53, 83, 84

[57] A. Dymarsky, I. R. Klebanov, and N. Seiberg, "On the moduli space of the cascading SU(M+p) x SU(p) gauge theory," *JHEP* **0601** (2006) 155, arXiv:hep-th/0511254 [hep-th]. 55

[58] H.-C. Chang and A. Karch, "Entanglement Entropy for Probe Branes," *JHEP* **1401** (2014) 180, arXiv:1307.5325 [hep-th]. 67

[59] J. M. Maldacena and H. S. Nastase, "The Supergravity dual of a theory with dynamical supersymmetry breaking," *JHEP* **0109** (2001) 024, arXiv:hep-th/0105049 [hep-th]. 67

[60] F. Canoura, P. Merlatti, and A. V. Ramallo, "The Supergravity dual of 3d supersymmetric gauge theories with unquenched flavors," *JHEP* **0805** (2008) 011, arXiv:0803.1475 [hep-th]. 67

[61] N. T. Macpherson, "SuGra on G_2 Structure Backgrounds that Asymptote to AdS_4 and Holographic Duals of Confining $2+1d$ Gauge Theories with $N=1$ SUSY," *JHEP* **1304** (2013) 076, arXiv:1301.5178 [hep-th]. 67

[62] J. Gaillard and D. Martelli, "Fivebranes and resolved deformed G_2 manifolds," *JHEP* **1105** (2011) 109, arXiv:1008.0640 [hep-th]. 68

[63] E. Caceres, N. T. Macpherson, and C. Núñez, "New Type IIB Backgrounds and Aspects of Their Field Theory Duals," *JHEP* **1408** (2014) 107, arXiv:1402.3294 [hep-th]. 72, 114

[64] A. Brandhuber, "G(2) holonomy spaces from invariant three forms," *Nucl.Phys.* **B629** (2002) 393–416, arXiv:hep-th/0112113 [hep-th]. 72

[65] J. D. Edelstein and C. Nunez, "D6-branes and M theory geometrical transitions from gauged supergravity," *JHEP* **0104** (2001) 028, arXiv:hep-th/0103167 [hep-th]. 73

[66] N. Kim, "Holographic entanglement entropy of confining gauge theories with flavor," *Phys.Lett.* **B720** (2013) 232–236. 74

[67] A. Brandhuber and Y. Oz, "The D-4 - D-8 brane system and five-dimensional fixed points," *Phys.Lett.* **B460** (1999) 307–312, arXiv:hep-th/9905148 [hep-th]. 75

[68] K. Balasubramanian, "Gravity duals of cyclic RG flows, with strings attached," arXiv:1301.6653 [hep-th]. 76

[69] J. Sonnenschein, "What does the string / gauge correspondence teach us about Wilson loops?," arXiv:hep-th/0003032 [hep-th]. 77, 78

[70] C. Nunez, I. Papadimitriou, and M. Piai, "Walking Dynamics from String Duals," *Int.J.Mod.Phys.* **A25** (2010) 2837–2865, arXiv:0812.3655 [hep-th]. 81

[71] F. Bigazzi, A. L. Cotrone, C. Nunez, and A. Paredes, "Heavy quark potential with dynamical flavors: A First order transition," *Phys.Rev.* **D78** (2008) 114012, arXiv:0806.1741 [hep-th]. 83, 114

[72] S. Bennett, "Wilson loops in warped resolved deformed conifolds," *Annals Phys.* **326** (2011) 2934–2956, arXiv:1102.5731 [hep-th]. 83

[73] N. T. Macpherson, "The Holographic Dual of 2+1 Dimensional QFTs with $N = 1$ SUSY and Massive Fundamental Flavours," *JHEP* **1206** (2012) 136, arXiv:1204.4222 [hep-th]. 113

[74] F. Bigazzi, A. L. Cotrone, A. Paredes, and A. Ramallo, "Non chiral dynamical flavors and screening on the conifold," *Fortsch.Phys.* **57** (2009) 514–520, arXiv:0810.5220 [hep-th]. 83

[75] F. Bigazzi, A. L. Cotrone, A. Paredes, and A. V. Ramallo, "The Klebanov-Strassler model with massive dynamical flavors," *JHEP* **03** (2009) 153, arXiv:0812.3399 [hep-th]. 88

[76] E. Conde, J. Gaillard, C. Nunez, M. Piai, and A. V. Ramallo, "Towards the String Dual of Tumbling and Cascading Gauge Theories," *Phys.Lett.* **B709** (2012) 385–389, arXiv:1112.3346 [hep-th]. 89

[77] N. Itzhaki, J. M. Maldacena, J. Sonnenschein, and S. Yankielowicz, "Supergravity and the large N limit of theories with sixteen supercharges," *Phys.Rev.* **D58** (1998) 046004, arXiv:hep-th/9802042 [hep-th]. 98

[78] U. Kol and J. Sonnenschein, "Can holography reproduce the QCD Wilson line?," *JHEP* **1105** (2011) 111, arXiv:1012.5974 [hep-th]. 99, 109

[79] J. Erlich, E. Katz, D. T. Son, and M. A. Stephanov, "QCD and a holographic model of hadrons," *Phys.Rev.Lett.* **95** (2005) 261602, arXiv:hep-ph/0501128 [hep-ph]. 102

[80] A. Karch, E. Katz, D. T. Son, and M. A. Stephanov, "Linear confinement and AdS/QCD," *Phys.Rev.* **D74** (2006) 015005, arXiv:hep-ph/0602229 [hep-ph]. 102

[81] A. Loewy and J. Sonnenschein, "On the holographic duals of $N = 1$ gauge dynamics," *JHEP* **0108** (2001) 007, arXiv:hep-th/0103163 [hep-th]. 104

[82] A. Butti, M. Grana, R. Minasian, M. Petrini, and A. Zaffaroni, "The Baryonic branch of Klebanov-Strassler solution: A supersymmetric family of SU(3) structure backgrounds," *JHEP* **0503** (2005) 069, arXiv:hep-th/0412187 [hep-th]. 113

[83] G. Itsios, C. Nunez, K. Sfetsos, and D. C. Thompson, "Non-Abelian T-duality and the AdS/CFT correspondence:new N=1 backgrounds," *Nucl.Phys.* **B873** (2013) 1–64, arXiv:1301.6755 [hep-th]. 114

[84] I. Kanitscheider, K. Skenderis, and M. Taylor, "Precision holography for non-conformal branes," *JHEP* **0809** (2008) 094, arXiv:0807.3324 [hep-th]. 114